WL-TR-96-2066

# HYDRAULIC AND THERMAL PERFORMANCE TESTS ON A HIGH FLUX HEAT EXCHANGER WITH PAO AS THE COOLANT

Afshin J. Ghajar, Professor
Michael Cutbirth, Graduate Student

School of Mechanical and Aerospace Engineering
Oklahoma State University
Stillwater OK 74078

MAY 1996

FINAL REPORT FOR 1 Sep 94 - 31 Dec 95

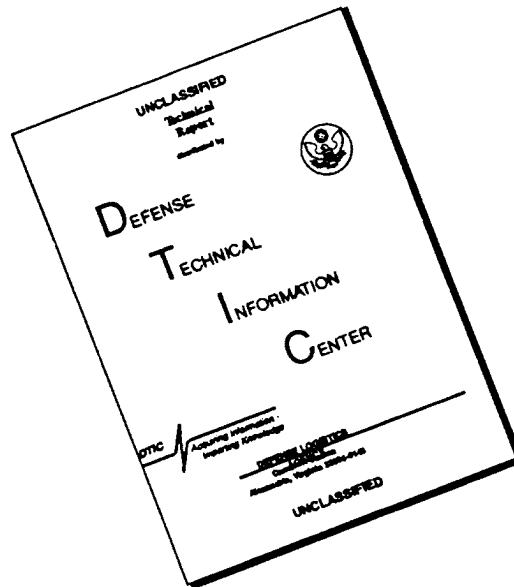**Approved for public release; distribution unlimited**

19960625 211

DTIC QUALITY INSPECTED 1

# DISCLAIMER NOTICE

THIS DOCUMENT IS BEST QUALITY AVAILABLE. THE COPY FURNISHED TO DTIC CONTAINED A SIGNIFICANT NUMBER OF PAGES WHICH DO NOT REPRODUCE LEGIBLY.
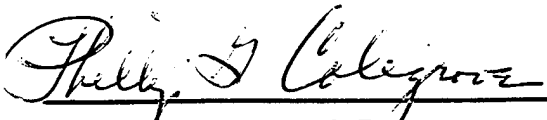
# NOTICE

WHEN GOVERNMENT DRAWINGS, SPECIFICATIONS, OR OTHER DATA ARE USED FOR ANY PURPOSE OTHER THAN IN CONNECTION WITH A DEFINITELY GOVERNMENT-RELATED PROCUREMENT, THE UNITED STATES GOVERNMENT INCURS NO RESPONSIBILITY OR ANY OBLIGATION WHATSOEVER. THE FACT THAT THE GOVERNMENT MAY HAVE FORMULATED OR IN ANY WAY SUPPLIED THE SAID DRAWINGS, SPECIFICATIONS, OR OTHER DATA, IS NOT TO BE REGARDED BY IMPLICATION, OR OTHERWISE IN ANY MANNER CONSTRUED, AS LICENSING THE HOLDER, OR ANY OTHER PERSON OR CORPORATION; OR AS CONVEYING ANY RIGHTS OR PERMISSION TO MANUFACTURE, USE, OR SELL ANY PATENTED INVENTION THAT MAY IN ANY WAY BE RELATED THERETO.

THIS REPORT IS RELEASABLE TO THE NATIONAL TECHNICAL INFORMATION SERVICE (NTIS). AT NTIS, IT WILL BE AVAILABLE TO THE GENERAL PUBLIC, INCLUDING FOREIGN NATIONS.

THE TECHNICAL REPORT HAS BEEN REVIEWED AND IS APPROVED FOR PUBLICATION.

JOHN E. LELAND
Project Engineer
Mechanical and Thermal Group

PHILLIP G. COLEGROVE
Chief
Mechanical and Thermal Group

MICHAEL D. BRAYDICH, Lt Col, USAF
Chief
Aerospace Power Division

# REPORT DOCUMENTATION PAGE

Public reporting burden for this collection of information is estimated to average 1 hour per response, including the time for reviewing instructions, searching existing data sources, gathering and maintaining the data needed, and completing and reviewing the collection of information. Send comments regarding this burden estimate or any other aspect of this collection of information, including suggestions for reducing this burden, to Washington Headquarters Services, Directorate for Information Operations and Reports, 1215 Jefferson Davis Highway, Suite 1204, Arlington, VA 22202-4302, and to the Office of Management and Budget, Paperwork Reduction Project (0704-0188), Washington, DC 20503.

| 1. AGENCY USE ONLY (Leave blank) | 2. REPORT DATE<br>May 1996 | 3. REPORT TYPE AND DATES COVERED<br>1 Sep 94 – 31 Dec 95 |
|---|---|---|

**4. TITLE AND SUBTITLE**
Hydraulic and Thermal Performance Tests on a High Heat Flux Heat Exchanger With PAO as the Coolant

**6. AUTHOR(S)**
Ghajar, Afshin J.
Cutbirth, Michael

**5. FUNDING NUMBERS**
C F33615-94-C-2419
PE 62203F
PR 3145
TA 32
WU Y6

**7. PERFORMING ORGANIZATION NAME(S) AND ADDRESS(ES)**
School of Mechanical and Aerospace Engineering
Oklahoma State University
Stillwater Oklahoma 74078

**8. PERFORMING ORGANIZATION REPORT NUMBER**

**9. SPONSORING/MONITORING AGENCY NAME(S) AND ADDRESS(ES)**
Aero Propulsion and Power Directorate
Wright Laboratory
Air Force Materiel Command
Wright Patterson AFB OH  45433-7251

**10. SPONSORING/MONITORING AGENCY REPORT NUMBER**
WL-TR-96-2066

**11. SUPPLEMENTARY NOTES**

**12a. DISTRIBUTION/AVAILABILITY STATEMENT**
APPROVED FOR PUBLIC RELEASE: DISTRIBUTION IS UNLIMITED.

**12b. DISTRIBUTION CODE**

**13. ABSTRACT (Maximum 200 words)**

With new aircraft navigation, communications and countermeasures equipment requiring numerous data processing units, today's military aircraft is experiencing an increasing dependence on electronics. Furthermore, the power densities and ensuing waste heat fluxes of electronic chips are increasing as designers strive to improve processing speeds. One concept being proposed to meet the stringent cooling requirements of these advanced electronics is the High Flux Heat Exchanger, HFHE, developed by McDonnell Douglas. The HFHE consists of 20 Compact High Intensity Coolers, CHICs, developed by Sundstrand and capable of handling 100 $W/cm^2$ each and arranged in a grid on a SEM-E card. This translates into a total cooling capacity of 2000 W. The design point for the HFHE was to deliver 2000 Watts of cooling while maintaining electronics junction temperatures at less than 90°C using polyalphaolefin (PAO) as the coolant. The purpose of this effort was to determine HFHE hydraulic and thermal performance. Results were obtained for flow rates of 1.0 to 4.0 kg/min over a temperature range of -10 to 40°C and for heat loads up to 100 W. Using these results, pump size and the flow rates needed for sufficient thermal performance of the HFHE were estimated.

**14. SUBJECT TERMS**
Electronics Cooling, Avionics Cooling, Polyalphaolephin, High Flux Heat Exchanger, Compact High Intensity Cooler

**15. NUMBER OF PAGES**
248

**16. PRICE CODE**

| 17. SECURITY CLASSIFICATION OF REPORT | 18. SECURITY CLASSIFICATION OF THIS PAGE | 19. SECURITY CLASSIFICATION OF ABSTRACT | 20. LIMITATION OF ABSTRACT |
|---|---|---|---|
| Unclassified | Unclassified | Unclassified | SAR |

TABLE OF CONTENTS

LIST OF FIGURES

LIST OF TABLES

## NOMENCLATURE

A     cross-sectional area of the individual channels of the CHIC, $m^2$

b     spacing in a dead-weight tester, cm

C     constant relating the Reynolds number and the friction factor for laminar flow

$C_n$     constants in the curve fit for the pressure, with n =1,2

d     diameter of the piston in the dead-weight tester, cm

D     diameter of the individual channels in the CHIC, m

f     friction factor for pipe flow, dimensionless

g     gravitational acceleration, $m^2/s$

$g_c$     gravitational constant, $kg\text{-}m/N\text{-}s^2$

h     enthalpy, N-m/kg

$h_f$     total frictional head loss, m

k     thermal conductivity of the HFHE (copper), 300 $W/m\text{-}°C$

$k_i$     minor loss coefficient for the CHIC for pipe flow, dimensionless

l     length of the piston in the dead-weight tester, cm

L     length of the individual tubes in the CHICs, m

$\dot{m}$     mass flow rate of the fluid, kg/hr

p     pressure, psi

Q     volumetric flow rate, $m^3/s$

$\dot{Q}$     heat transfer, $W/cm^2$ or W per CHIC (each CHIC has a surface area of 1 $cm^2$)

Re     Reynolds number (= $\rho VD/\mu$), dimensionless

$R_{xy}$     thermal resistance from x to y, $°C/(W/cm^2)$

$r_n$     distance from CHIC center to symmetry boundary in n-direction, m

t     conduction thickness of the target plate, 0.001143 m

$T_n$     temperature of n, where n is a subscript referring to the coolant fluid, surface of the HFHE, wall of the CHIC, and the junction, °C

v     volume of fluid, mL

V     velocity of the fluid in the test section, m/s

w     work, J/kg

$\dot{W}$     power, W/s

z     potential energy term, m


## Greek letter symbols

$\Delta p$     pressure drop across the HFHE, psi

$\varepsilon$     error term, dimensionless

$\phi_n$     constant in the $\dot{Q}_{loss}/\dot{Q}_{applied}$ curve fit, n=1,....,7

$\gamma$     specific weight of the coolant fluid, $N/m^3$

$\lambda_n$     constant in the wall temperature curve fit, n=0,1,2,3

$\mu$     absolute viscosity of the coolant fluid, $N-s/m^2$

$\nu$     kinematic viscosity of the coolant fluid, $m^2/s$

$\theta_n$     constant in the surface temperature curve fit, n=1,2,3

$\rho$     density of the coolant fluid, $kg/m^3$

$\xi$     dummy variable to express the direction of the radial heat flow, cm

$\psi$     temporary coefficient for the wall temperature, dimensionless


## Subscripts

c     refers to the case housing of the electronics

e     exit of the control volume

f     refers to the coolant fluid

i     inlet to the control volume

j     refers to the junction of the case housing and the electronic chip

mech     mechanical (i.e. mechanical work)

s     refers to the surface of the HFHE

$s_\tau$     Viscous stress

w     refers to the outer wall of the CHIC in the HFHE

# FOREWORD

Afshin J. Ghajar
Michael Cutbirth

# CHAPTER I

## INTRODUCTION

This chapter will first present background as it relates to the study of the hydraulic and thermal performance of the High Flux Heat Exchanger. The purposes of the investigation will be given and a summary of the performed experimental work will be included. Finally, brief statements about the previous work of other investigations, relating to the development of the High Flux Heat Exchanger, will justify the need for experimentation such as this.

## 1.1 Background

Modern aircraft has seen an increase in dependence on electronics. New on-board electronics require more data processing units for improvements in navigation and high-powered radar. In addition, computer technology is constantly creating more powerful electronic chips without increasing the surface area. The combination of these factors has created a need for improved coolant systems to dissipate the increasing amount of thermal energy created by

the electronics. In past electronic components that have low power densities, the preferred cooling approach was air cooling due to its simplicity, leakage tolerance, and reliability. However, with the increase of electronic chip technology, processors have higher heat fluxes; thus, liquid cooling becomes more attractive even though the liquid cooling systems add an intermediate cooling loop. One of the most effective processes for liquid cooling is jet impingement. However, an analysis can be made that leads to the conclusion that a multiple number of small jets will be more effective in cooling the same area than a single large jet. Furthermore, the cooling performance can be enhanced by extending the surface areas. Therefore, a greater surface density per unit volume can be achieved leading to higher fin efficiencies all resulting from the use of shorter conduction path lengths that are vigorously scrubbed by high heat transfer coolant jets. The shorter path lengths are a result from using thin lamination plates in close proximity to the heat source. This concept of using multiple jet impingement with the enhancement of multiple plates let to Sundstrand's Compact High Intensity Cooler, CHIC. However, this concept only satisfies the requirement for higher heat fluxes caused by modern electronics. To meet the need for the increased number of electronic processors, McDonnell Douglas developed the High Flux Heat

Exchanger, HFHE. The HFHE consists of 20 CHICs arranged in parallel flow, with each CHIC being 1 cm$^2$ in contact area and capable of absorbing 100 W/cm$^2$.

Because of this need for liquid cooling to absorb higher heat fluxes, additional considerations must be introduced. With the added intermediate cooling loop, in the aircraft, associated with liquid cooling, leaking and handling of the liquid coolant are of immense concern. Also, with the increase of emphasis on safety and environmental hazards, this liquid coolant must be non-toxic, non-corrosive, and be an adequate dielectric. Because of these concerns, the Navy and Air Force have replaced Coolanol, a silicate based ester that forms flammable components when exposed to water, with polyalphaolefin, PAO, a synthetic oil.

## 1.2  Objectives

The long range goal of this investigation is to accurately model the thermal and hydraulic performance of the High Flux Heat Exchanger, HFHE, under actual performance conditions. The specific objectives of this research are:

1.  To investigate the influence of the coolant flow rate and temperature on the pressure drop across the inlet and outlet of the HFHE. This

investigation should result in a hydraulic performance equation and corresponding performance curve with the flow rate and temperature as the dependent variables.

2.  To investigate the influence of the coolant flow rate and temperature on the heat flux removal capabilities of the HFHE for steady-state heat loads.  This investigation should result in a thermal performance curve and correlating equation for the necessary coolant flow rate with respect to the coolant temperature to achieve a given amount of heat flux removal (e.g.  one performance curve for 100 Watts of heat flux removal, one performance curve for 80 Watts of heat flux removal, etc.)

3.  To investigate the influence of the coolant flow rate and temperature on the heat flux removal capabilities of the HFHE for transient heat loads.  This investigation should result in graphical presentation of the thermal lag of the HFHE.

4.  To develop a guideline for the overall performance of the HFHE.  This will consist of a performance chart and correlating equation combining the

hydraulic performance and the steady-state performance curves.

## 1.2.1  Long Term Goals

This thesis details the preparations of a suitable experimental apparatus with inherent versatility for the successful fulfillment of all long term objectives.  In addition, this thesis concerns itself with both the methodology and the analysis of accurate modeling of the High Flux Heat Exchanger.  The methodology was developed to be used not only on the HFHE but any other high flux heat exchanger developed for the purpose of cooling the avionics' electronic system.  The common methodology will allow for comparison between the different proposed cooling systems.  Furthermore, the test loop was designed to accommodate any heat exchanger that fits the SEM-E configuration (the SEM-E configuration is described in detail in the literature review).

## 1.2.2  Data Base

This thesis discusses the hydraulic and thermal performance of the High Flux Heat Exchanger over a wide range of mass flow rates, coolant temperatures, and heat loads.  To provide the necessary data base, 104 experimental

runs were performed for the hydraulic tests, 1236 experimental runs were performed for the steady-state thermal tests, and 150 experimental runs were performed for the transient thermal tests. At the beginning of the research, it was determined that for each run, a minimum of fifteen data points were necessary for sufficient accuracy, due to the fluctuations of the data collection equipment. This reasoning is shown in Appendix A.

The hydraulic tests were performed over the following ranges: coolant temperature, -10°C to 50°C by an increment of 10°C, with the addition of -15°C to fully cover the effects of sub-zero coolant temperature, and mass flow rate, 1.0 kg/min to 4.0 kg/min by an increment of 0.25 kg/min.

The steady-state thermal tests were performed on six of the twenty CHICs in the HFHE, shown in Figure 1.1. The first three CHICs tested (CHICs: A, B, C) were evaluated in full to develop all of the correlations, and covered the following ranges: a coolant temperature of -10°C to 40°C by an increment of 10°C, a mass flow rate of 1.0 kg/min to 4.0 kg/min by an increment of 0.25 kg/min, and a heat load of 20 W to 100 W by an increment of 20 W. However, due to the constraints explained below, the flow rate and heat load ranges were truncated for certain coolant temperatures. One of the constraints states that the maximum HFHE wall

temperature be 50°C; therefore, the 100 W heat load for the 30°C coolant temperature and the 80 W and the 100 W heat load for the 40°C coolant temperature were eliminated. In addition, for these coolant temperatures, the minimum mass flow rate was raised to 2.0 kg/min. Also, due to the constraint of high pressure, the maximum flow rate was lowered to 3.0 kg/min for the 0°C and 10°C coolant temperatures.

The last three CHICs (CHICs: D, E, F) were then evaluated in part to cross-correlate with the first three CHICs. For these CHICs, the coolant temperature and heat load ranges were retained from the first three CHICs. However, the flow rate range was truncated to contain the following data points: the lowest flow rate, the lowest flow rate increased by 0.5 kg/min, the median flow rate, the highest flow rate decreased by 0.5 kg/min, and the highest flow rate for the corresponding coolant temperature (e.g. 1.0, 1.5, 2.5, 3.5, and 4.0 kg/min for a coolant temperature of 10°C).

Finally for the transient tests, the full coolant range, -10°C to 40°C, was retained. In addition, the flow rate data points were the same as the flow rate data points for the last three CHICs; the lowest flow rate, the lowest
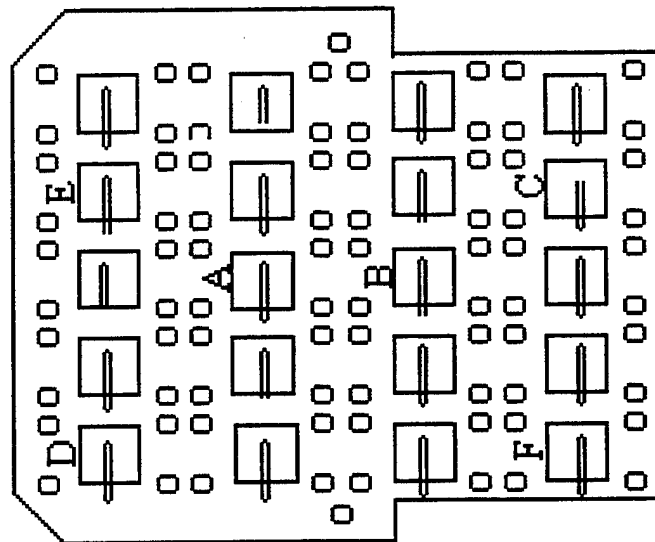
Figure 1.1.  The Location of the Tested CHICs.

flow rate increased by 0.5 kg/min, the median flow rate, the highest flow rate decreased by 0.5 kg/min, and the highest flow rate for the corresponding temperature, as shown in the example above. Finally, the heat load range was reduced to 10 W to 50 W by an increment of 10 W.

## 1.2.3 Correlation Comparisons

For this data base, few correlations are possible due to the small amount of existing data on the High Flux Heat Exchanger.

For the hydraulic tests, Sundstrand has existing computer programs that are capable of predicting the hydraulic performance of the Compact High Intensity Cooler in any geometric arrangement. However, these programs only predict the hydraulic performance for the turbulent flow regime. In addition, the experimental analysis backing these existing performances are for fluids other than polyalphaolefin. For this research, only the combination of the extreme end of the flow range, 4.0 kg/min, and the extreme end of the coolant temperature, 50°C, results in non-laminar flow. For these parameters, the Reynolds number is 2176 which is slightly in the transitional flow region. Therefore, the flow regime and the fluid used in this research have not previously been examined in detail, and

all previous predictions for the HFHE must be used roughly.

In addition, the thermal performance, both steady-state and transient, have been previously examined by McDonnell Douglas. However, this previous research covered only three discrete flow rates and a temperature range of 10°C to 40°C. Furthermore, the stacking of the laminates for the HFHE examined by McDonnell Douglas differs from the stacking of the laminates for the HFHE used in this research. Therefore, the thermal data in this research should theoretically differ from the thermal performance data recorded by McDonnell Douglas. In conclusion, the data collected in this research is unique, and all previous results for the HFHE are used as very rough approximations.

## 1.3  Literature Survey

Modern aircraft has seen an increase in dependence on electronics. Mackowski [1] performed an industrial survey to determine future requirements for the high flux heat removal in advanced electronics systems. The study focused on the technology requirements for military avionics systems. The results of this survey can be sorted into four broad application categories:  commercial digital systems, military data processors, power processors and radar and optical systems. The commercial digital systems can be

divided into sub-categories, the first being the central processor units (CPUs) and gate arrays (customizable processors).  Some thermal management researchers predict that future power dissipation in these devices will increase to 100 W per device, while each device's surface area will decrease to 1 cm$^2$; thereby creating a maximum heat flux of 1 W/cm$^2$.  However, Mackowski states that these devices will have power consumptions that remain under 30 W.

The second sub-category is the mainframe computer.  The modern mainframe itself can have power consumption of 500 W; however, the thermal load per individual chip is low due to the large number of chips used.  One example given by Mackowski is a Motorola multi-chip module that can accommodate a heat load of up to 500 W.  However, this module is 4 inches by 4 inches, yielding a heat flux of 14 W/cm$^2$.  The second category includes military data processors.  These processors range from the general data processor to missiles and smart weapons.  However, even though it is predicted that the total power for each board may go as high as 400 W for these digital systems, the localized heat flux should not exceed 50 W/cm$^2$.

The third category, which includes general power processors, low-voltage power supplies, high-power systems, and neutral particle beam, require a cooling capability of at least 100 W/cm$^2$.  However, the cooling capability could

be even higher because the solid state power switching devices can produce a pulsed heat flux of over 400 W/cm$^2$. The final category includes conventional radar, solid state RF arrays, laser radar, optical sensors, and laser communications. The most likely driver for high flux cooling from this category will be the solid state RF arrays and laser device. However, the localized heat fluxes for both of these devices are under 25 W/cm$^2$. As seen, the most challenging thermal problems were found to lie with the power controllers. The power controllers contain steady-state heat fluxes reaching at least 100 to 200 W/cm$^2$. In addition, pulsed heat loads of short duration, on the order of a second or less, could exceed 400 W/cm$^2$. The heat dissipation of future high-performance data processors was predicted to be somewhat lower, with steady-state levels reaching perhaps 50 to 100 W/cm$^2$.

Flynn [2] made an evaluation of cooling concepts for high power avionics applications. Based on the results of Mackowski [1], a steady-state chip heat flux of 100 W/cm$^2$ and a maximum chip junction temperature of 90°C was selected as representative thermal requirements for the near-future high power avionics. Several additional constraints were also imposed on the cooler due to the intended application of cooling fighter aircraft electronics. These constraints included a practical lower limit on coolant supply

temperature, the preference for a non-toxic, nonflammable, and nonfreezing coolant, the need to minimize weight and volume, and operation in an accelerating environment. Evaluation factors included aircraft system impact, cooler development status, and qualitative assessments of life cycle cost, reliability, maintainability, and safety. Among the emerging cooling technologies, seven concepts were identified which could meet the cooling requirements. The evaluated cooling concepts were: Compact High Intensity Cooler (CHIC), Curved Channel Flow with Subcooled Boiling, Evaporative Spray Cooler, Heat Pipe, Jet Impingement with Subcooled Boiling, Microchannel Cooler, and Pumped Capillary Evaporator. These seven cooling concepts were investigated in detail and an assessment of their performance was made against the evaluation factors. The Compact High Intensity Cooler (CHIC) concept was selected to meet the demanding thermal requirements foreseen for near-future avionics.

The CHIC device was first introduced by Sundstrand in 1983 (Bland, et al. [3]). The original CHIC was developed to provide a heat rejection of 50 W to a 1 cm by 1 cm surface, which results in a heat flux intensity of 50 $W/cm^2$ of heat removal with tight requirements for surface isothermality. This liquid single phase cooler combines the thermal efficiency of multiple jet impingement with a large

fin area to produce a high effective heat transfer
coefficient.

In the development of the multi-CHIC High Flux Heat
Exchanger, Flynn, et al. [4] made a comparison of a single
jet impingement to multiple jet impingement. Ordinary jet
impingement for a single jet can be divided into three
zones: the stagnation zone, the turning region and the wall
jet region. For jet impingement with multiple jets a fourth
region occurs, the jet interaction zone. These four zones
can be seen in Figure 1.2. The heat transfer rates are high
for both of the inner regions. This leads to the conclusion
that a multiple number of small jets will be more effective
in cooling the same area than a single large jet.

Furthermore, the cooling performance can be enhanced by
extending the surface areas. Therefore, a greater surface
area density per unit volume can be achieved leading to
higher fin efficiencies resulting from the shorter
conduction path lengths. This is accomplished by using thin
lamination plates in close proximity to the heat source
being vigorously scrubbed by high heat transfer coolant
jets. This maximizing the surface area and fin
effectiveness is in actuality minimizing the thermal
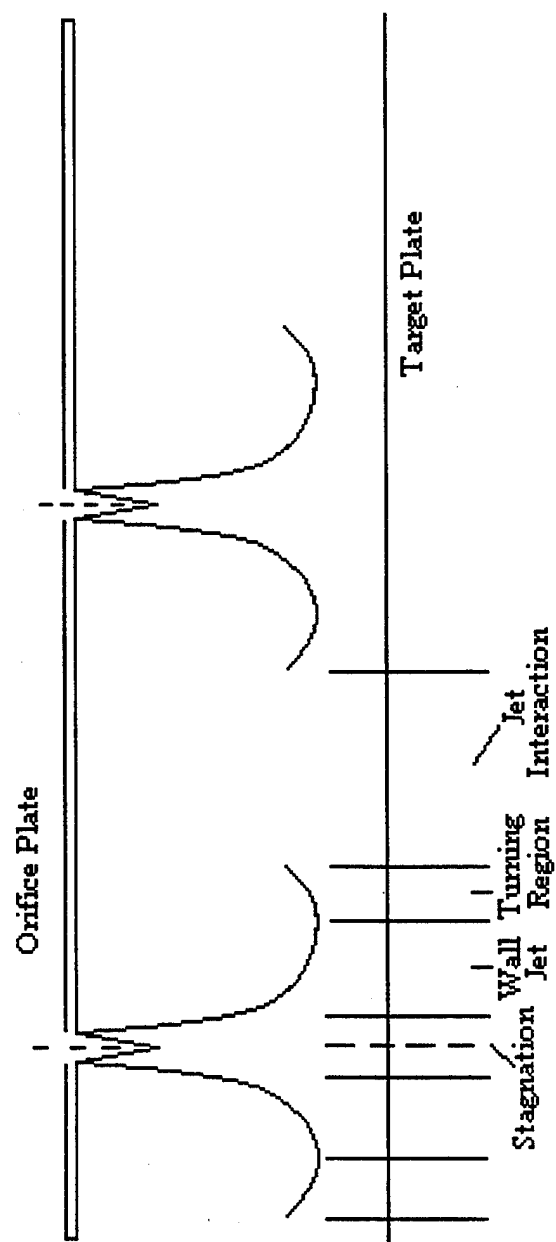
Figure 1.2.  Four Characteristic Regions for Multiple Jet Impingement Heat Exchanger.

resistance. This concept of using multiple jet impingement with the enhancement of multiple plates is the basis for Sundstrand's development of the CHIC.

The operating principle of a CHIC device is relatively simple, as shown in Figure 1.3. The liquid enters the inlet port in the end cover, flows through a succession of thin laminates towards the heat acquisition surface, or target plate. The liquid impinges on the target plate, and then isdirected back to the drain manifold attached and ultimately to the exit port of the end cover. The electronics device is attached to the opposite side of the target plate. As shown in Figure 1.3, the fluid en route to the target plate passes through a jet orifice plate and a spacer plate. The jet orifice plate usually contains about 50 to 200 small circular holes. In a typical CHIC device, the orifice plate and the spacer plate are repeated several times, with each successive orifice plate acting as a target for the jets from the orifice plate immediately upstream. The orifices are offset by one-half their pitch from plate to plate, so that the liquid impinges on solid metal, then cascades downward as it passes through subsequent orifice plates. The jet interaction of the multiple jets increases the turbulence and mixing, enhancing the heat transfer. Increasing the number of orifice plates, increases the fin
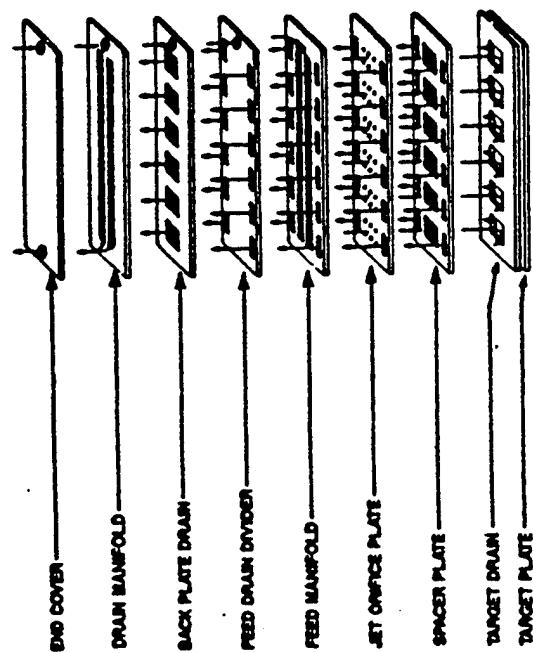
Figure 1.3. CHIC Basic Elements and Operating Principle [4].

Labels (reading the diagram): END COVER, DRAIN MANIFOLD, BACK PLATE DRAIN, FEED DRAIN DIVIDER, FEED MANIFOLD, JET ORIFICE PLATE, SPACER PLATE, TARGET DRAIN, TARGET PLATE.

area and produces a higher effective heat transfer
coefficient. The penalty for a larger number of orifice
plates is higher pressure drop and a thicker heat exchanger.
Since the 1983 prototype [3], several versions of CHICs have
been built from copper and aluminum. The devices have been
tested with Freon-11 [3], Freon-113 [5], and water [6].

However, this concept only satisfies the requirement
for higher heat fluxes caused by modern electronics. To
meet the need for an increase in the number of electronic
processors, McDonnell Douglas developed the High Flux Heat
Exchanger, HFHE. The HFHE consists of 20 CHICs arranged in
parallel flow, with each CHIC being 1 $cm^2$ and capable of
absorbing 100 $W/cm^2$. The HFHE was designed to integrate
into the Lockhart LOC-E-JECT liquid cooled Navy Standard
Electronic Module (SEM-E) used for F-2 avionics cooling.
The actual design requirement used for the development of
the HFHE is that size must fit the SEM-E, approximately 15
by 17 cm, on 1.5 cm pitch, for a total of 200 $cm^2$ mounting
area per side. Furthermore, the module must absorb 2180 W
of steady-state heat load, distributed as 100 $W/cm^2$ to 20
$cm^2$ of board surface area, consisting of the 20 one $cm^2$
CHICs, and 1.0 $W/cm^2$ heat flux over the remaining 180 $cm^2$ of
surface area. Further details of the high flux heat
exchanger design are documented in [4]

To ease the process of manufacturing this complex array of CHICs, Sundstrand has developed a process [7] of photo-etching laminae allowing for very accurate location of the orifices on the plates. The laminae are then stacked and bonded. Diffusion bonding was used for the copper boards and vacuum brazing was used for the aluminum boards. This photo-etching process allows virtually anything that can be drawn to be fabricated.

Because of this need for liquid cooling to absorb higher heat fluxes, additional considerations must be introduced. With the added intermediate aircraft cooling loop associated with liquid cooling, leaking and handling create a selection process for the liquid coolants. And with the increase of emphasis on safety and the environment, this liquid coolant must be non-toxic, non-corrosive, and be an adequate dielectric. In the past, silicate-ester based fluids, Coolanol 25R, were widely used as the liquid coolant in military avionics systems. These fluids have caused significant and sometimes catastrophic problems due to their hygroscopic nature and subsequent formation of flammable alcohols and silica gel. The alcohol by-product lowers the fluid flash point, increasing the risk of aircraft fires. The gelatinous precipitate called the "black plague", deposits on the surfaces of the electronics components, causing avionics equipment to malfunction. In order to

solve the problems associated with Coolanol, the Air Force and the Navy investigated the possibility of direct replacement of silicate-ester based fluids with hydrogenated polyalphaolefin based fluids. Their studies concluded that polyalphaolefin (PAO) fluids are chemically more stable, (do not hydrolyze to form either silica gel or alcohol by-products), are less costly, offer equal or improved dielectric characteristics, and meet or exceed military requirements for a dielectric coolant [8,9]. Due to these desirable properties of PAO, the Air Force and the Navy, for some selected fighter aircraft, have both replaced the liquid coolant, Coolanol, used in their fighter aircraft electronic cooling systems with PAO.

In a recent study [10], the hydraulic and thermal performance of PAO and Coolanol 25R in different flow regimes, laminar and turbulent, were compared. The results indicated that at normal operating temperatures the two coolants were reasonably close and fairly independent of the flow regime. However, at low temperatures, dependent on the flow regime, there could be a substantial difference between the hydraulic and thermal performance of the two fluids. Particularly, at temperatures below 0°C, PAO's hydraulic performance in the laminar flow region, and its thermal performance in the turbulent flow region, are inferior to those of Coolanol 25R at comparable conditions.

Coolanol has been a standard coolant of fighter aircraft, but is currently being phased out by PAO, which is much less prone to decomposition. Therefore, in this study of the performance for the High Flux Heat Exchanger, PAO was selected as the liquid coolant.

In the following chapters, the experimental setup, the experimental procedure, and the presentation of the completed objectives are presented.

# CHAPTER II

## EXPERIMENTAL APPARATUS

Because of the extreme ranges of pressure and temperature and the wide array of information garnered, the analysis of the hydraulic and thermal performances of the High Flux Heat Exchanger, HFHE, required a specialized experimental setup. A schematic diagram of the top view of the laboratory setup is shown in Figure 2.1. Also, presented in this chapter is a description of the experimental apparatus used in the laboratory test setup, including the necessary instrumentation details on the individual components. Following the apparatus descriptions, an explanation of the necessary calibration procedures is given ensuring the accuracy of each data processing component. Next, the operational procedure of the test setup for the hydraulic, steady-state thermal, and the transient thermal tests are given. The final section of this chapter is concerned with the detailing of the reduction of the raw data output from the data processing

components of the experimental setup to a presentable form, including the software incorporated in this process.

## 2.1  Test Section

The test section consisted of the following materials: circular steel tubing and Swegelock fittings, a variable speed motor and gear pump, a reservoir for the loop coolant, a shell and tube heat exchanger, a mass flow meter, a filter, two analog pressure gauges, a differential pressure transducer, a cold temperature bath, four metering valves, power supply and heat source, fifteen surface thermocouples, the HFHE, and a data acquisition system.

The test loop and its components rest upon a wooden table, with the exception of the reservoir, filter, and flow meter, in order to keep the fluid in a horizontal plane. This allows for the elimination of the change in potential energy throughout the test loop.  The reservoir, filter, and flow meter are all suspended from the tubing from the edges of the table.  Furthermore, to reduce vibrations from the motor/pump causing inaccuracies in the data measurements, rubber mats were placed under the motor/pump, HFHE, and the differential pressure transducer.
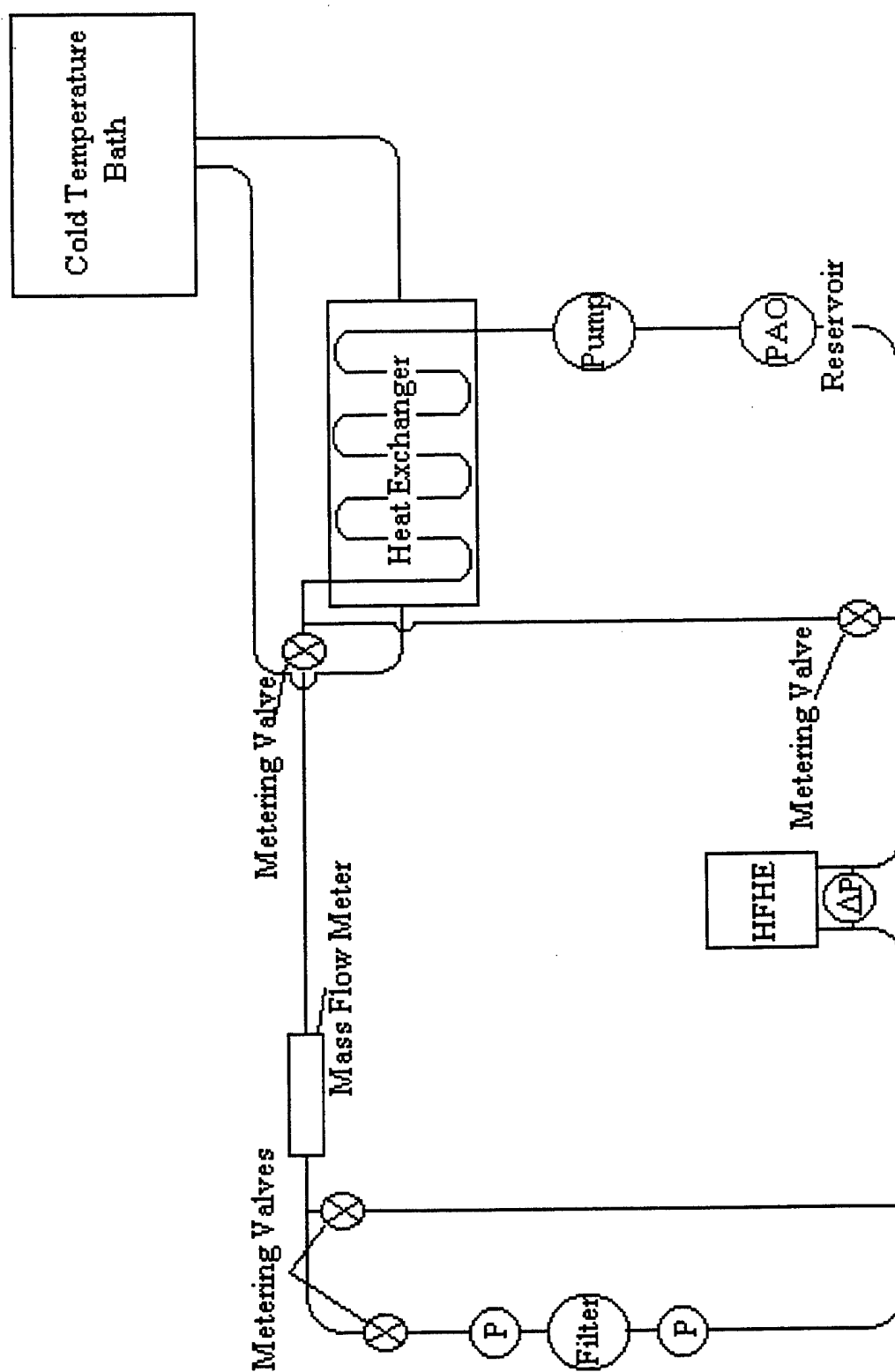
**Figure 2.1. Schematic of the Experimental Apparatus.**

## 2.1.1  Tubing

The test section consisted of seamless 316 stainless steal circular tube with an average inside diameter of 15.850 ± 0.0127 mm (0.624 ± 0.0005 inches) and outside diameter 18.999 ± 0.0127 mm (0.748 ± 0.0005 inches). The connections for the joints of the tubing and the setup components consisted of Swegelock™ compression fittings. The test setup is arranged in a rough rectangular shape. The dimensions of the test setup are 1.8288 m (6 ft) by 1.2192 m (4 ft). These dimensions are adhered to because of the need for a large length to diameter ratio, L/D, for the mass flow meter. Figure 2.2 shows the compression fittings and the individual dimensions of the piping throughout the test loop. Furthermore, because one bypass loop must transverse the heat exchanger, the tubing was bent out of the horizontal plane as shown in Figure 2.3.

## 2.1.2  Pump-motor

The pump-motor combination consisted of a variable speed DC Scott motor magnetically coupled with a gear pump from Tuthill. The coupling for the motor and pump was capable of handling pressures up to 150 psi. The variable speed DC motor allowed for the necessary variation in the
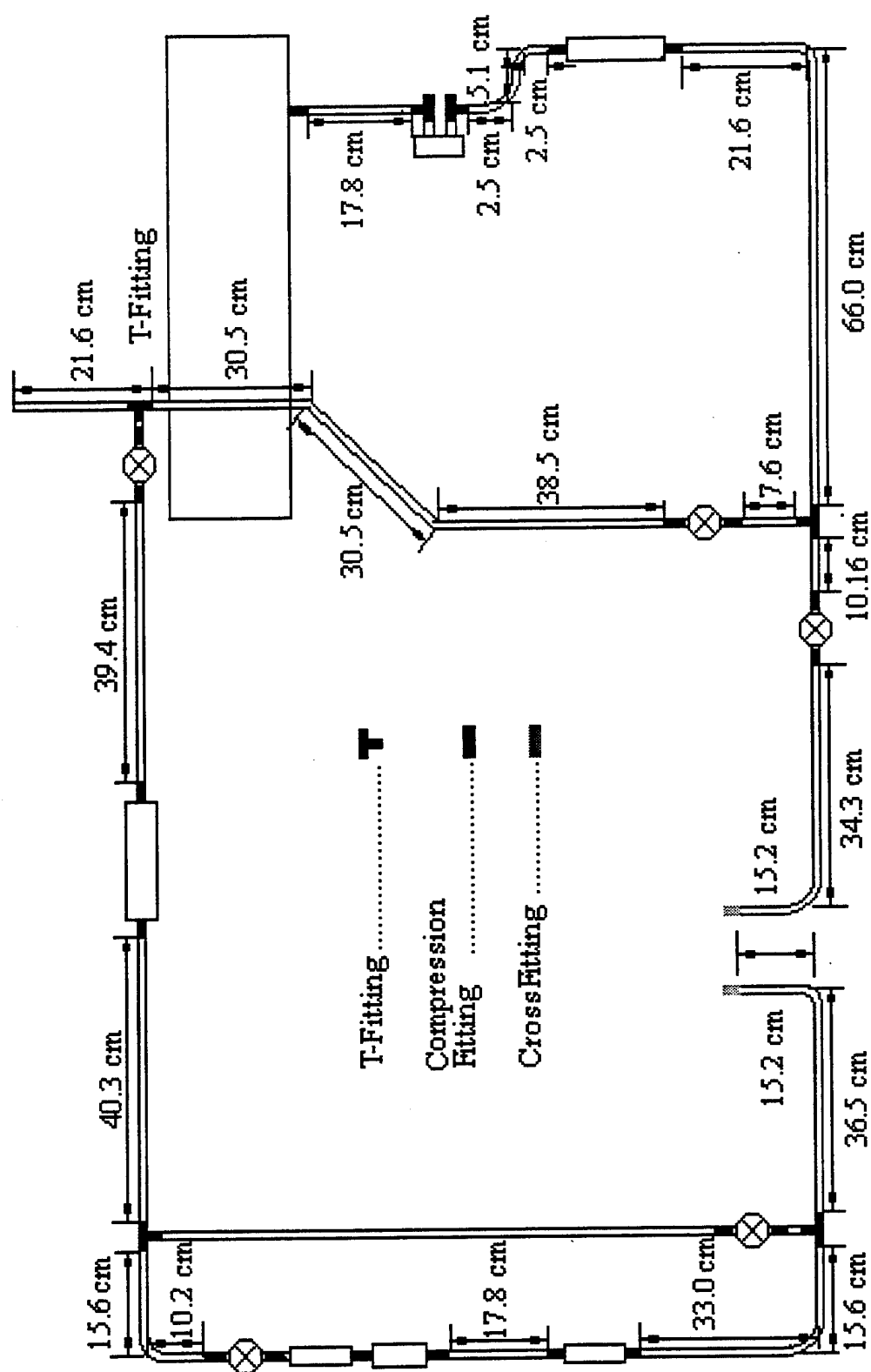
Figure 2.2. Dimensions and Fittings for the Test Loop.
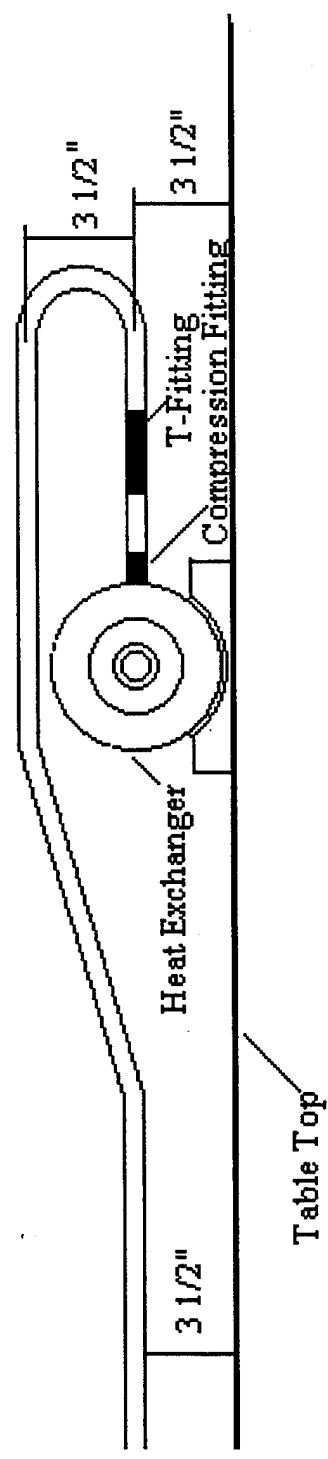
Figure 2.3.  Side View of the Bypass Loop in the Test Section.

range of flow rates analyzed.  The pump-motor was capable of
a range of flow rates from 0.50 to 4.5 kg/min.


### 2.1.3  Reservoir

The reservoir for the test loop coolant consisted of
the shell casing of a large flow rate filter with the
capability of containing two liters of fluid.  Because of
the placement of the reservoir before the pump in the test
loop, the fluid flow was induced flow.  In addition to the
induced flow, the physical design of the filter used for the
reservoir, shown in Figure 2.4, in which the exiting fluid
was from the bottom of the container, allowed for air
pockets to be alleviated from the test loop.

Because of the weight of the reservoir, support must be
provided to alleviate any deflection of the pipe.  For this
support, a wooden block with a cross section of 1 inch by
1 inch was attached to the table top by the use of 3/8 inch
diameter wood screws with a length of 2 inches.  Two 5/8
inch holes were drilled four inches apart through this
wooden block.  A four inch u-bolt was then attached to the
block and secured by two lock nuts.  This support system can
be seen in Figure 2.5.
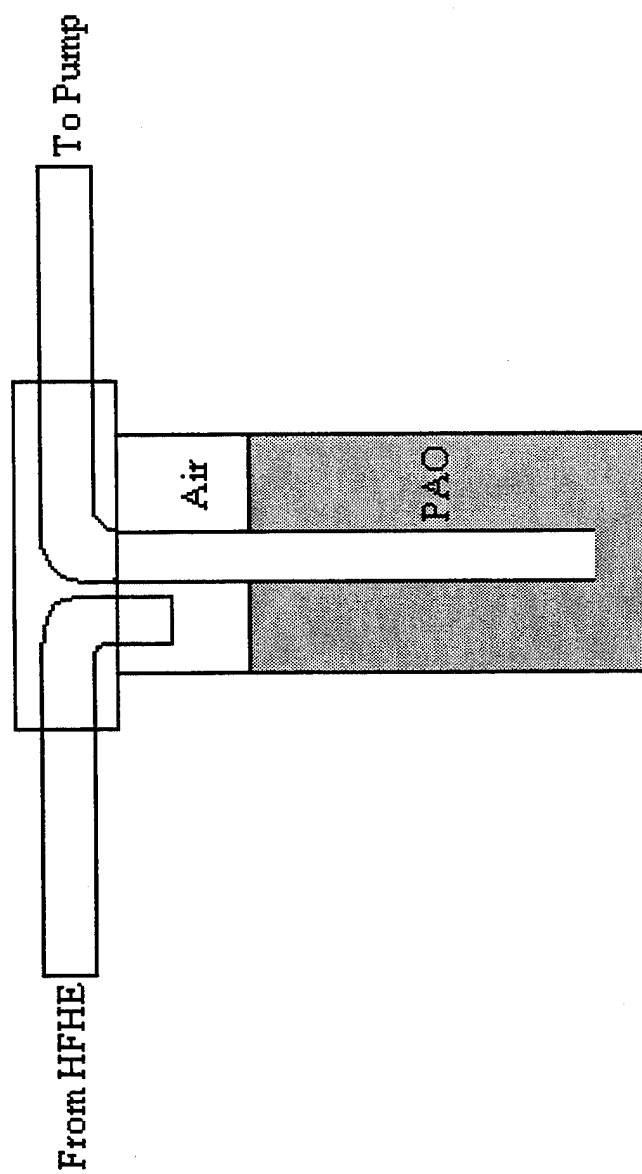
Figure 2.4. PAO Reservoir for the Experimental Setup.

Side View

Coolant Inlet

Table Top

PAO Reservoir

Top View

4" U-bolt

Table Top

Screws

Wooden Block
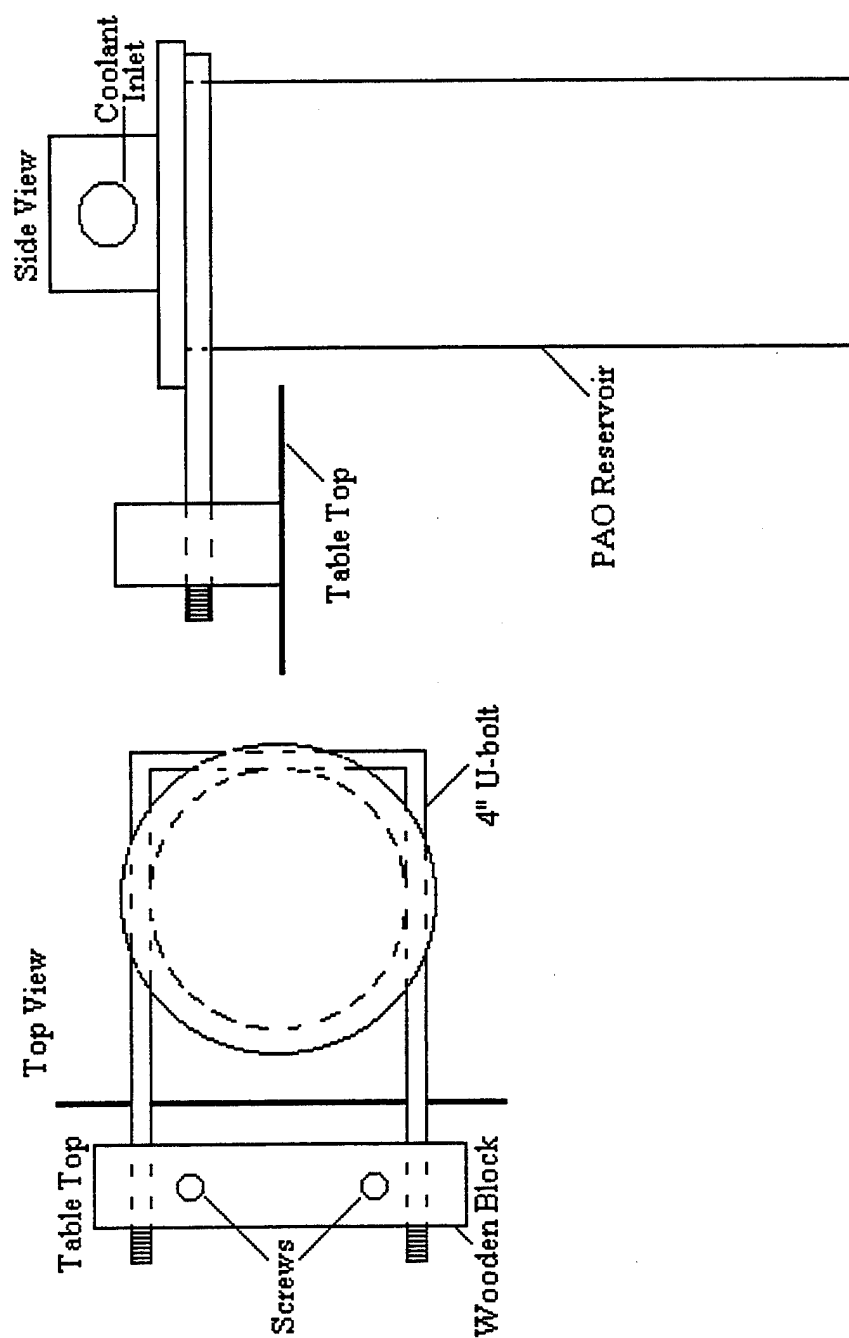
**Figure 2.5.  Support System for the PAO Reservoir.**

## 2.1.4 Heat Exchanger

Because the coolant for the HFHE was required to be
PAO, the test section fluid was also required to be PAO.
However, because this fluid is a light hydraulic oil, it was
deemed that it not be used inside the cold temperature bath.
Therefore, an additional in-loop heat exchanger was needed.
This heat exchanger consisted of a shell and tube counter
flow heat exchanger appropriated from Wright Laboratories.
The purpose of this heat exchanger was to remove the heat
flux added to the PAO from the applied heat load and from
the frictional forces induced by the test loop and its
components.

## 2.1.5 Flow Meter

One of the three dependent variables used for the
spectrum of analysis is the flow rate. Therefore a flow
meter was included into the test loop. The flow meter
consisted of a MicroMotion DS25 mass flow meter that
delivers an output of 4 to 24 mA of current. This current
output was directly monitored by the data acquisition
system. The mass flow meter is capable of a density range
from 0.0 to 5.0 $g/cm^3$, with a minimum span of 0.1 $g/cm^3$ and
a maximum span of 5.0 $g/cm^3$. In addition the flow meter has

a temperature range of -240°C to 450°C with a minimum span of 20°C and a maximum span of 690°C. The flow meter has a turn-on time of 15 seconds and reaches stable operation within 30 minutes.

For the MicroMotion mass flow meter, the flow meter is flagged upward for gases and downward for liquids. Therefore, for the coolant PAO, the mass flow meter must be flagged downward in this test loop. A mass flow meter was chosen, as opposed to a volumetric flow meter, due to dependency of the density of PAO on temperature. A mass flow meter allowed for accurate measurements of the mass flow rate for all operating coolant temperatures.

## 2.1.6  Filter

Because of the relatively small diameter of the orifices in the HFHE, any substantial particulates will clog the passages of the HFHE causing higher pressure losses and reduced flow through some of the impingement jets. This partial loss of flow through the impingement jets will cause unequal cooling throughout the HFHE. Therefore, a 20 micron HYCON filter was used to remove particulates large enough to do damage to the HFHE.

## 2.1.7  Analog Pressure Gauges

Two 250 psi analog pressure gauges were included in the test loop immediately upstream and downstream of the filter to monitor the pressure drop across the filter.  A high pressure drop would indicate that the filter needed to be cleaned.  However, because the test loop is closed to the atmosphere, after a large number of hours of testing, all of the particulates should be filtered out of the test loop and the filter can be removed from the fluid path to reduce the pressure loss in the test loop.

## 2.1.8  Differential Pressure Transducer

One substantial element of the analysis of the HFHE is its hydraulic performance.  This hydraulic performance corresponds to the pressure drop across the HFHE. Therefore, a pressure tap was formed immediately before the inlet and after the exit of the HFHE and connected by a differential pressure transducer.  Both pressure taps were constructed by using a cross fitting with a 0.635 cm (0.25 inches) inside diameter attached vertically into the test section.  The in-line legs of the cross fitting allowed for the flowing coolant, the bottom leg allowed for a thermocouple probe, and the top leg was used as a pressure tap.  These cross fittings are shown in Figure 2.6.  Vinyl

tubing with an inner diameter of 0.635 cm (0.25 inches) was used to connect the pressure tap and the pressure transducer.   A Validyne P305D-50 wet-wet pressure transducer provided the pressure drop measurements with an output of ± 5.0 V at 0.5 mA and a pressure range of  0-861.75 kPa (0-125 psi) with a possible overpressure of 200% of full scale with less than a 0.5% zero shift.   The P305D is a differential pressure transducer with symmetrical pressure cavities of stainless steel.   Fluid pressures act directly on a central diaphragm in a balanced variable reluctance design which eliminates the need for internal isolation fluids.   The transducer diaphragm is replaceable. The transducer has an accuracy of ± 0.25% of full scale including linearity, hysteresis, and repeatability.   In addition, the transducer is capable of an operating temperature range of -53.89°C (-65°F) to 121.11°C (250°F).

## 2.1.9  Cold Temperature Bath

The second of the three dependent values that was used for the spectrum of tests was the inlet coolant temperature. Therefore, a cold temperature bath was included into the test loop via the heat exchanger.   The cold temperature
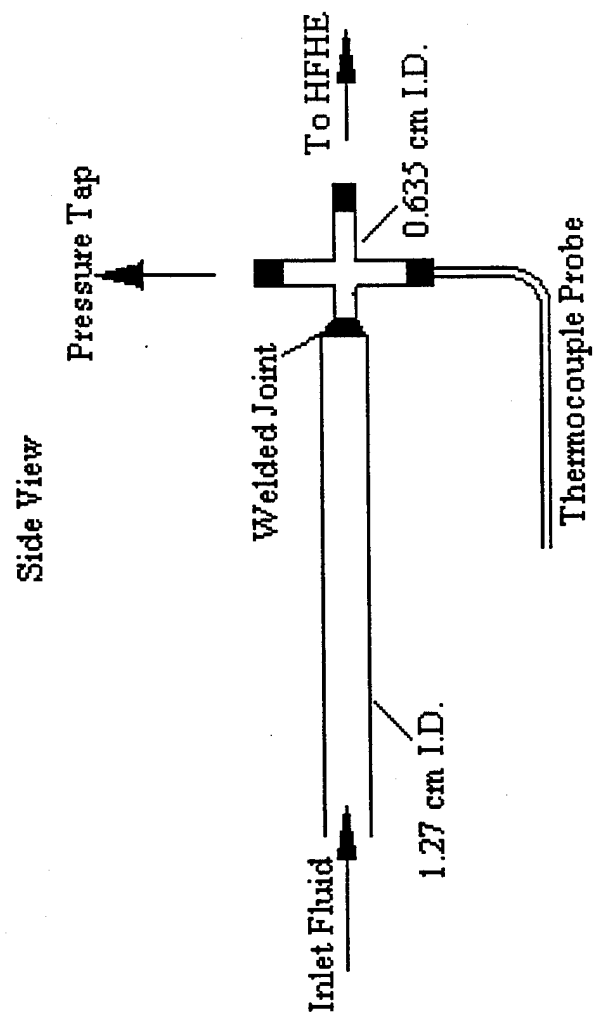
Figure 2.6. Cross Fitting for the Inlet and Outlet of the HFHE.

bath, a RC-50LT with the deluxe control package, was selected from FTS Systems because of its capability of holding the bath fluid temperature constant from -40 °C to 75 °C. This increased range was necessary to hold the PAO temperature constant from -15 °C to 50 °C. The losses in temperature are due to the inefficiencies of the heat exchanger. Three-eighths inch vinyl tubing was used to complete the secondary cooling loop with the heat exchanger. The coolant used, HT-30 silicone oil heat transfer fluid, remained in liquid state well beyond the range of temperatures resulting from the temperature bath, and was purchased from FTS Systems.

## 2.1.10  Metering Valves

The test loop configuration contains two sets of metering valves. The first set of valves are for the filter. During the initial hours of testing, the filter needs to be part of the test loop to remove any particulates from the fluid. However, because the test setup is a closed loop, the filter becomes unnecessary after the initial hours of testing are complete. Therefore, the additional loss of pressure from the filter can be removed by taking the filter out of the test loop. This removal of

pressure losses decreases the burden on the motor by
allowing the pump to operate at a lower pressure.  The
second set of metering valves were used for the modeling of
the hydraulic startup of the HFHE.  Because the PAO is
cooled by the HT-30 fluid in the heat exchanger, the PAO
must have an actual flow rate to achieve any cooling.
Therefore, to achieve the low temperatures the motor-pump
must be operating.  However, to test the start-up
capabilities of the HFHE, the test must begin with no flow
rate through the HFHE.  Therefore, to accommodate both the
cooling of the PAO and zero flow rate through the HFHE, a
set of metering valves are used to separate the
refrigeration cycle of the PAO from the rest of the test
setup.


## 2.1.11   Heat Source

The last dependent variable used for the spectrum of
tests is the applied heat load.  Therefore, the test setup
must include a power source and heat source for the HFHE
capable of handling a heat flux of 100 W/cm$^2$.  This high
heat flux eliminates most conventional heat sources.
Therefore, McDonnell Douglas developed a heat flux
amplifier, similar to the one used by Grote, et al. [6].  The
heat flux amplifier is designed to increase the contact

surface from 1.0 cm$^2$ to 40.3 cm$^2$. Therefore, a low heat flux heating element can be used to produce a high heat flux at the amplifier/HFHE interface.

This amplifier is shown in Figure 2.7. The lower 1.3 cm of the amplifier has a constant area of 1.0 cm$^2$. In this section, there are three parallel planes of thermocouples spaced 0.25 cm apart. Eight thermocouples were placed in each of the three planes of the constant cross-sectional area "neck" of the amplifier. These thermocouples were 36 gage type T, copper/constantan, from Omega. A 0.5 mm diameter hole was drilled 0.5 mm deep at each thermocouple location. The thermocouple bead was peened into each hole. A hole was also drilled to the center of each plane, and each thermocouple was covered with Ecco-Bond 56C epoxy and inserted. The other thermocouples were also bonded with epoxy and their leads secured with Kapton tape. The ninth temperature in each plane was extrapolated during the data reduction process. The temperature at the amplifier/HFHE interface plane A, from Figure 2.7, will be calculated by projecting the temperatures in planes "B", "C", and "D" using a linear least squares fit. This technique provides very accurate temperature estimates at the interface correlating with the measured temperature in the HFHE wall.

To provide the actual heat source for the steady-state thermal tests, a Minco mica heater, 5.08 cm (2 inches) in diameter, with a resistance of 19 ohms was used as the heat source. For the transient thermal tests a 32 ohm MiniSystems thick filmed resistor was used. A Variac was used to regulate the AC wall voltage for the mica heater. The voltage output of the Variac and the amperage, measured by a current shunt, was sent directly to the data acquisition system.

## 2.1.12   Thermocouples

In addition to the 24 thermocouples that are located in the heat flux amplifier, the experimental setup contains fifteen more surface thermocouples and two thermocouple probes. The surface thermocouples consist of Omega 30 gage type T (copper/constantan) thermocouples. These thermocouples are necessary to both measure the wall temperature of the High Flux Heat Exchanger and estimate the radial heat loss due to conduction through the HFHE. This radial heat loss is caused by the simplification of applying a heat load to one CHIC at a time. When only one heat load is applied, heat is lost to the surrounding CHICs. Therefore, the actual heat flux through the tested CHIC is less than the heat load applied. Hence, it is necessary to
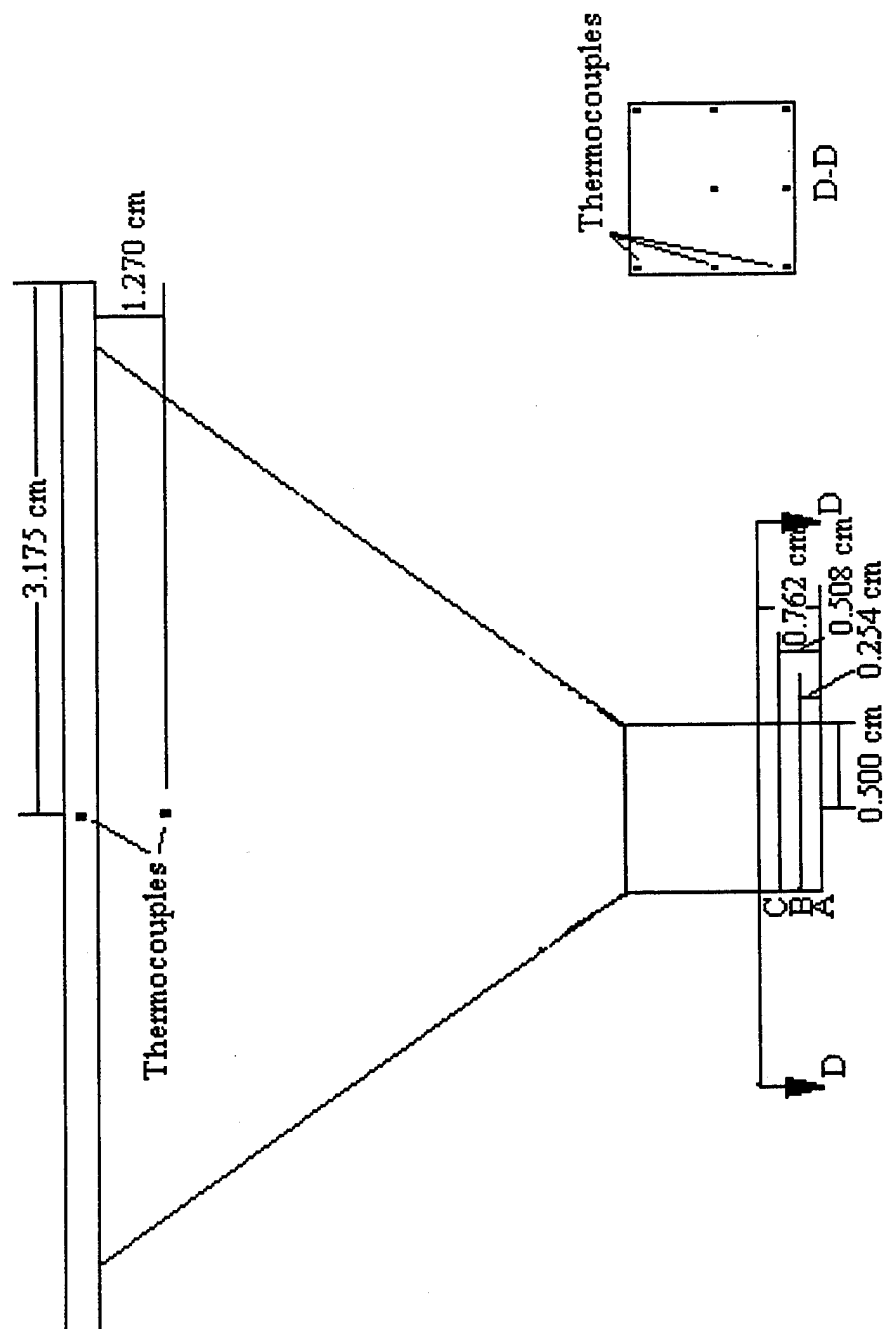
Figure 2.7. Heat Flux Amplifier.

estimate the difference in heat flux.  To obtain this difference, the wall temperature profile must be calculated.

Therefore, the thermocouples are placed on the HFHE surface using Omega's Omegabond 101.  This bond is a high heat conducting epoxy used to temporarily cement the thermocouples onto the HFHE.  This placement can be seen in Figure 2.8.  For the thermocouple underneath the amplifier, a groove was made in the HFHE for each CHIC.  The groove consisted of a channel cut 0.05 cm deep and 0.6 cm long. This length of channel allows for the placement of the thermocouple wire under the amplifier.  The channel does not reach the center of the CHIC footprint; however, the heat flux should be uniform across the entire surface area of the footprint.  Therefore, the wall temperature should also be uniform across the entire surface of the CHIC footprint. The channel cut was made with a 1/16 inch  router bit.

The thermocouple probes consisted of a type T Cole-Parmer general-purpose temperature probe.  These 0.3175 cm (0.125 inch) diameter, 20.32 cm (8 inch) long probes consisted of 316 stainless steel with a maximum temperature of 399°C (750°F) and a time constant of 10 seconds.  These probes were placed at the inlet and outlet of the HFHE, shown in Figure 2.6.  The temperature probes are placed into
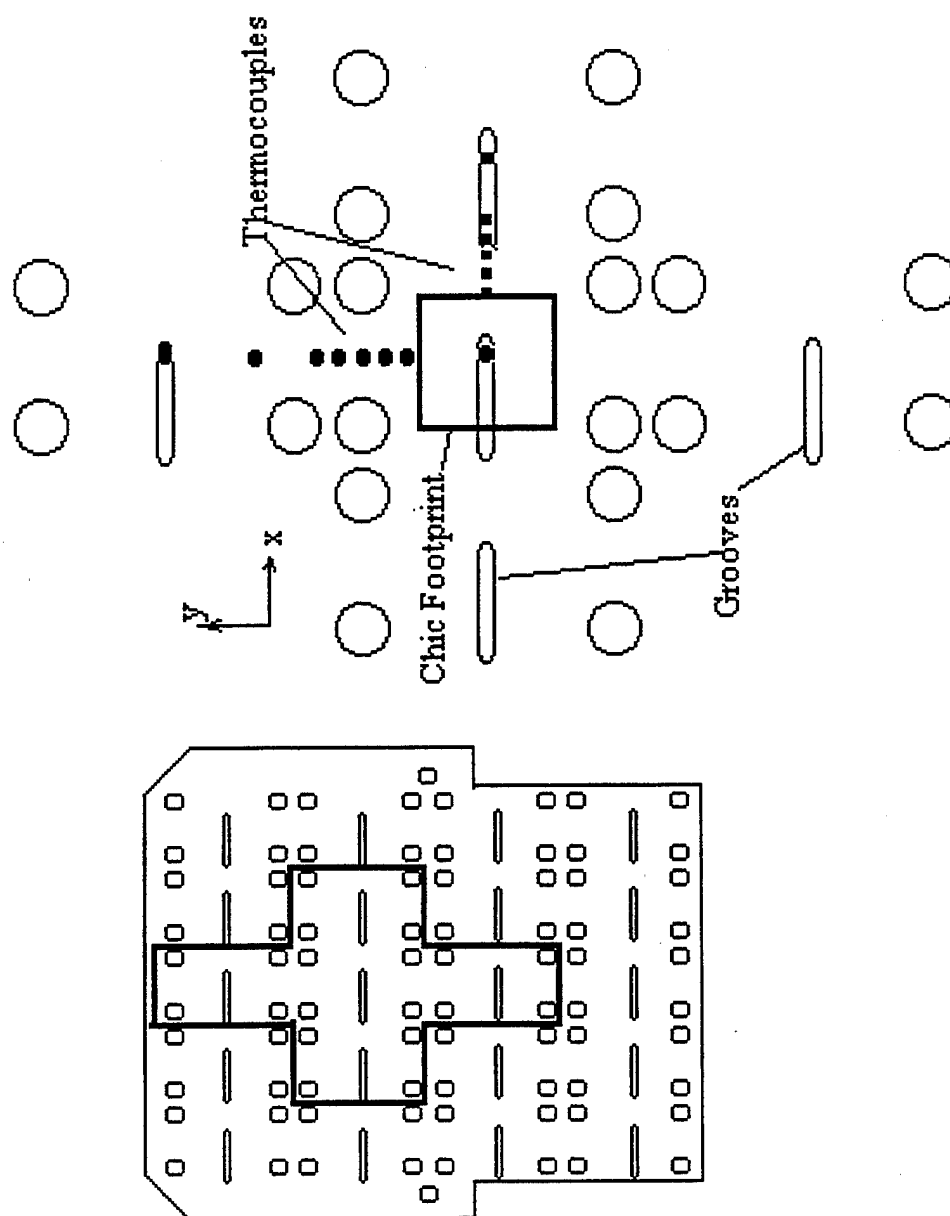
Figure 2.8. Placement of the Surface Thermocouples.

the cross fitting, to where 0.3175 cm (0.125 inch) of the

probe extends into the fluid flow, thereby ensuring

sufficient immersion into the fluid without causing a large

obstruction of the flow.  The inlet and outlet temperature

measurements are necessary for varying the coolant

temperature and heat addition to the fluid, respectively.

## 2.1.13  Securing Plate

To guarantee sufficient contact pressure between the

amplifier and the CHIC surface, the amplifier was bolted

onto the HFHE.  This was accomplished by four 1/4 inch bolts

and a securing plate.  The plate consisted of an aluminum

sheet 6.35 cm (2.5 inch) by 6.35 cm (2.5 inch) with 0.9525

cm (0.375 inch) holes designed to align with the amplifier

holes and the HFHE.  In addition, a 1.905 cm (0.75 inch)

notch was made to keep from damaging the lead of the mica

heater under compression.  This securing plate can be seen

in Figure 2.9.  In addition, thermal grease was applied to

the amplifier and HFHE interface.

## 2.1.14  High Flux Heat Exchanger

The High Flux Heat Exchanger, HFHE, originally was

designed to consist of a copper alloy insert into a

stainless steel header-frame.  The outer dimensions of the
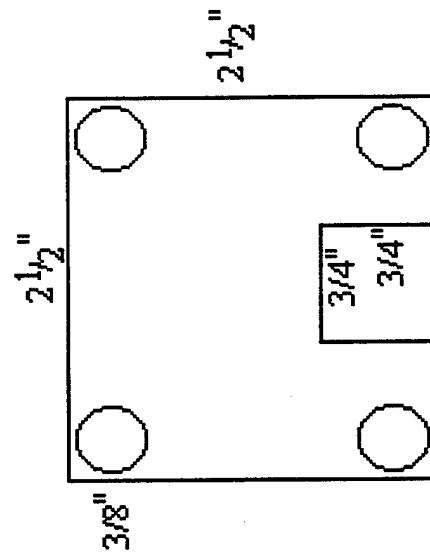
**Figure 2.9. Configuration of the Securing Plate.**

header-frame was required to meet SEM-E, Standard Electronics Module, Type E, specification, or 15 cm by 17 cm.  Because a SEM-E size liquid flow-through module was recently developed under a separate Air Force program, McDonnell Douglas and the maker of the module, Lockhart Industries, Inc., combined to modify the SEM-E liquid cooled module (part number 101456, shown in Figure 2.10) by blocking the normal active flow zone and instead porting the flow into a flush-mounted removable CHIC plate.  The porting locations and sizes are shown in Figure 2.11.  Because the Lockhart module is fabricated from aluminum alloy, a departure from the original design was necessary.

The overall assembly of the HFHE consists of two principal components: an aluminum header-frame and a copper insert which contains the twenty high flux cooling locations.  The header and the insert are then bolted together.  The entire assembly measures 14.9 cm by 15.6 cm, with a total thickness of 1.52 cm.  The copper insert contains the CHIC coolers, and the aluminum frame adds stiffness to the overall assembly and extends the outer dimensions to SEM-E specifications. To seal the copper insert and header-frame a VITON-A gasket seal was used.  The copper insert contains twenty CHIC coolers arranged in a four-by-five array and coolant distribution channels in an
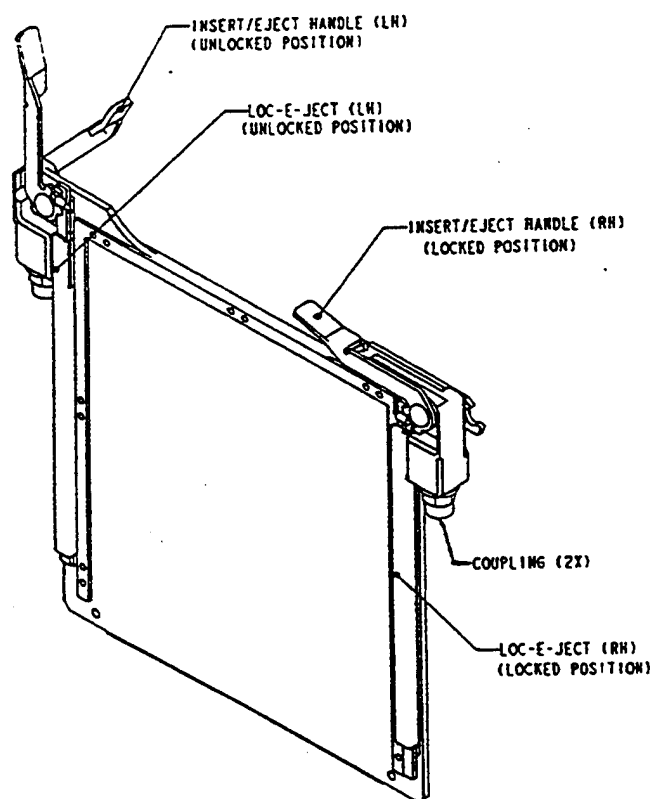
Figure 2.10. Modification to the SEM-E Module.
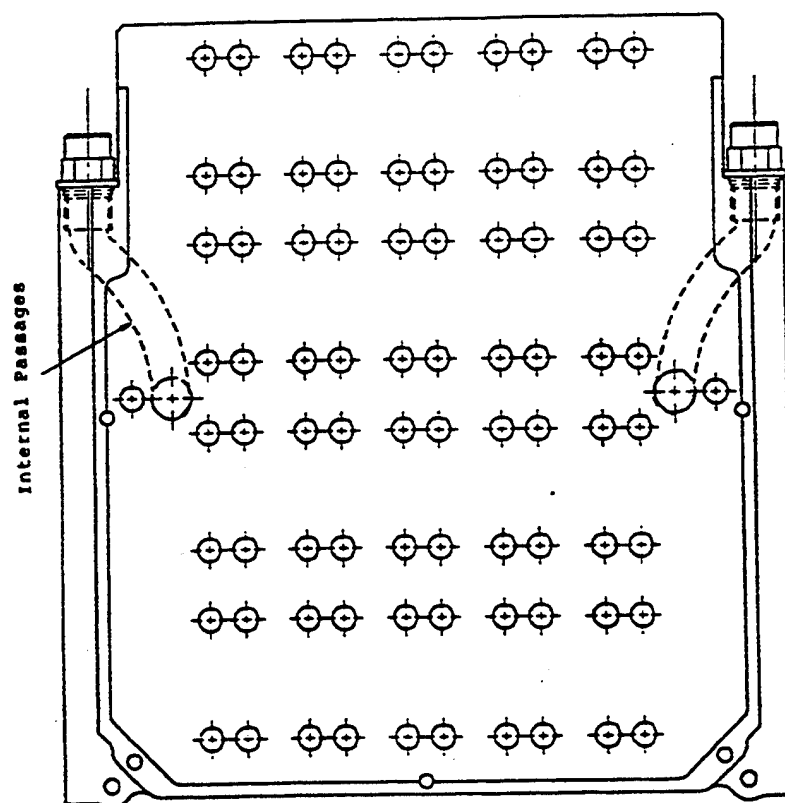
Figure 2.11.  Porting Locations and Sizes.

integral structure. It was formed by stacking 24 photo-etched copper alloy laminates, each of 0.010 or 0.038 cm thickness, and diffusion bonding them to create a platelet heat exchanger. Total thickness of the insert is 0.467 cm. The alloy is CDA 15100 (copper, 0.10% zirconium). The module is designed for single-sided heat application. Each CHIC cools a surface area of 1.0 $cm^2$, contains nine orifice plates, and sixty holes per plate arranged in three parallel slots, and is fed coolant in parallel.

The HFHE design and performance requirements were based on a maximum local heat flux of 100 $W/cm^2$ (steady or transient) for each 1 $cm^2$ CHIC surface area and 1.0 $W/cm^2$ heat flux over the remaining 180 $cm^2$ for a total heat flux capability of 2180 W. In addition, the HFHE designs were based on a maximum junction temperature of 90°C, and PAO as the liquid coolant. Other constraints included a lower limit on the coolant supply temperature (0°C), an upper limit on the flow rate (1000 kg/hr), and pressure drop (690 kPa for a cold start and 311 kPa at the design point). The HFHE consists of a set of bonded laminates using 8 different types of plates and a total of 24 plates. Appendix B shows each type of plate as well as the configuration of the bonded plates for the HFHE tested. Depending on the number of orifice plates that are used, the thermal performance,

cost , heat exchanger thickness, and pressure drop vary. Therefore, the results shown in chapter III are dependent on the stacking of the individual plates.

## 2.1.15   Data Acquisition

The final component of the test loop is the data acquisition system.  This system consists of two parts, the data logger and a personal computer.  The Fluke 1703 data logger was capable of containing individual programs to record the different data needed by the separate tests. These programs require no computer programming.  Instead, the Fluke programs consist of listing the channels to be recorded, indicating the name and units for each channel, and calculating any pseudochannel (channel 82 (Wattage) = channel 81 (voltage) x channel 82 (amperage)).  In addition, the programs include the mode of recording (a time interval scan of the channels or continuous scan of the channels) and the device for the output file (a printed output or disk file).  All of these parameters of the Fluke program are prompted by the Fluke.  The output of the Fluke program consists of an ASCII data file.  This data file is then input into a DOS data reduction routine on a Pentium-60 personal computer.  Finally, all of the final calculations were made with the use of Microsoft Excel and MathCad.

## 2.2  Experimental Calibrations

Upon the completion of the experimental setup construction, calibrations of all the data processing equipment were performed.  The following sections outline the details of the calibrations for the cold temperature bath, the thermocouples, the mass flow meter, and the differential pressure transducer.

### 2.2.1  Cold Temperature Bath

The calibration procedure for the FTS Systems RC50 recirculating cooler is defined in the operating manual. To calibrate the cold bath a previously calibrated temperature indicator and a heater must be present.  The calibration setup is then as follows:

- A "short circuit" hose is placed between the fluid inlet and outlet to provide a short fluid path which introduces minimal heat to the process.

- The temperature standard sensor, provided by FTS Systems, is placed in the reservoir inside the fluid return tube. Place the sensor between 2 inches and 4 inches into the tube.

- On larger systems the cooling system may be difficult to stabilize without a heat load.  This is due to the high

refrigeration capacity of the equipment causing extreme drops in temperature when activated.

- To eliminate this problem, a heater rated at 50% of the heat removal capacity of the system at 0°C may be immersed in the reservoir and energized. This will provide a load to stabilize the temperature.

After the setup is completed, the actual calibration is performed by the following:

- While turning on the power to the unit, dress the O/I (off/on) button.

- The SP (set point) prompt and present SP will appear on the display. Adjust the SP to 0.0 and press enter (O/I) button.

- By setting the SP to 0.0 the RC (recirculating cooler) will attempt to cool to 0.0°C. Allow the system to stabilize at zero (wait at least 15 minutes to allow electronics to stabilize). Once the O/I button is pressed the display will begin to alternate between "C oS" (cal offset) and the process temperature. At any time while the "C oS" is displayed, the up/down buttons will adjust the measured process temperature up and down, approximately 0.1 degree per step. Adjust the reading to match the temperature standard.

- After the zero has been adjusted, press the O/I button again and the SP prompt will return. The span may be adjusted either using a low temperature or using a high temperature.

Once the zero temperature has been established, the cold bath calibration is performed for low temperatures and high temperatures separately. For the calibration at low temperatures the following procedure was followed:

- If a heater was added for the zeroing procedure it must be removed. Wait for the temperature to stabilize at its maximum low temperature. (Caution, the fluid being used must be pumpable at the maximum low temperature.) Because the thermocouples will be calibrated to -20°C, the cold bath was calibrated to -30°C.

- Adjust the setpoint to it's minimum setting and then press O/I again. The "C Gn" prompt will appear. When the temperature stabilizes adjust the temperature to read the same as your calibration device.

- When complete press O/I. The prompt "rFC" (restore factory calibration?) appears. If the user calibration was unsuccessful then you will want to restore the factory calibration. To save the adjust calibration

answer 0 (no), to restore factory calibration answer 1 (yes) and press O/I.

- The "Fin?" (finished) prompt will appear. If you are finished answer (yes) and press O/I. In not, entering 0 will loop back to the beginning and start over.

To calibrate the cold bath for high temperatures, the following procedure was performed:

- A heater is required to heat the unit up to it's maximum temperature. If the RC is supplied without heat, an external heater must be added to the reservoir. (Caution, the fluid being used must be pumpable at the maximum temperature and must not be flammable.)

- Adjust the setpoint to it's minimum setting and then press O/I again. The "C Gn" prompt will appear. When the temperature stabilizes adjust the temperature to read the same as your calibration device.

- When complete press O/I. The prompt "rFC" (restore factory calibration?) appears. If the user calibration was unsuccessful then you will want to restore the factory calibration. To save the adjust calibration answer 0 (no), to restore factory calibration answer 1 (yes) and press O/I.

- The "Fin?" (finished) prompt will appear. If you are finished answer (yes) and press O/I. In not, entering 0 will loop back to the beginning and start over.

## 2.2.2  Thermocouples

For all of the thermocouples, including the surface thermocouples, amplifier thermocouples, and temperature probes, the calibration usually consists of three data points. However, because of the difficulty in reaching known steady state temperatures, the thermocouples can usually be calibrated by submersing the thermocouples in ice water, (0°C), using room temperature (25°C), and submersing the thermocouples in boiling water (100°C). However, after the calibration of the cold temperature bath is completed, the cold bath can be used to calibrate the thermocouples. Moreover, because the cold temperature bath was selected to provide the temperature range necessary to complete the experimental tests, the cold temperature bath is capable of providing a suitable temperature range for the calibration of the thermocouples. Therefore, the thermocouples were submersed in the cold temperature bath at steady state temperatures between -20°C and 60°C at an interval of 10°C. As a reference temperature guide, an Omega Platinum DP50

temperature gage was used to correlate the temperature
reading of the cold temperature bath. Both the temperature
gage and the cold temperature bath were capable of output
readings of tenths of a degree Celsius. The output reading
of the submersed thermocouples were taken from the Fluke
data processor. Finally, a calibration curve was obtained
by using least squares in a linear regression. A typical
calibration curve is shown for surface thermocouple 15 in
Equation (2.1).

$$T_{act} = 1.009 T_{meas} - 0.6048 \qquad\qquad (2.1)$$

A complete listing of the calibration curves can be seen in
Appendix C. Because the thermocouples yield data directly,
the uncertainty results from only two factors. The first
factor is the uncertainty from the thermocouple itself.
From Omega's catalog, the type T (copper/constantan)
thermocouple, between -20°C and 60°C, has an accuracy of
±0.5°C. However, when calibrating the thermocouples, it was
evident that the thermocouples had an accuracy of ±0.1°C.
The second factor comes from any non-linearity of the curve
fit. However, as can be seen from Figure 2.12, when the
uncertainty of the thermocouple is factored into the
calibration curve, each data point fits within the

confidence interval. Therefore, it can be assumed that the thermocouples have an uncertainty of ±0.1°C.

The curve fitted data for this thermocouple, surface thermocouple 15, has a standard deviation of 0.044 and a maximum error of -0.09°C (at -20°C) from the actual temperature. Both the standard deviation and the maximum error are typical of the calibrations of all of the thermocouples. The standard deviations and the maximum errors for the remaining thermocouples can also be found in Appendix C.

## 2.2.3 Mass Flow Meter

For calibration of the flow meter, a "bucket and stopwatch" approach was used. First, the test setup was modified by removing the HFHE, leaving an open loop, seen in Figure 2.13. Next, the time to fill a 500 ml graduated cylinder was measured for flow rates ranging from 0.7 kg/min to 4.0 kg/min. This data combined with the density of the PAO was charted, and a linear curve fit was performed. These can be seen in Figure 2.14. However, no measurements are 100% accurate; therefore, an error analysis for both the "bucket and stopwatch" approach and the measured flow was performed. An example of the methodology is as follows:

$$T_{act}=1.0009*T_{meas}-0.6048$$

Measured Temperature (C)
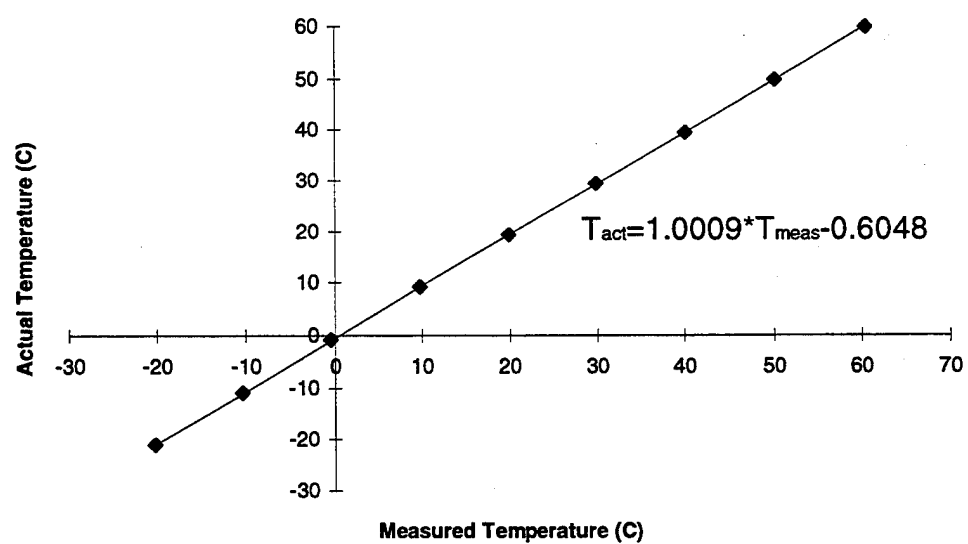
**Figure 2.12. Typical Thermocouple Calibration Curve.**

For the "bucket and stopwatch" approach, the equation for the mass flow rate is:

$$\dot{m} = \frac{\rho v}{time} \qquad (2.2)$$

Next, the uncertainty factor is calculated by the following equation:

$$\varepsilon_{\dot{m}} = \left[ \left( \frac{\partial \dot{m}}{\partial \rho} \varepsilon_\rho \right)^2 + \left( \frac{\partial \dot{m}}{\partial t} \varepsilon_t \right)^2 + \left( \frac{\partial \dot{m}}{\partial v} \varepsilon_v \right)^2 \right]^{\frac{1}{2}} \qquad (2.3)$$

Performing the partial derivatives for each independent variable, dividing by the mass flow rate, and multiplying by 100 to get the percentage yields:

$$\frac{\varepsilon_{\dot{m}}}{\dot{m}} = 100 \times \left[ \left( \frac{\varepsilon_\rho}{\rho} \right)^2 + \left( \frac{\varepsilon_v}{v} \right)^2 + \left( \frac{\varepsilon_t}{t} \right)^2 \right]^{\frac{1}{2}} \qquad (2.4)$$

Next, determine the uncertainty factors for each independent variable.

- The density is calculated as a function of the temperature of the PAO. This function and its'
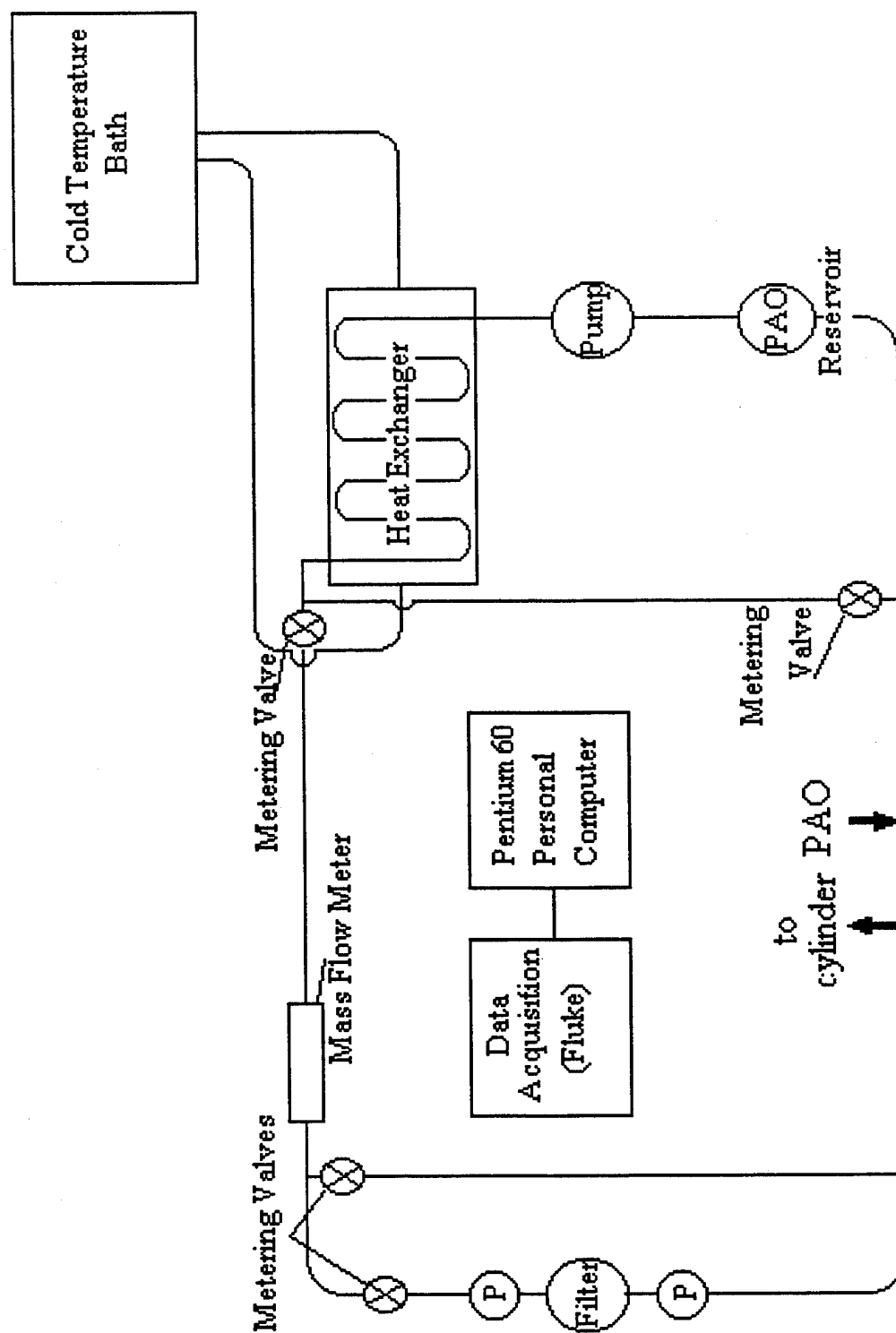
Figure 2.13. Schematic of the Mass Flow Rate Calibration.

uncertainty factor is given by Ghajar [10]. This curve fitted equation for the density has a maximum deviation of less than ±0.5%. For the flow rate measurements, the coolant temperature was room temperature, 25°C. Therefore, then density of the PAO was 0.792 kg/L. A 0.5% deviation from this value represents an uncertainty factor of ± 0.004 kg/L.

- The graduated cylinder used in the measurements consisted of increments of 5 ml. Therefore, the uncertainty of the volume is one half of the smallest increment or 2.5 ml.

- The time was measured with a stopwatch with an increment of 0.01 seconds. However, after many tests, it was concluded that the smallest increment of time that could accurately be measured was 0.25 seconds. Therefore, half of the smallest increment translates to an uncertainty of 0.125 seconds.

Finally, substitute the uncertainty factors and the following independent variables values to achieve a maximum uncertainty into Equation (2.4)

$$\rho = 0.79 \text{ kg/L}$$

$$v = 450 \text{ ml}$$

$$t = 6.5 \text{ s}$$

61

This yields an uncertainty factor for the measured mass flow rate of 4.09%.

For the error analysis on the flow meter itself, we must look at the fluctuations and perform a least squares analysis for each flow rate. The equation for the least squares analysis is as follows:

$$\varepsilon = \sqrt{\frac{1}{n}\sum_{i=1}^{n}\left[(x_i)_{meas} - (x_i)_{act}\right]^2} \qquad (2.5)$$

Where i is the individual data point and the sum is taken from i = 1 to i = n and x is an individual data point. At a flow rate of 2.5 kg/min, this analysis yields an error of 0.009517 kg/min.

## 2.2.4  Differential Pressure Transducer

The next data gathering component of the test setup in need of calibration was the differential pressure transducer from Validyne, (Validyne P305D-50) capable of differential pressures up to 125 psi. For the calibration of the pressure transducer, the procedure must be performed in two steps. The two step procedure is necessary due to the large range of possible pressures. The first step, for the low pressures, was performed by using a Dwyer 60-0-60 inch

The graph shows Measured Mass Flow Rate (kg/min) versus Flow Meter Output (mA) with the text:

"Conversion from Flow Meter Output to Mass Flow Rate: $\dot{m} = 0.2406(mA)$-"
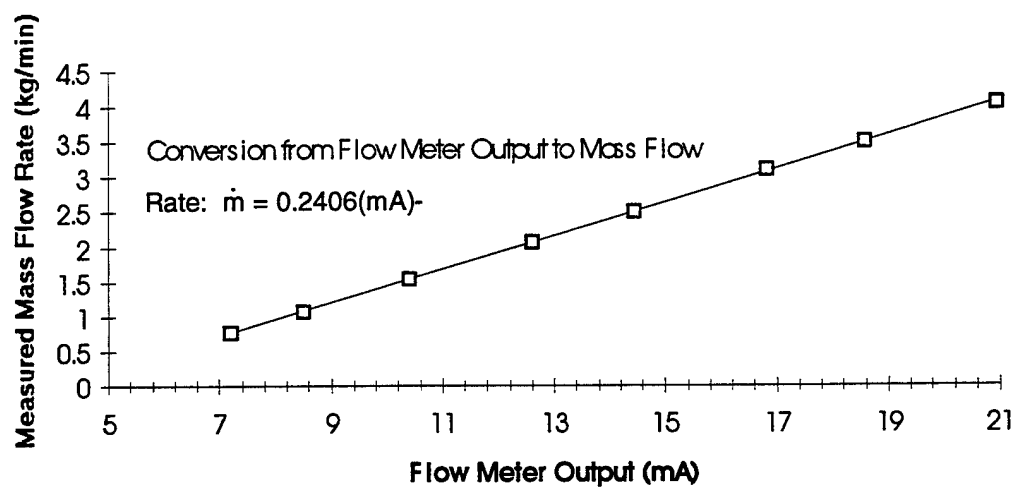
**Figure 2.14.** **Mass Flow Meter Calibration Curve.**

mercury U-tube manometer and compressed air. The test configuration consisted of an input of compressed air into the calibration system, which then branched off to the manometer and the pressure transducer, this system is seen in Figure 2.15. However this method only completed the 0-50 psi range of the transducer.

For the upper end of the scale, a dead-weight tester was used. The dead-weight tester, shown in Figure 2.16, is set up for calibration of the pressure gage G. The chamber and cylinder of the tester are filled with a clean oil by first moving the plunger to its most forward position and then slowly withdrawing it while the oil is poured in through the opening for the piston. The gage to be tested is installed and the piston inserted in the cylinder. The pressure exerted on the fluid by the piston is now transmitted to the gage when the valve is opened. This pressure may be varied by adding weights to the piston or by using different piston-cylinder combinations of varying areas. The viscous friction between the piston and the cylinder in the axial direction may be substantially reduced by rotating the piston-weight assembly while the measurement is taken. As the pressure is increased, it may be necessary to advance the plunger to account for the compression of the oil and any entrapped gases in the apparatus. High-pressure
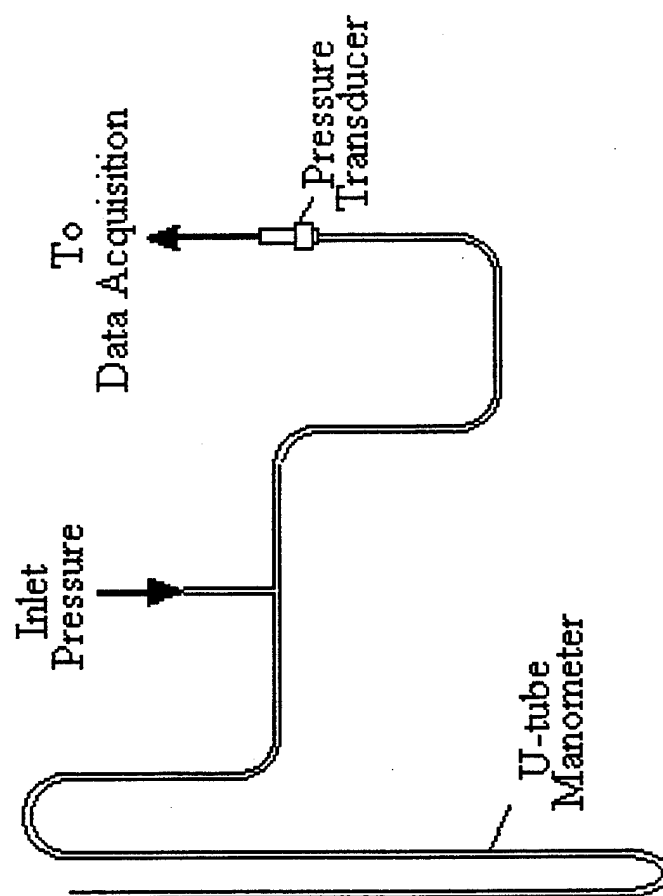
Figure 2.15. Schematic of the Pressure Transducer Calibration.
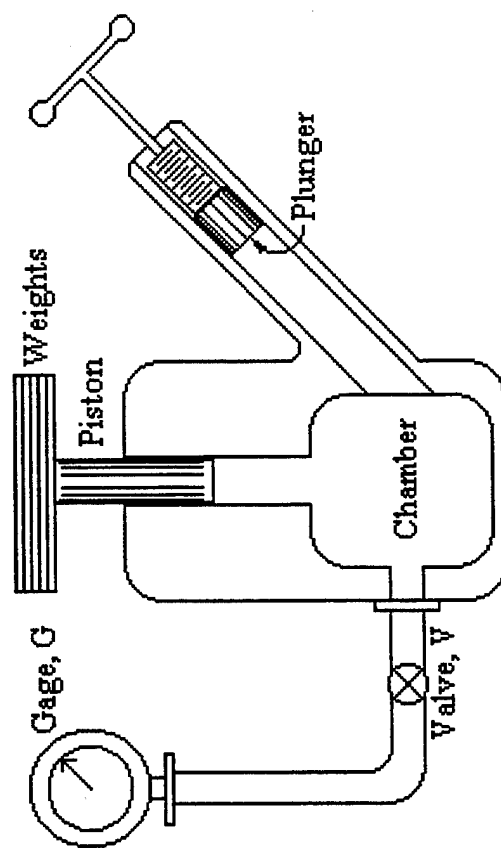
Figure 2.16.  Schematic of a Dead-Weight Tester.

dead-weight testers have a special lever system which is used to apply large forces to the piston.

The result of this calibration is shown in Figure 2.17, as a plot of the output of the transducer in Volts versus the measured pressure in pounds per square inch.

An error analysis was performed for the pressure transducer. The accuracy of dead-weight testers are limited by two factors: (1) the friction between the cylinder and the piston and (2) the uncertainty in the area of the piston. The friction is reduced by rotation of the piston and use of long enough surfaces to ensure negligible flow of oil through the annular space between the piston and the cylinder. The area upon which the weight acts is not the area of the piston nor the area of the cylinder; it is some effective area between these two which depends on the clearance spacing and the viscosity of the oil. The smaller the clearance, the more closely the effective area will approximate the cross-sectional area of the piston. The percent error due to the clearance varies according to the following equation:

$$\% \, error \propto \frac{(\rho \Delta p)^{1/2} b^3}{\mu d l} \tag{2.6}$$

Where the density (ρ) and the viscosity (μ) refer to the

oil, the diameter (d) and length (l) refer to the piston, b

is the clearance spacing, and the pressure differential

(Δp) is the difference of pressure across the cylinder.

Therefore, to obtain the error associated with the dead-

weight tester, the same uncertainty approach described

earlier is used.  The result of this analysis is that the

maximum percent error for the dead-weight tester is

approximately 0.5%, and occurs at a pressure differential of

100 psi.  This translates to a maximum uncertainty of 0.5

psi.

For the manometer, the final data consisted of

multiplying the measured change in mercury heights by a

constant resulting from the change in units.  Therefore,

this error is straightforward and no complicated error

analysis needs to be performed.  However, a least squares

analysis is still required for the transducer output.

- For the pressures using the manometer:

    The manometer is calibrated in increments of 0.1 inch

    of mercury.  Therefore, the uncertainty of the reading

    is one half the smallest increment, or 0.05 inch of

    mercury.  However, when using an U-tube manometer, a

    reading must be taken on both sides; therefore, the

    total uncertainty is sum of the individual

uncertainties, or 0.1 in. of mercury. Converting this into psi yields an uncertainty of 0.049 psi.

- For pressures using the pressure transducer:

  Because the differential pressure is measured by a pressure transducer whose output consists of an electrical signal, voltage, to the Fluke, some error will occur as this signal fluctuates. Therefore, for the error analysis on the pressure transducer itself, we must look at the fluctuations and perform a least squares analysis for each pressure measurement. This least squares analysis is the same used for the mass flow meter calibration and can be seen in Equation (2.5). The maximum error for the fluctuations occurs for the pressure measurement of 26.4 psi. The corresponding least squares analysis yields an error of 0.125 psi. Furthermore, the minimum error for the pressure transducer occurs for the pressure measurement of 8.6 psi. The corresponding least squares analysis yields an error of 0.095 psi.

Combining these uncertainties yield the following: for pressures below 50 psi (manometer calibrated), the differential pressure has a maximum uncertainty of 0.174 psi and for pressures above 50 psi (dead-weight calibrated), the

Curve Fit:
P = 14.3627*(V)+6.7044
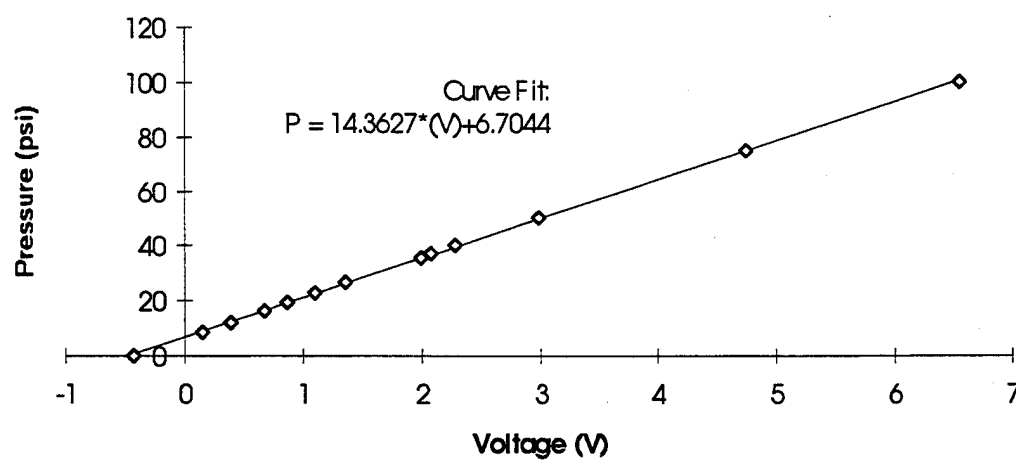
**Figure 2.17.   Differential Pressure Transducer
              Calibration Curve.**

differential pressure has a maximum uncertainty of 0.625 psi.

## 2.3  Experimental Procedures

The system warm up, data collection, and shut off procedures were conceived with consideration for accuracy, repeatability, safety, and ease of performance. Furthermore, because the experimentation on the High Flux Heat Exchanger consisted of three distinct categories, the experimental procedure was designed to overlap the different tests.

### 2.3.1  Warm Up

Before each data collection experiment occurred a quick check of all apparatus and equipment was performed to ensure no leaks nor failed components were present in the system. These checks included the following:

1. First, switch the Fluke data logger on, and select the proper data acquisition program needed for the current experiments.

2. After initiating flow through the test loop, set the flow rate to its maximum, 4.0 kg/min, and check for PAO leaks around the filter, reservoir, and the inlet and outlet of the HFHE.

3.  Start the pump on the cold temperature bath (do not start the cooling cycle), then check for coolant leaks at the inlet/outlet to the in-loop heat exchanger and the inlet/outlet of the cold temperature bath.

4.  Set the Set Point temperature of the cold temperature bath to cool the test loop to 20°C (at the maximum flow rate and zero heat load, this equates to approximately 18.5°C for the cold temperature bath) and initiate the cooling cycle. If the test-loop temperature measurement (at the inlet of the HFHE) does not measure approximately 20°C, then the thermocouple probes should be recalibrated.

5.  Once the test-loop temperature has steadied at 20°C, then check the pressure drop across the HFHE.  This pressure drop should be approximately 47 psi.  If the measurement from the differential pressure transducer does not match this value, the transducer should be recalibrated.

6.  Finally, if a substantial pressure drop occurs across the filter, the filter should be changed.

## 2.3.2  Operational Procedure

The operating procedures for the three distinct sets of experiments are similar, but retain significant difference to present three distinct sets of operational standards. The first to be presented is the operational procedure for the hydraulic tests.

1.  Set the Fluke data logger to the hydraulic test data acquisition program.  This program consists of recording the incoming data on the inlet coolant temperature and outlet coolant temperature of the HFHE, the mass flow rate, and the pressure drop across the HFHE.

2.  After the test-loop checks have been made, select a coolant temperature and set a corresponding Set Point temperature on the cold temperature bath. The corresponding Set Point temperature will vary depending on the coolant temperature and the room temperature (e.g.  If the coolant temperature is set for 50°C and room temperature is 25°C, the Set Point temperature will be greater than 50°C). Retain the maximum mass flow rate of 4.0 kg/min, for all coolant temperatures above 0°C.  However, if the selected coolant temperature is below 0°C, then reduce the mass flow rate to 3.0 kg/min.

3. Allow the inlet coolant temperature to reach thermal equilibrium. Thermal equilibrium is defined in this report as when the measured temperature does not increase or decrease more than 0.1°C in a time span of two minutes. The ±0.1°C in temperature allows for the uncertainty of the thermocouples. The time span of two minutes allows for both the thermal lag between the inlet coolant temperature and the HFHE surface, in addition to the maximum time needed for the data collection.

4. Initiate the data acquisition program, allowing fifteen data points to be recorded.

5. After stopping the data acquisition program, decrease the mass flow rate by 0.25 kg/min.

6. Repeat steps 3 through 5 until the minimum mass flow rate, 1.0 kg/min, has been reached.

7. Once the entire flow spectrum has been completed, select a new coolant temperature and repeat the procedure. (Periodically, after the entire flow spectrum has been completed, perform the hydraulic tests in reverse, starting with the minimum flow rate and increasing to the maximum flow rate, to determine any hysteresis in the data collection.)

8. Repeat the above steps until the entire temperature spectrum has been completed.

The second set of experiments consisted of the thermal performance of the HFHE in steady-state operation. To complete this set of experiments the following procedure was followed:

1. Select the individual CHIC of the HFHE to be tested, and perform the thermocouple set up and amplifier set up described in section 2.1.12.

2. Set the Fluke data logger to the steady state thermal test program. This program records the inlet coolant temperature and outlet coolant temperature, the pressure drop across the HFHE, the mass flow rate, the surface thermocouples, the heater thermocouple, the amplifier thermocouples, and the voltage and amperage of the mica heater. The program also calculates the power supplied by the mica heater through the use of the measured voltage and amperage.

3. Set the Set Point temperature to maintain a test-loop temperature of 20°C and a power load of 40 W.

4. Allow for thermal equilibrium of the test-loop temperature. This temperature will be slightly lower than 20°C at zero heat load.

5. Switch on the heater and set the heat load to 40 W. This must be done by monitoring the voltage and amperage from the data logger, and self calculating the power.

6. Allow for thermal equilibrium of the embedded thermocouple (thermocouple measuring the surface temperature of the HFHE beneath the heat flux amplifier). From Flynn [11], this temperature should be approximately 60°C.

7. Once this check has been made, the power to the mica heater is switched off. Then, select a coolant temperature and set a corresponding Set Point temperature on the cold temperature bath. Retain the maximum mass flow rate of 4.0 kg/min, for all coolant temperatures above 0°C. However, if the selected coolant temperature is below 0°C, then reduce the mass flow rate to 3.0 kg/min.

8. Allow thermal equilibrium of the inlet coolant temperature to be reached. Then switch on the power to the mica heater, and set the heat load to 20 W.

9. Allow thermal equilibrium of the heater thermocouple. The heater thermocouple was chosen because the heater has the greatest temperature of

all the components involved in the heat removal, the HFHE, the amplifier, and the mica heater.

10. Initiate the data acquisition program, allowing fifteen data points to be recorded. After stopping the data acquisition program, decrease the mass flow rate by 0.25 kg/min.

11. Once again allow for the thermal equilibrium of the heater temperature, and repeat step 10 until the minimum mass flow rate has been achieved.

12. After the entire spectrum of flow rates has been completed, increase the power setting by 20 W. (Periodically, after the entire spectrum of flow rates has been completed, perform the procedure in reverse, starting with the minimum mass flow rate and increasing to the maximum mass flow rate to check for hysteresis in the data collection.)

13. Repeat steps 9 through 12 until the entire spectrum of heat loads has been completed. Then select a new coolant temperature and repeat the data collection procedure.

14. After the entire spectrum of coolant temperatures has been completed, select a new individual CHIC and perform the entire procedure again until all the required CHICs have been completed.

The final set of experiments consists of the thermal performance of the HFHE in a transient state of operation. To complete this set of experiments, the following procedure was followed:

1. Select the individual CHIC to be evaluated, and set up the thermocouples and the ceramic heater as described in section 2.1.12

2. Set the Fluke data logger to the transient state thermal test program. This program records the imbedded thermocouple temperature, the inlet temperature, and the voltage and the amperage of the mica heater. The acquisition program only records this data to optimize the number of data points collected in the transient time span.

3. Follow the procedure steps 3 through 7 from the steady-state test procedure.

4. While allowing for thermal equilibrium of the coolant temperature, turn on the power to the heater and set the Variac to create 10 W of power. Then turn off the power to the heater while retaining the settings for the 10 W of power.

5. After attaining thermal equilibrium for the coolant temperature, start the data acquisition program. Then turn on the power to the heater and record data points for thirty seconds, then turn

off the power to the heater and record data points
for thirty seconds. Repeat the data collection
process a sufficient enough times to achieve
satisfactory accuracy. This number of repititions
was assumed to be three.

6.  Stop the data acquisition program, and lower the
    mass flow rate by 0.5 kg/min.

7.  Repeat steps 5 and 6 until the entire mass flow
    rate spectrum has been completed. Then increase
    the power setting by 10 W, and follow steps 5 and
    6. Repeat this step until the entire power
    spectrum has been completed.

8.  After the power spectrum has been completed,
    select a new coolant temperature and repeat the
    entire procedure.

## 2.3.3  Shut Down

For proper safety, the following procedure should be
completed at the end of each set of experiments.

1.  Turn off the power to the mica heater, and allow
    the temperature of the embedded thermocouple to
    reach room temperature.

2.  Then turn off the motor/pump, the cold temperature
    bath, and the Fluke data logger.

3.   Finally, inspect the test section apparatus and ensure that no leaks have become evident.

## 2.4   Problems

It was discovered that due to the large spectrum of coolant temperatures, sufficient thermal expansion occurs in the rubber hoses inside of the cold temperature bath and in the vinyl tubing connecting the cold temperature bath and the in-loop heat exchanger to cause significant leakage at the fittings.   Therefore, after each cycle of coolant temperatures, the fittings inside of the cold temperature bath and the tubing connecting the cold temperature bath and the in-loop heat exchanger were tightened.

Another problem during experimentation occurred at the check on the embedded thermocouple temperature during steady state tests.   It was determined if the surface temperature is greater than the referenced value the following must be checked.   First, the amplifier is not making significant contact with the CHIC surface due to a lack of contact pressure.   This can be checked by slightly tightening the nuts on the securing plate.   If the embedded thermocouple temperature decreases, then the contact pressure is not sufficient.

Second, if the amplifier is not making significant contact with the CHIC surface, the reason is due to the

improper alignment between the footprint of the CHIC and the footprint of the amplifier. To check this, remove the insulation and securing plate. Then ease the amplifier off the HFHE and check the footprint in the thermal grease. If the footprint does not overlay the footprint of the CHIC, then the contact between the HFHE and the amplifier is not sufficient.

The third problem that may arise is a non-uniform heat removal by the amplifier. This can be checked by evaluating the amplifier thermocouples. If the thermocouple readings on each plane of the amplifier are not uniform, then the amplifier needs to be replaced.

Finally, a lack of proper impingement on the target plate due to clogged passages of the CHIC passages by particulates in the fluid. This is assumed if no other cause is ascertained. To overcome this problem, the HFHE will need to be removed from the test loop and soaked in a solvent, and rinsed out by compressed air.


## 2.5  Data Reduction Procedures

A computer program called LAB was the major data reduction tool. A listing of the computer program LAB is given in Appendix D. The program's input is the data output file from the Fluke data logger and the number of inputs

(e.g. for the hydraulic tests, the number of inputs is four: inlet and outlet temperatures, mass flow rate, and pressure drop across the HFHE). The program averages each input and arranges the file in order to create a summary file that includes each flow rate, heat load, and coolant temperature for each CHIC tested (a sample output file is also given in Appendix D). The output file is then in a form to derive the final presentation of the data collected. This derivation of the data is presented in the results and discussion chapter.

# Chapter III

RESULTS AND DISCUSSION

## 3.1  Hydraulic Results

The hydraulic tests consisted of pressure drop measurements across the HFHE for ranges of flow rate and inlet coolant temperature of 1.0 kg/min to 4.0 kg/min by 0.25 increments and -10°C to 50°C by increments of 10°C, respectively.  In addition, because of the emphasis on low temperature measurements for system start up the -15°C was also included.  The actual pressure taps are immediately before and after the inlet and outlet of the HFHE. Therefore, the pressure drop measured is the actual pressure drop.  The results of these tests are in the form of a family of curves of pressure drops across the range of flow rates and coolant temperatures.  and the corresponding curve fit equation as a function of flow rate and viscosity and as a function of flow rate and coolant temperature.  Figure 3.1 shows the family of curves for the hydraulic performance of the High Flux Heat Exchanger.
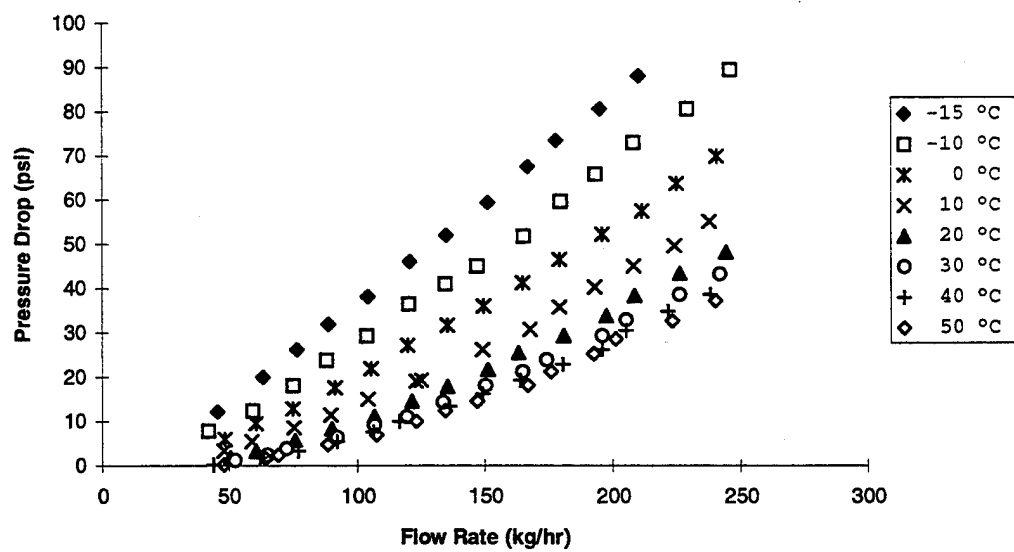
**Figure 3.1.   Pressure Drop Measurements.**

## 3.1.1 Analytical Hydraulic Model

The next step in the analysis of the hydraulic performance for the HFHE is to determine the equation governing the pressure drop. This is done by the following procedure.

First, beginning with the energy equation [12] for a control volume in a pipe for laminar flow and assuming steady state conditions the following equation for the conservation of energy is developed:

$$\dot{W}_{mech} = \int_{A_e} \rho_e \left( h + \frac{V^2}{2} + gz \right)_e dQ_e - \int_{A_i} \rho_i \left( h + \frac{V^2}{2} + gz \right)_i dQ_i - \dot{W}_{s_\tau} - {}_i\dot{Q}_e \quad (3.1)$$

If the fluid properties vary at most in one direction, and if the control volume has a number of inlet and exit stations through which the fluid flows, then the energy equation can be divided by the mass flow rate and the viscous work term, $\dot{W}_{s_\tau}$, and the heat transfer term, ${}_i\dot{Q}_e$, can be combined into a total friction loss term, $h_f$. This new equation can be seen as Equation (3.2).

$$w_{mech} = \sum_e \left( \frac{p}{\gamma} + \frac{V^2}{2g} + z \right)_e - \sum_i \left( \frac{p}{\gamma} + \frac{V^2}{2g} + z \right)_i + h_f \quad (3.2)$$

However, if the entire HFHE is considered the control volume, only one inlet and one exit station occurs. Also, the friction head loss, $h_f$, can be expressed by a viscous-frictional loss term and a dynamic loss term. Therefore, the energy equation can be expressed in its final form.

$$\left(\frac{p}{\gamma}+z+\frac{V^2}{2g}\right)_1+\left(_1W_2\right)_{mech}=\left(\frac{p}{\gamma}+z+\frac{V^2}{2g}\right)_2+f\frac{L}{D}\frac{V^2}{2g}+\sum k_i\frac{V^2}{2g} \qquad (3.3)$$

Now applying this form of the energy equation to the HFHE in the test loop, the following modifications can be made. First, for the HFHE, the mechanical work term is negligble, no pumps or turbines exist in the control volume. Next, the HFHE is located in the horizontal plane, therefore the change of potential energy across the HFHE, $z_1-z_2$, can be neglected. In addition, because the hydraulic tests were performed for an isothermal condition, the density of the PAO can be considered a constant across the HFHE. Applying a constant density with the fact that the cross-sectional area of the inlet equals the cross-sectional area of the outlet, from conservation of mass, translates to the velocity entering the HFHE being equal to the velocity exiting the HFHE. Therefore the change in kinetic energy, $(V^2/2)_1-(V^2/2)_2$, across the control volume can also be

neglected. Finally, both the viscous-friction term and the dynamic term can be modeled by a summation of the individual viscous-friction terms and dynamic terms associated with the individual plates in each CHIC. Therefore, the equivalent tube-orifice model can be expressed as:

$$\Delta p = \sum_{i=1}^{n} k_i \frac{V_i^2 \rho}{2 g_c} + \sum_{i=1}^{n} f_i \frac{L_i}{D_i} \frac{\rho V_i^2}{2 g_c} \qquad (3.4)$$

Now assuming that the flow is predominately laminar flow, the friction factor can be expressed as a function of only the Reynolds number. This friction factor is expressed as:

$$f = \frac{C}{\mathrm{Re}} = \frac{C\mu}{\rho V D} \qquad (3.5)$$

Substituting Equation (3.5) and the expression that the velocity is equal to the volumetric flow rate divided by the cross-sectional area, V=Q/A, yields the following equation for the pressure drop across the HFHE:

$$\Delta p = \sum_{i=1}^{n} \rho Q^2 \left( \frac{k_i}{2 A_i^2 g_c} \right) + \sum_{i=1}^{n} \mu Q \left( \frac{C L_i}{2 g_c A_i D_i^2} \right) \qquad (3.6)$$

The terms in the parentheses represent the minor loss coefficient, the cross-sectional area of the individual tubes, the gravitational constant, the length of the individual tubes, the diameter of the individual tubes, and the constant relating the Reynolds number and the friction factor. All of these are independent of the flow rate and the coolant temperature. Therefore, Equation (3.6) can be simplified as the pressure drop across the HFHE is equivalent to the viscous-frictional head loss, $\mu Q$, plus the dynamic head loss, $\rho Q^2$.

$$\Delta p = C_2 \rho Q^2 + C_1 \mu Q \tag{3.7}$$

However, the flow rate measured was in terms of the mass flow rate instead of the volumetric flow rate. Therefore, using the expression that the volumetric flow rate is equivalent to the mass flow rate divided by the density of the fluid, $Q = \dot{m}/\rho$, the final equation for the pressure drop across the HFHE is:

$$\Delta p = \frac{\left( C_1 \mu \dot{m} + C_2 \dot{m}^2 \right)}{\rho} \tag{3.8}$$

Because the pressure drops are dependent on the viscosity, density, and flow rate, this set of curves are indicative to the inert properties of the coolant PAO. Therefore, to complete the modeling of the hydraulic performance of the HFHE, equations for the density and the viscosity of the coolant must be developed as functions of the fluid temperature. These equations were developed by Ghajar, et al. [13], and shown below. First, the viscosity of the PAO follows the following equation, in which the viscosity is in terms of m²/s and the temperature is in terms of K:

$$\nu = \left( 10^{\left( \frac{10^{9.67}}{T^{3.923}} \right)} - 0.70 \right) \times 10^{-6} \qquad (3.9)$$

From this equation, it can be seen that the viscosity increases exponentially below 291.7 K or 18.5 °C. This exponential increase can be seen in Figure 3.1. In addition, the density of the coolant fluid PAO, in kg/m³, is given as a function of the coolant temperature, in K, by the following equation:

$$\rho = 1.36 \times 10^3 - 4.56T + 0.0157T^2 - 0.280 \times 10^{-4} T^3 + 0.174 \times 10^{-7} T^4 \qquad (3.10)$$

Now substituting the expressions for the density and viscosity into Equation (3.8), and realizing that the kinematic viscosity is equal to the absolute viscosity divided by the density, $v = \mu/\rho$, the final equation for the pressure drop across the HFHE, psi, in terms of the mass flow rate, kg/hr, and inlet coolant temperature, K, is expressed as the following:

$$\Delta p = C_1 \left[ \left( 10^{\left( \frac{10^{9.67}}{T_f^{3.923}} \right)} - 0.70 \right) \times 10^{-6} \right] \dot{m}$$
$$+ C_2 \frac{\dot{m}^2}{\left( 1.36 \times 10^3 - 4.56 T_f + 0.0157 T_f^2 - 0.28 \times 10^{-4} T_f^3 + 0.174 \times 10^{-7} T_f^4 \right)} \quad (3.11)$$

## 3.1.2 Overall Hydraulic Performance

Combining the experimental and analytical models for the pressure drop across the HFHE, the constants for Equation (3.11) can be derived from a curve fit. These constants for $C_1$ and $C_2$ were determined to be 7354.83 and 0.428, respectively, for all of the inlet coolant temperatures. These constants yield an equation that fits the experimental data at each discrete temperature with a standard deviation of 1.813 psi and a maximum error of 3.5 psi at a coolant temperature of -15°C and flow rate of 180 kg/hr. This model, as shown in Figures 3.2 and 3.3, fits

the data well, especially at medium and high flows.
However, the form of the equation of this model is
constrained to pass through the origin. This constraint may
affect the fit at the low flow conditions. Evaluation of
the hydraulic performance shows at normal flow, 200 kg/hr,
and an inlet temperature of -10°C, the pressure losses are
28% dynamic and 72% viscous-frictional. For the same flow
at an inlet temperature of 50°C the losses are 78% dynamic
and 22% viscous-frictional. At reduced flow, 100 kg/hr, and
an inlet temperature of -10°C, the pressure losses are 16%
dynamic and 84% viscous-frictional. For the same flow rate
and at an inlet temperature of 50°C the losses are 64%
dynamic and 36% viscous-frictional.

3.1.3 HFHE Flow Regime

For the development of the hydraulic performance
equation, shown in section 3.1.1, the assumption of a
laminar flow regime was made. Therefore, a check on this
assumption is necessary. For this check, the following
procedure was performed, starting with the Reynolds number
equation.

$$Re = \frac{VD}{\nu} \qquad (3.12)$$
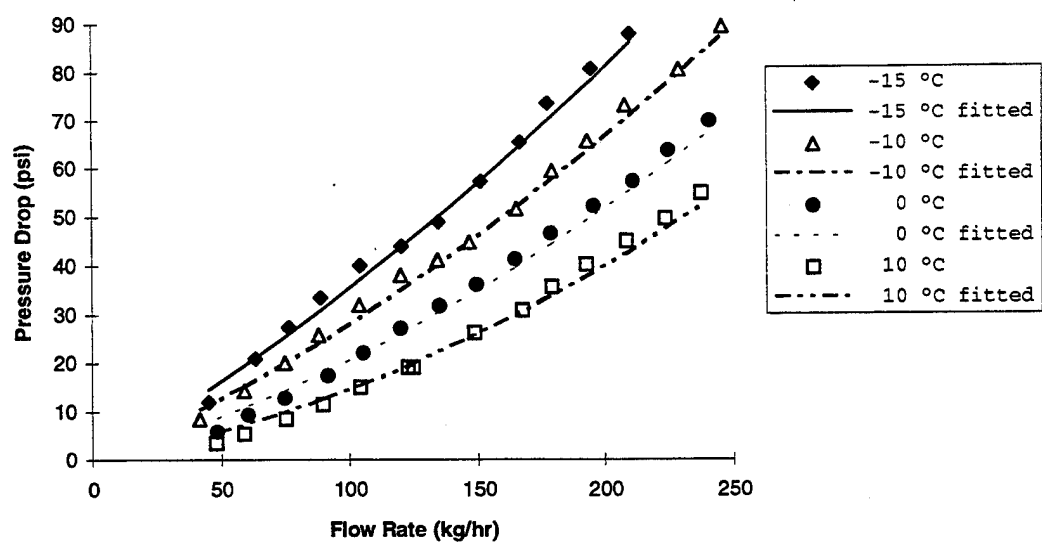
**Figure 3.2  Curve Fit for the Pressure Drop (-15°C to 10°C).**
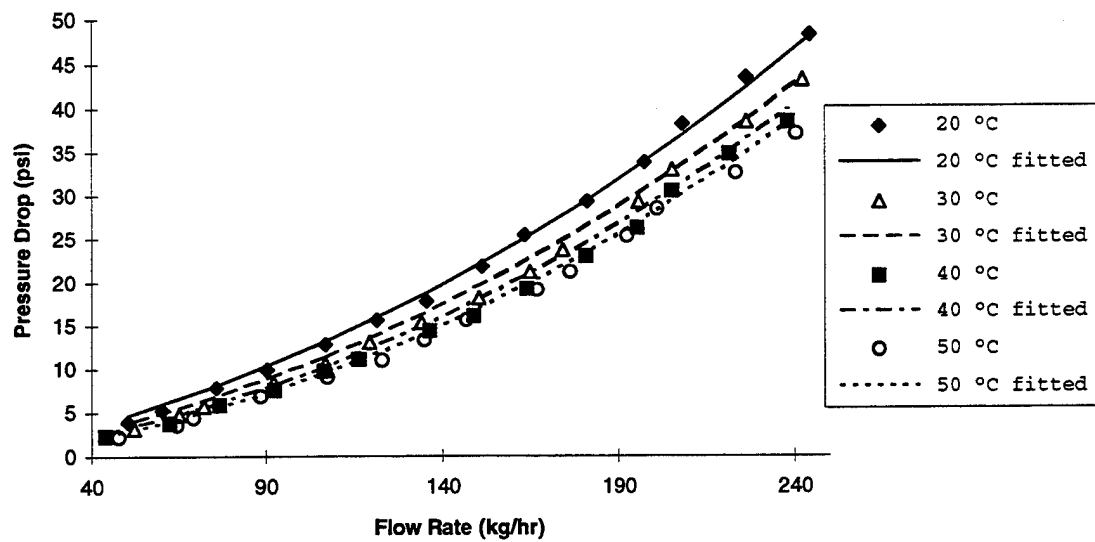
**Figure 3.3.  Curve Fit for the Pressure Drop (20°C to 50°C).**

Now rearranging this equation in terms of the mass flow rate yields the following:

$$Re = \frac{4\dot{m}}{\pi D \rho \nu} \qquad (3.13)$$

Now substituting Equations (3.9) and (3.10) for the density and the viscosity yields an equation for the Reynolds number in terms of the mass flow rate, diameter of the tubing, and the coolant temperature.

$$Re = \frac{4\dot{m}}{\pi D \left(1.36 \times 10^{3} - 4.56 T_f + 0.0157 T_f^{2} - 0.28 \times 10^{-4} T_f^{3} + 0.174 \times 10^{-7} T_f^{4}\right)}$$

$$\times \frac{1}{\left[\left(10^{\left(\frac{10^{9.67}}{T_f^{3.923}}\right)} - 0.70\right) \times 10^{-6}\right]} \qquad (3.14)$$

Now examining this equation for the outlet and inlet of the HFHE yields that the maximum Reynolds number, occurring at the extreme temperature of 50°C, flow rate of 4.0 kg/min, and pipe diameter of 1.27 cm (0.5 inch), corresponding to the inlet and outlet of the HFHE, is 2176. The Reynolds number occurring at the extreme temperature of -10°C, flow rate of 1.0 kg/min, and pipe diameter of 1.27 cm (0.5 inch)

is about 50.    Therefore, the Reynolds number over the entire flow rate range, 1.0 kg/min to 4.0 kg/min, and coolant temperature range, -10°C to 40°C, is laminar.

Furthermore, although the individual tubes in the HFHE are much smaller than the inlet/outlet pipe, the flow rate through each CHIC is only 1/20 the flow rate through the inlet/outlet pipe.  In addition, the individual jets diameter are on the order of 0.018 cm (0.007 in).  However, each CHIC contains sixty jets, three rows of twenty. Therefore the mass flow rate of the individual jet is 1/1200 of the total mass flow rate through the HFHE. At the maximum Reynolds number case, a coolant temperature of 50°C and a mass flow rate of 4.0 kg/min, the Reynolds number through the individual jets translates to about 130.  Therefore, once again the assumption of laminar flow through the individual jets of the HFHE is valid.

Some turbulence does occur through the abrupt turning of the flow through the CHICs; however, the increased pressure drop due to this turbulence is modeled in the dynamic pressure loss term.  Therefore, the assumption that the flow is predominately laminar throughout the entire HFHE is valid.

### 3.1.4  Hydraulic Performance Comparison

Because the Compact High Intensity Cooler was designed in 1983, previous examinations have been performed on the hydraulic performance that have led to an analytic model predicting the pressure drop through the CHIC. In addition, the predictions have been extrapolated to encompass various geometric arrangements of the CHICs, such as the High Flux Heat Exchanger. These predictions can be seen in Flynn, et al. [4] and in Figure 3.4. If the predicted pressure drop seen in Figure 3.4 is compared to the experimental pressure drop seen in Figure 3.1, one can see the experimental pressure drops at high flow rates are 50 to 100% higher than the predicted pressure drops. However, the predicted pressure drops follow a model that assumes ideal bend, split, merge, and area transition losses. However, the actual geometry tested will have more losses. In addition, assumed flow channels and orifices for the prediction model are as designed; however, some flow blockage or deformation of passages from fabrication may occur. Finally, most of the predicted pressure drop in a CHIC is spent in the viscosity over the range of expected operating temperatures. The impingement pressure drops are more predictable. Therefore, the predictions of this HFHE design will have more impingement jets; however, in the HFHE design, the

ADIABATIC PRESSURE DROP
(Does not include OD pressure drop)
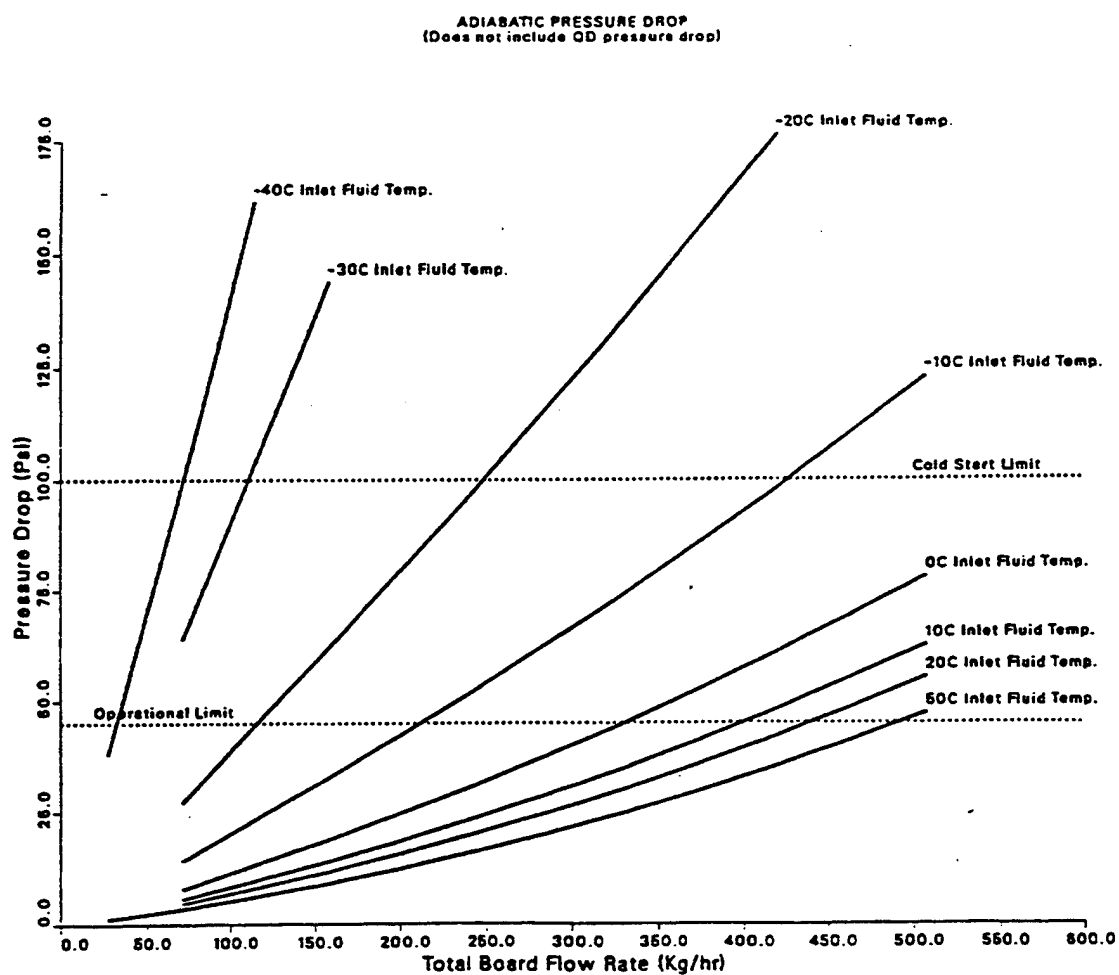
Figure 3.4.  Predicted Hydraulic Performance of the
HFHE [4].

majority of the pressure losses are line-type frictional losses that occur outside of the orifice plate losses. This is because the HFHE was designed to operate with PAO. All of these factors contribute somewhat to the poor correlation between the previously hydraulic predictions and the experimental analysis.

However, the largest contributor is that in the predictions for the pressure drop across the HFHE seen in Figure 3.4, the flow regime is assumed to be turbulent flow. However, as described earlier, the flow regime for this experimentation is laminar. The effect of this invalid assumption can be shown in the calculation of the constants for Equation (3.11). Upon examination of Equation (3.4), shown below with the velocity replaced with the mass flow rate, the only variable that is dependent on the assumption of laminar flow is the friction factor.

$$\Delta p = \sum_{i=1}^{n} \frac{k_i \dot{m}^2}{2 \rho g_c A_i^2} + \sum_{i=1}^{n} f_i \frac{L_i \dot{m}^2}{2 D_i \rho g_c A_i^2} \qquad (3.15)$$

The minor loss coefficient, $k_i$, the length of the tubes, $L_i$, the diameter of the tubes, $D_i$, and the cross sectional area of the tubes, $A_i$, are inherent properties of the HFHE and are independent of the flow. The density, $\rho$, is dependent

on only the coolant temperature.  Therefore, the density is independent of the flow.

Finally, the gravitational constant, $g_c$, is a universal constant and is independent of all the input parameters. Therefore, a comparison between the friction factor for laminar flow and the friction factor for turbulent flow through the HFHE is presented. For the majority of the actual flow regime representing the experimentation with the coolant PAO, the Reynolds number is below 1000 (see section 3.1.3).  Using the Moody Chart in [12], this yields a friction factor of over 0.06.  However, for the previous predictions of the HFHE, the friction factor for a relatively smooth pipe (such as drawn tubing) is less than 0.03.  Therefore, the friction factor is at least 2 times greater for the laminar flow than turbulent flow.  Hence, the viscous-frictional term for laminar flow will be twice that of the turbulent flow.  This indicates that for laminar flow, the pressure drop across the HFHE should be larger than the predictions for the pressure drop across the HFHE for turbulent flow.

This realization is consistent with the results obtained from this thesis and not consistent with the results obtained by McDonnell Douglas' report [4].

## 3.2   Thermal Steady-state Performance

The thermal tests include the same flow rate range as
the hydraulic tests, but the range of inlet coolant
temperatures was reduced to -10°C to 40°C.  This reduction
is due to the fact that the cold temperature bath used to
keep the temperature of PAO constant, must actually cool the
PAO below -10°C to remove the power that is added in the
thermal tests.  In addition, heat loads were applied to the
HFHE ranging from 20 W to 100 W by an increment of 20 W.

## 3.2.1 Radial Heat Loss

Because the HFHE consists of twenty parallel CHICs, an
assumption that all CHICs are identically independent is
made.  Therefore, the thermal tests consisted of applying a
heat load to only one of the CHICs in the HFHE at a time.
To check the assumption, numerous CHICs were tested to
indicate conformity.  However, because of the layout of the
CHICs in the HFHE, each CHIC is surrounded by channels of
PAO.  This results in radial heat loss due to conduction
heat transfer when only one CHIC is tested at a time.
Therefore, the actual heat flux absorbed by the CHIC is less
than the heat load applied.  So, a two-dimensional heat
transfer model was constructed by taking temperature
measurements surrounding the testing CHIC, shown in

Figure 2.8. The temperature was then plotted and an exponential decaying curve was fitted. This curve fit followed the following equation:

$$T_s = \theta_1 + \theta_2\, e^{\theta_3 \xi} \qquad\qquad (3.16)$$

Where the variable $\xi$ is a dummy variable representing the distance from the edge of the CHIC in the x or y direction, in cm, and the surface temperature is given in °C.

A typical curve for the surface temperature profile is shown in Figures 3.5 and 3.6 for the heat loss in the x-direction and the heat loss in the y-direction, respectively. The coordinate system for the HFHE can be seen in Figure 3.7. The constants $\theta$ are determined by the curve fit and are dependent on the heat load, fluid temperature, flow rate, and CHIC location. The equation is then differentiated and evaluated at the $\xi$ value representing the symmetry line, shown in Figure 3.7. From this temperature gradient, the heat conducted across the line of symmetry in the x and y direction can be approximated from the following equations, respectively:
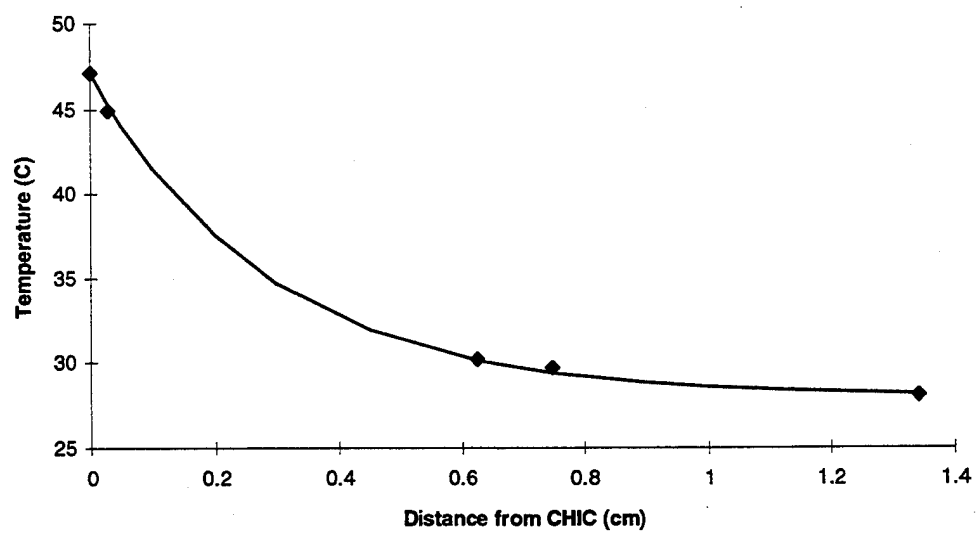
Figure 3.5.   X-Directional Temperature Profile.
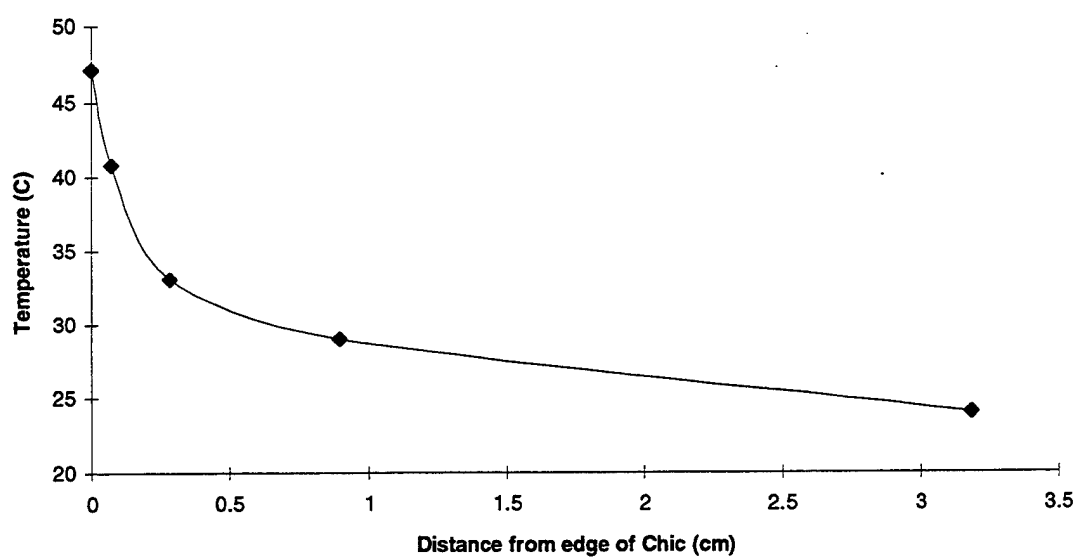
**Figure 3.6. Y-Directional Temperature Profile.**

$$\dot{Q}_{+/-x} = \pi k r_x t \frac{dT_s}{dx}$$

<div align="right">(3.17)</div>

$$\dot{Q}_{+/-y} = \pi k r_y t \frac{dT_s}{dy}$$

This process is a double sided heat transfer model. Therefore, the total heat loss in the radial direction due to conduction heat transfer for a CHIC surrounded by four CHICs would be the sum of the total heat loss in the x-direction and the y-direction.

However, if the CHIC being tested was surrounded only by two CHICs (the four corner CHICs), the total heat loss would be one half the sum of the total heat loss in the x-direction and the y-direction. In addition, if the CHIC was surrounded by three CHICs (edge CHICs excluding the corner CHICs), then the total heat loss would be the sum of the heat loss in the direction of the two similar CHICs and one half the heat loss in the direction of the third CHIC.

Once the location of the CHICs were accounted for in the total heat loss in the radial direction, it was determined that the individual CHICs tested behaved in similar fashion. This validated the identically independent assumption. The next step in the evaluation of the thermal performance was to develop an analytic equation for the
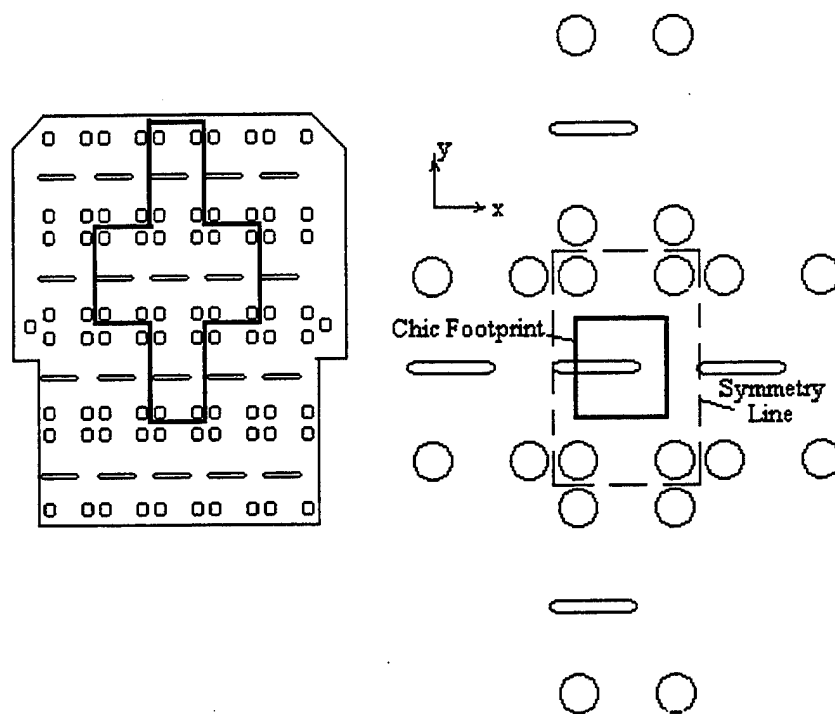
Figure 3.7.  Line of Symmetry.

radial heat loss due to conduction heat transfer. In
theory, the radial heat loss should be a function of the
flow rate only. However, if the energy balance is
inspected, it can be shown that the direct path through the
CHIC is capable of more heat transfer than the radial path.
Therefore, as the heat load is increased, a greater
percentage must be transferred directly into the CHIC. This
generalization can also be made for the fluid temperature.
The affect of the fluid temperature is felt more by the
direct route than the radial route. Therefore, as the fluid
temperature decreases, a greater percentage of the heat
transfer will travel directly into the CHIC. Hence, the
actual radial heat loss due to conduction is a function of
the flow rate, inlet temperature, and the applied heat load.
This is validated by the fact that the largest heat loss
occurs at an inlet temperature of 40°C, a flow rate of 60
kg/hr, and a heat load of 20 W. The experimental data was
fitted with a curve that was expressed as Equation (3.18).
The mass flow rate is expressed in terms of kg/hr and the
coolant temperature is expressed in K.

$$\frac{\dot{Q}_{loss}}{\dot{Q}_{applied}} = \phi_1 + \left(\phi_2 + \phi_3 e^{(\phi_4 T)}\right)e^{\left(\left(\phi_5 + \phi_6 e^{(\phi_7 T)}\right)\dot{m}\right)} \tag{3.18}$$
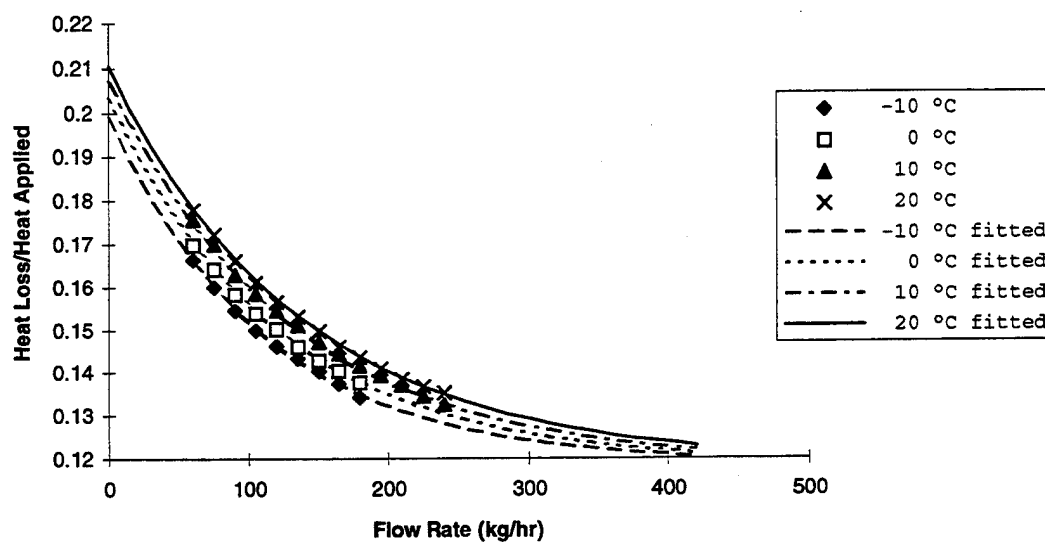
**Figure 3.8. Radial Heat Loss Due to Conduction Heat Transfer for an Applied Heat Load of 100 W.**

The constants $\phi_n$ are dependent on the applied heat load. For a heat load of 100 W the constants are as follows: $\phi_1$ (0.11858), $\phi_2$ (0.11897), $\phi_3$ (-0.7860), $\phi_4$ (-0.011485), $\phi_5$ (-0.0046646), $\phi_6$ (-0.37727), and $\phi_7$ (-0.017087). The curve fit for the 100 W case is shown in Figure 3.8. This curve fit produces equations that have a standard deviation of 0.000525 and a maximum error of 0.001536. The error analysis for this equation can be seen in Appendix E.

## 3.2.2 Wall Temperature

The next step in the thermal performance analysis is to develop a thermal resistance equation for the HFHE. To accomplish this, an analytical model must be developed for the wall temperature of the HFHE. This wall temperature theoretically should be a linear function of the heat flux, W/cm$^2$ as shown below with the wall and fluid temperatures in °C or K:

$$T_w - T_f = \psi \dot{Q} \qquad (3.19)$$

However, the flow rate influences the efficiency of the jet impingement heat exchanger. Therefore, the wall temperature should be a linear function of the heat flux, but the

constant, $\psi$, will be exponentially dependent on the flow rate. To curve fit the experimental data, the heat load used in Equation (3.19) must be the net heat load. This is because the wall temperature data was generated by applying a heat load to only one CHIC. However, when a heat load is applied to all twenty CHICs simultaneously, the radial heat loss will be negligible. Thus the net heat load will be approximately the applied heat load. Therefore, the equation for the wall temperature is shown in Equation (3.20) with the wall and fluid temperatures in °C or K:

$$T_w - T_f = \lambda_0 + \left(\lambda_1 + \lambda_2 e^{(\lambda_3 \dot{m})}\right)\dot{Q} \qquad (3.20)$$

The constants $\lambda_n$ are independent of the flow rate, heat load, and fluid temperature and have the following values: $\lambda_0$ (2.25), $\lambda_1$ (0.19779), $\lambda_2$ (0.19968), and $\lambda_3$ (-0.013115). In addition, the mass flow rate is in kg/hr, and the heat load is in W/cm$^2$. This curve fit, shown in Figure 3.9, produces a standard deviation of 0.275°C and a maximum error of 0.707°C. This error analysis can be also be seen in Appendix E.


## 3.2.3 Thermal Resistance

The last step in the procedure for determining the
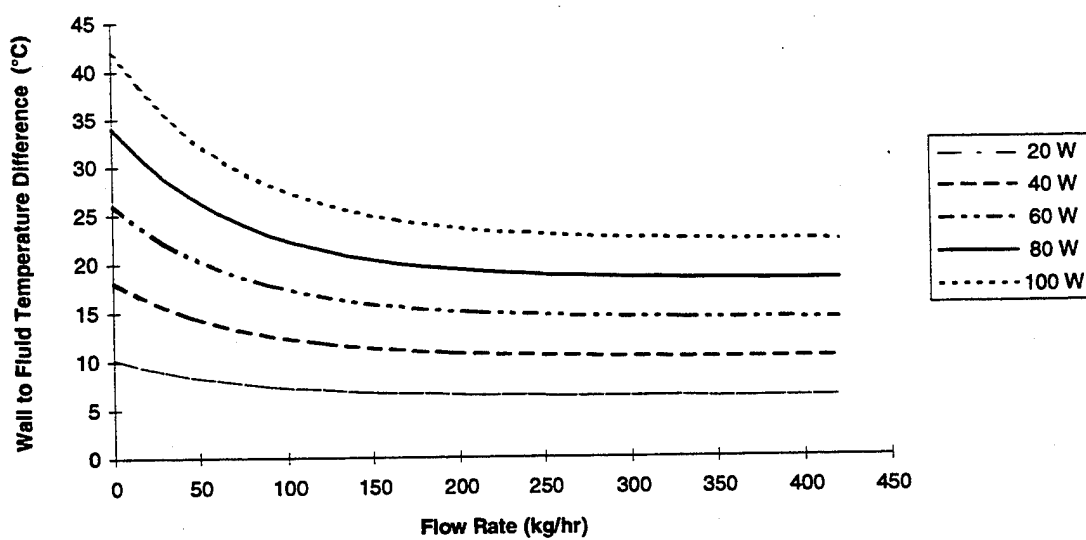
**Figure 3.9. Wall Temperature as a Function of the Flow Rate.**

properties of the HFHE is the thermal resistance. This thermal resistance of the HFHE, $°C/(W/cm^2)$, can be obtained by the following equation:

$$R_{wf} = \frac{T_w - T_f}{\dot{Q}}$$

(3.21)

This equation can be also expressed in terms of the mass flow rate, kg/hr, and the heat load, $W/cm^2$, by substituting Equation (3.20) into Equation (3.21). This expression is shown in Equation (3.22). In addition the thermal resistance for the HFHE is shown as the mass flow rate and heat load vary in Figure 3.10.

$$R_{wf} = \frac{2.25 + \left(0.20 + 0.20e^{(-0.013\dot{m})}\right)\dot{Q}}{\dot{Q}}$$

(3.22)

3.2.4 Thermal Performance

Once the thermal resistance is calculated, the maximum heat flux capable for the HFHE as a function of the inlet temperature and the flow rate can be calculated using the following equation:
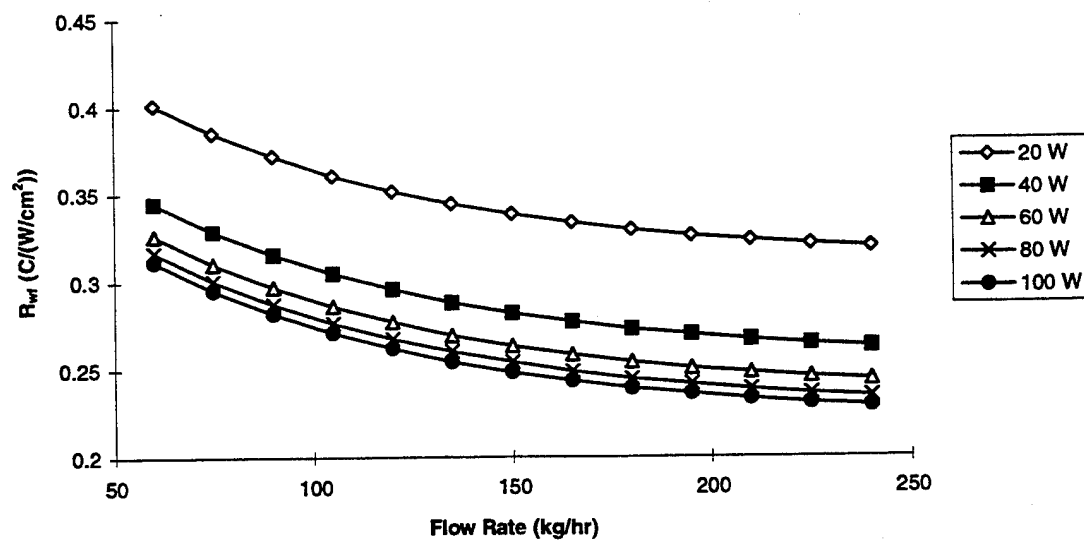
**Figure 3.10.  Thermal Resistance of the HFHE.**

$$\dot{Q} = \frac{T_j - T_f}{R_{jc} + R_{cw} + R_{wf}}$$

(3.23)

The junction temperature, $T_j$, was designated by the design requirements of the HFHE to be 90° C. The thermal resistance, $R_{jc}$, from the junction to the case interface and the thermal resistance, $R_{cw}$, from the case interface to the wall of the HFHE are dependent on the material consistency.

The location of these thermal resistances and the junction temperature are shown in Figure 3.11. McDonnell Douglas [4] assumed the values of these thermal resistances both to be 0.2 °C/(W/cm$^2$). Therefore, Equation (3.23) reduces to a function of the fluid temperature, mass flow rate, and the heat load. Therefore, if Equation (3.22) is substituted into Equation (3.23), and the resulting equation is solved for the **minimum** mass flow rate required, $\dot{m}$ (kg/hr), for removal of a given applied heat load in terms of the applied heat load, $\dot{Q}$ (W/cm$^2$), fluid temperature, $T_f$ (K), thermal resistances from the junction to the case and the case to the wall, $R_{jc}$ and $R_{cw}$ (°C/(W/cm$^2$)), and junction temperature, $T_j$ (K), the following equation is generated:
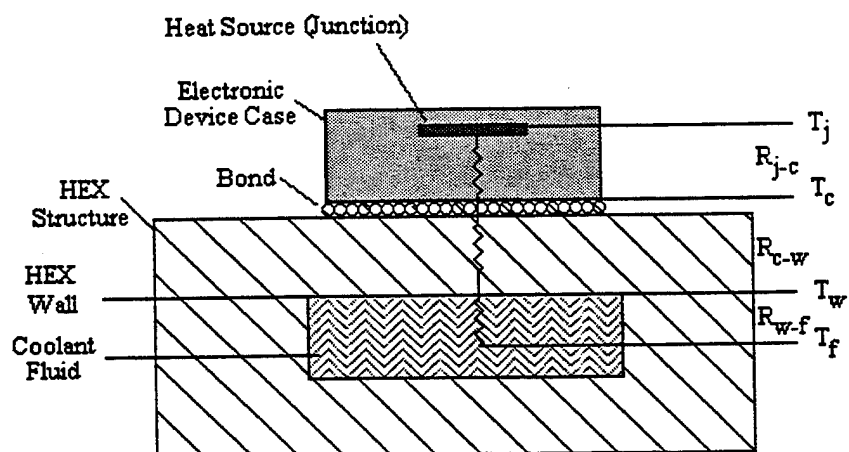
**Figure 3.11. Thermal Resistance and Junction Temperature Placement.**

$$\dot{m} = -76.24 \ln\left[5.01\left(\frac{-R_{cw}\dot{Q} - R_{jc}\dot{Q} - 2.25 - 0.20\dot{Q} + T_j - T_f}{\dot{Q}}\right)\right] \qquad (3.24)$$

$$IF\ \dot{m}_{measured} \le 0.0: \quad THEN\ \dot{m}_{actual} = 0.0$$

$$ELSE\ \dot{m}_{actual} = \dot{m}_{measured}$$

A logical expression must be inserted into Equation (3.24) because the equation itself does not discern positive and negative values of the mass flow rate. This logical expression can be added into any control device or computer program and does not invalidate the equation for the mass flow rate. The meaning of this logical expression can be explained as follows. The equation will produce a heat flux capability for the HFHE at zero mass flow rate. The reason for this error is that the equation assumes a constant coolant temperature. However, when zero flow occurs in the HFHE and a heat load is supplied, the coolant temperature increases, thereby invalidating Equation (3.24). Therefore, an asymptote must be manually added to the thermal performance curves at zero flow rate. This manual addition is the logical expression. The logical expression itself indicates that any negative values for the flow rate resulting from the input parameters in Equation (3.24) in

actuality mean that any positive non-zero flow through the
HFHE is sufficient to remove the input heat flux.
Furthermore, a positive value for the mass flow rate
resulting from the input parameters in Equation (3.24)
reflects the actual *minimum* mass flow rate necessary to
remove the given heat flux.


## 3.2.5 Design Heat Load Performance

Now if the heat load is held constant, and the values
for the thermal resistance, 0.2 °C/(W/cm$^2$) and the junction
temperature, 90°C, are assumed to be the values described
above, then the flow rate can be calculated as a function of
the fluid temperature.  Because the HFHE was designed to
remove 100 W per CHIC, the applied heat load, $\dot{Q}$, was given
the value of 100 W.  Therefore, the optimum performance
curve can be constructed using the flow rates generated by
Equation (3.24) over the possible range of coolant
temperatures.  This performance curve for the heat load of
100 W per CHIC is shown in Figure 3.12.  As seen in this
figure, the flow rate necessary to generate a maximum
cooling rate of 100 W per CHIC remains small until the
coolant temperature approaches a value of 28°C (301 K).  At
this temperature the minimum flow rate necessary for a

cooling rate of 100 W per CHIC increases to infinity. This was reflected in the experimental data. For the value of 0.2 °C/(W/cm$^2$), for the thermal resistance, $R_{jc}$ and $R_{cw}$, a heat load of 100 W per CHIC, and a junction temperature of 90°C, the corresponding wall temperature of the HFHE must be 50°C.

During experimentation, at coolant temperatures of 30°C and above, the wall temperature exceeded 50°C over the entire range of flow rates. For a coolant of 40°C, the required 50°C wall temperature, for the removal of 100 W per CHIC, was exceeded at 60 W per CHIC. Furthermore, for a coolant of 30°C, the required 50°C wall temperature was exceeded at 80 W and flow rates less than 3.5 kg/hr. However, the maximum possible coolant temperature can be increased from 28°C by decreasing the thermal resistances of $R_{jc}$ and $R_{cw}$. If the thermal resistances were reduced from 0.2 to 0.15 °C/(W/cm$^2$), the corresponding maximum possible coolant temperature is increased from 28°C to 38°C. In addition, if the thermal resistances were increased from 0.2 to 0.25 °C/(W/cm$^2$), the corresponding maximum possible coolant temperature decreases from 28°C to 18°C. The affect of the thermal resistance values between the junction and
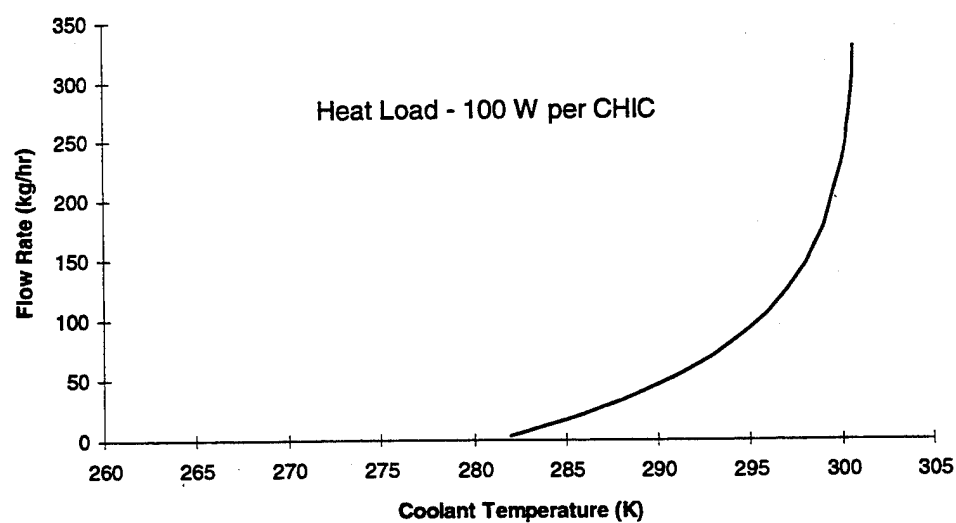
**Figure 3.12. Design Specification Thermal Performance Curve
for the Minimum Cooling Rate of 100 W per CHIC ( $R_{cw}$ and $R_{jc}$, 0.20 °C/(W/cm$^2$),
and $T_j$, 90°C).**
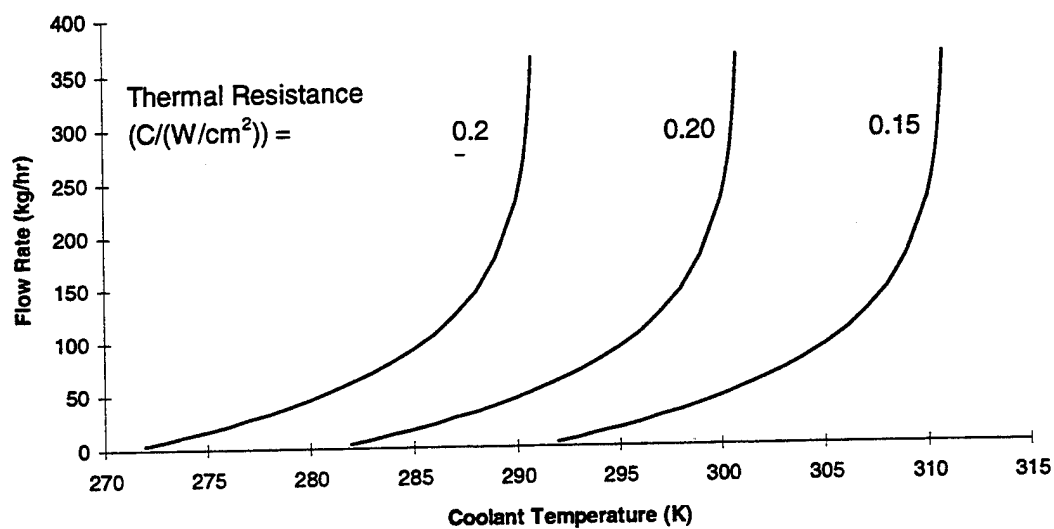
**Figure 3.13.    Thermal Performance as a Function of the
Thermal Resistances.**

the case and between the case and the wall of the HFHE on the performance curves are shown in Figure 3.13.

### 3.2.6 Overall Steady-State Performance

This optimum performance for the HFHE of 100 Watts per CHIC is based on possible future needs in electronic cooling. However, current cooling demands do not reach this high heat flux. Therefore, a complete range of heat loads were examined for the HFHE. So, using Equation (3.24) with the constants for the thermal resistances, $R_{wc}$ and $R_{jc}$, of 0.2 °C/(W/cm$^2$), and a constant junction temperature of 90°C, a family of performance curves can be constructed by varying the coolant temperature and heat load. As a note, in previous sections it has been stated that for a junction temperature of 90°C, the corresponding wall temperature, for thermal resistance values of 0.2 °C/(W/cm$^2$), is 50°C. However, this wall temperature corresponds to a heat load of 100 Watts per CHIC. Tables 3.1 to 3.3 show the corresponding wall temperature for the spectrum of heat ranges considered.

Figures 3.14 through 3.16 show the family of curves for the corresponding thermal resistances, $R_{wc}$ and $R_{jc}$, and heat loads shown in Tables 3.1 through 3.3.

**Table 3.1.** Correlation Between the Wall and Junction Temperature for Thermal Resistances of 0.15 °C/(W/cm²).

| Heat Load (W/cm²) | $R_{wc}$ (°C/(W/cm²)) | $R_{jc}$ (°C/(W/cm²)) | $T_j$ (°C) | $T_w$ (°C) |
|---|---|---|---|---|
| 20 | 0.15 | 0.15 | 90 | 84 |
| 40 | 0.15 | 0.15 | 90 | 78 |
| 60 | 0.15 | 0.15 | 90 | 72 |
| 80 | 0.15 | 0.15 | 90 | 66 |
| 100 | 0.15 | 0.15 | 90 | 60 |

**Table 3.2.** Correlation Between the Wall and Junction Temperature for Thermal Resistances of 0.20 °C/(W/cm²).

| Heat Load (W/cm²) | $R_{wc}$ (°C/(W/cm²)) | $R_{jc}$ (°C/(W/cm²)) | $T_j$ (°C) | $T_w$ (°C) |
|---|---|---|---|---|
| 20 | 0.2 | 0.2 | 90 | 82 |
| 40 | 0.2 | 0.2 | 90 | 74 |
| 60 | 0.2 | 0.2 | 90 | 66 |
| 80 | 0.2 | 0.2 | 90 | 58 |
| 100 | 0.2 | 0.2 | 90 | 50 |

**Table 3.3.** Correlation Between the Wall and Junction Temperature for Thermal Resistances of 0.25 °C/(W/cm²).

| Heat Load (W/cm²) | $R_{wc}$ (°C/(W/cm²)) | $R_{jc}$ (°C/(W/cm²)) | $T_j$ (°C) | $T_w$ (°C) |
|---|---|---|---|---|
| 20 | 0.25 | 0.25 | 90 | 80 |
| 40 | 0.25 | 0.25 | 90 | 70 |
| 60 | 0.25 | 0.25 | 90 | 60 |
| 80 | 0.25 | 0.25 | 90 | 50 |
| 100 | 0.25 | 0.25 | 90 | 40 |
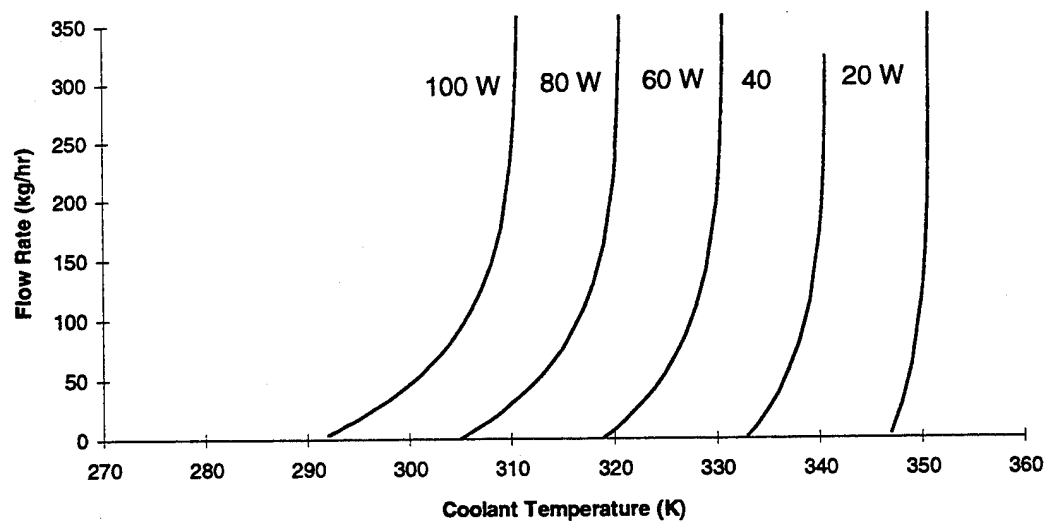
Figure 3.14.  Thermal Performance as a Function of the Heat
Load with Thermal Resistances of 0.15 °C/(W/cm$^2$).
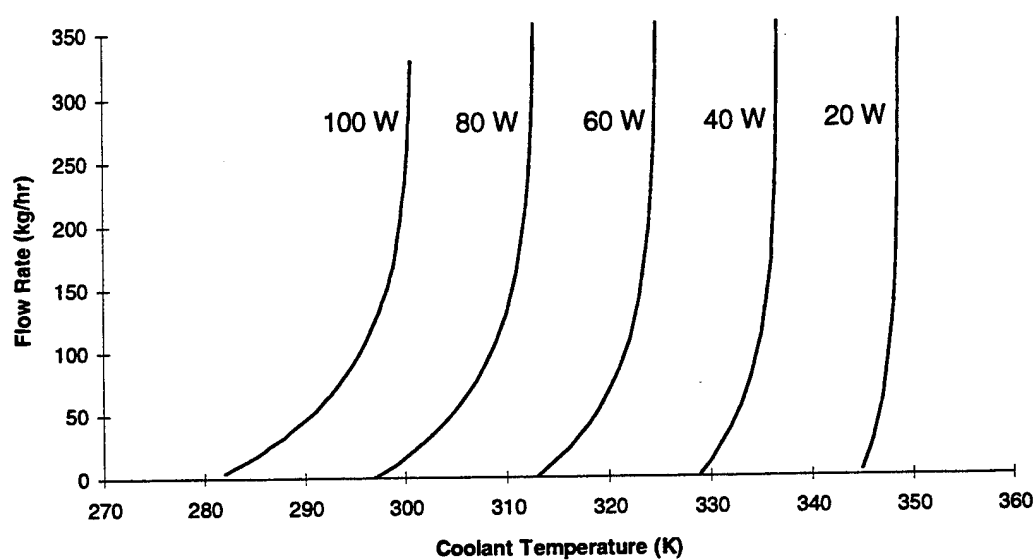
Figure 3.15.   Thermal Performance as a Function of the Heat Load with Thermal Resistances of 0.2 °C/(W/cm²).
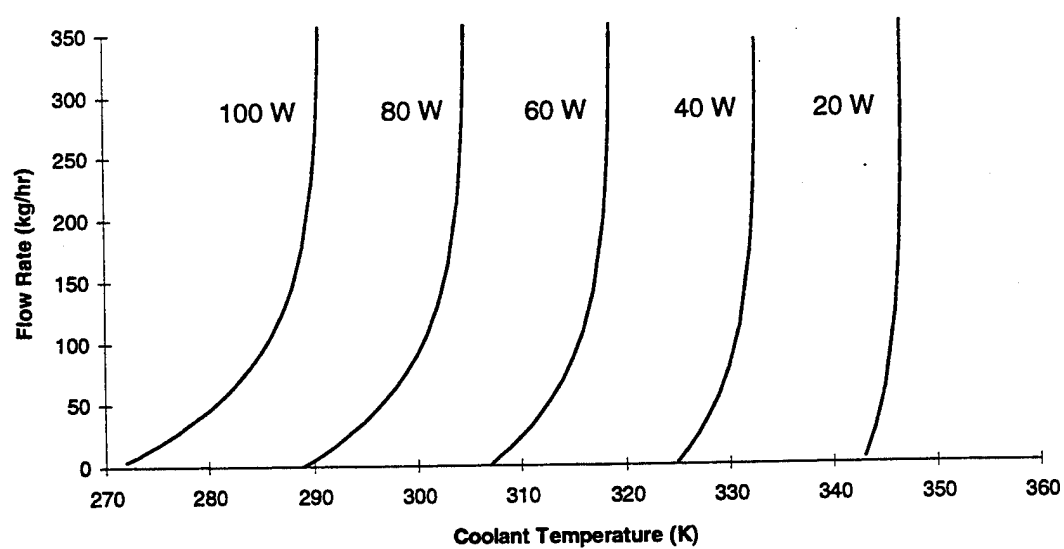
Figure 3.16. Thermal Performance as a Function of the Heat Load with Thermal Resistances of 0.25 °C/(W/cm$^2$).

These curves represent the minimum mass flow rate necessary to remove the inputted heat flux for an inputted coolant temperature. In addition, Figures 3.14 through 3.16, are for the required junction temperature of 90°C. As these plots show, for the lower heat loads (less than 20 W), the necessary mass flow rate is independent of the coolant temperature. For example, if the coolant temperature is below 348 K (75°C), then any flow rate through the HFHE is sufficient to remove a heat flux of 20 W/cm$^2$. However, as the heat load is increased, the necessary mass flow rate becomes dependent on the coolant temperature. For example, to remove a heat flux of 100 W/cm$^2$ with thermal resistances of 0.20 °C/(W/cm$^2$), the minimum necessary mass flow rate is 150 kg/hr at a coolant temperature of 298 K (25°C). However, if the coolant temperature is reduced to 290 K (17°C), then the minimum necessary mass flow rate through the HFHE reduces to 50 kg/hr. Furthermore, if the coolant temperature is reduced below 281 K (8°C), then any mass flow rate through the HFHE will remove 100 W/cm$^2$.

### 3.2.7 Maximum Heat Flux Capability

The heat flux capability of the HFHE may be estimated by extrapolating the results from Equation (3.11) using the operating conditions specified by the Air Force. These operating conditions include a coolant temperature of 0°C and a pressure drop across the HFHE of 311 kPa (45 psi). Therefore, solving Equation (3.11) for the mass flow rate and substituting the operating condition values for the coolant temperature and the pressure drop across the HFHE yields a mass flow rate of 182 kg/hr. Using this value in the HFHE thermal resistance equation, Equation (3.22), the thermal resistance is then solved as a function of the heat flux. This equation can then be substituted into Equation (3.23), and solved for the heat flux, shown as Equation (3.25).

$$\dot{Q} = \frac{T_j - T_f - 2.25}{-\left(R_{cw} + R_{jc}\right) - 0.20 - 0.20e^{(-0.013\dot{m})}} \qquad (3.25)$$

The operating conditions for the HFHE are as follows: a junction temperature, $T_j$, of 363 K (90°C), a coolant temperature, $T_f$, of 273 K (0°C), thermal resistances, $R_{cw}$ and $R_{jc}$, of 0.20 °C/(W/cm$^2$), and a mass flow rate, $\dot{m}$, of 182 kg/hr. With these inputs, the maximum heat flux capability of the HFHE is calculated to be 142.4 W/cm$^2$. However, this

maximum heat flux capability is not an absolute. The maximum heat flux is dependent on the operating coolant temperature and thermal resistances between the case and the junction and between the case and the wall. Therefore, the variation in the heat flux capability for the HFHE is shown in Table 3.4. As a note, for each new coolant temperature, the mass flow rate must be recalculated for the total pressure drop to remain constant at 45 psi (311 kPa). As can be seen, although a higher mass flow rate is possible at the higher coolant temperatures, the coolant temperature remains as the driving factor in the heat flux capability.

As can be seen from Table 3.4, if the refrigeration cycle for the avionic electronic system is capable of coolant temperature below 293 K (20°C) or if the thermal resistance between the junction and the wall of the HFHE can be maintained below 0.2 °C/(W/cm$^2$), then the HFHE's cooling capacity is well above the required 100 W/cm$^2$.

## 3.2.8 Steady-State Comparison

In the only previous study of the thermal performance, McDonnell Douglas [4] presented the thermal performance through plots of the thermal resistance for the HFHE and a maximum heat flux capability. Therefore, the final presentation of the thermal performance curves in this

Table 3.4  Maximum Heat Flux Capability.

| Pressure Drop | | Mass Flow Rate | Junction Temperature | Coolant Temperature | Thermal Resistance (junction to case) | Thermal Resistance (case to wall) | Maximum Heat Flux Capability |
|---|---|---|---|---|---|---|---|
| kPa | (psi) | kg/hr | K | K | $^\circ$C/(W/cm$^2$) | $^\circ$C/(W/cm$^2$) | W/cm$^2$ |
| 311 | 45 | 181.68 | 363 | 273 | 0.20 | 0.20 | 142.40 |
| 311 | 45 | 181.68 | 363 | 273 | 0.25 | 0.25 | 122.52 |
| 311 | 45 | 181.68 | 363 | 273 | 0.15 | 0.15 | 169.99 |
| 311 | 45 | 220.47 | 363 | 293 | 0.20 | 0.20 | 111.27 |
| 311 | 45 | 220.47 | 363 | 293 | 0.25 | 0.25 | 95.57 |
| 311 | 45 | 220.47 | 363 | 293 | 0.15 | 0.15 | 133.14 |

report are unique. Furthermore, it is impossible to compare the thermal resistance of the HFHE presented by McDonnell Douglas and the thermal resistance of the HFHE presented in this report. This is because the thermal resistance presented by McDonnell Douglas is only dependent on the flow rate. This conclusion for the thermal resistance was reached because McDonnell Douglas [4] performed a shotgun test matrix. This analysis with the shotgun approach is shown in Figure 3.17. This figure shows the correlation between conduction heat loss and the flow rate. For this correlation, McDonnell Douglas presents a linear curve dependent on only the flow rate. The data used in this analysis is shown in Table 3.5. In this table, McDonnell Douglas' CHIC site D corresponds to CHIC B, see Figure 1.1, evaluated in this report.

Furthermore, in this table, McDonnell Douglas used the volumetric flow rate for the variance in the flow rate. However, the volumetric flow rate does not reflect the change in density with the coolant temperature. Therefore, comparisons between the different temperatures cannot be made at the same volumetric flow rate. Therefore, the volumetric flow rate used by McDonnell Douglas has been converted into the mass flow rate used in this report. As stated previously, Figure 3.17 indicates a linear function

$$Q_{loss}/Q_{incident} = (0.218 - 0.06313*W_{tot})*N/4$$

where "$W_{tot}$" is the module flow rate in gpm and "N" is the number of adjacent CHICs (N = 4 at Site D).

Note: 100 kg/hr = 0.558 gpm
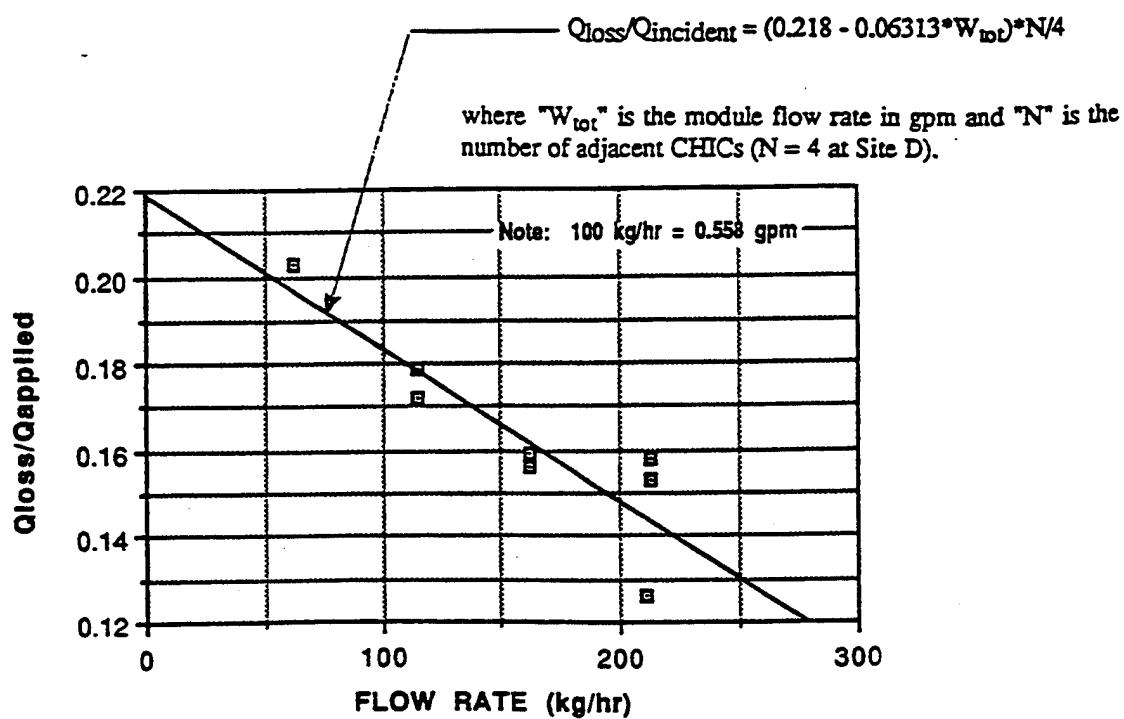
Figure 3.17.   Correlation Between Conduction Heat Loss and Flow Rate [12].

Table 3.5.  McDonnell Douglas' Approach for the Radial Heat Loss.

| Test I.D. | CHIC Site | Coolant Temperature | Coolant Flow Rate | | Amplifier Heat Flux |
|---|---|---|---|---|---|
| | | °C | gpm | kg/min | W |
| 86 | D | 18.80 | 1.18 | 3.56 | 118.94 |
| 83 | D | 20.24 | 1.19 | 3.58 | 101.00 |
| 81 | D | 20.25 | 1.19 | 3.58 | 82.13 |
| 78 | D | 20.25 | 0.90 | 2.71 | 79.41 |
| 80 | D | 20.53 | 0.90 | 2.71 | 79.92 |
| 76 | D | 19.87 | 0.64 | 1.93 | 76.83 |
| 60 | D | 20.01 | 0.64 | 1.93 | 45.47 |
| 74 | D | 20.36 | 0.35 | 1.05 | 78.73 |

dependent on only the flow rate; however, as shown in Figure 3.7, the heat loss due to conduction is also dependent on the coolant temperature. Moreover, as shown in Appendix F, the heat loss due to conduction is dependent on the coolant flow rate, the coolant temperature, and the heat load and this dependency is not a linear relationship.

In the shotgun test matrix used by McDonnell Douglas, only four flow rates were examined: 0.3 gal/min, 0.6 gal/min, 0.9 gal/min, and 1.2 gal/min. In addition, only two heat loads, 50 W/cm$^2$ and 100 W/cm$^2$, and four coolant temperatures, 10°C, 20°C, 30°C, and 40°C, were examined. However, in contrast to the research performed at Oklahoma State University, McDonnell Douglas did not fully represent the heat loads nor the coolant temperatures with all of the flow rates. Therefore, the interpretation of their results did not indicate a dependency of the thermal resistance on the heat load. Any variation in the thermal resistance with the heat load was explained due to the curve fit error.

Because all of the thermal performance characteristics of the HFHE, the radial heat loss due to conduction, the thermal resistance, and the temperature difference between the wall and the fluid temperatures, were considered as functions of only the flow rate by McDonnell Douglas, comparisons between their thermal results and the thermal

performance results presented in this thesis are impratical. Furthermore, McDonnell Douglas did not formulate any thermal performance curves or a thermal performance equation as seen in sections 3.2.4 through 3.2.6. Therefore, the only true comparison that can be made is the maximum heat flux capability of the HFHE. This "maximum" heat flux capability represents the operating conditions of the HFHE: a coolant temperature of 0°C, a pressure drop of 311 kPa (45 psi), and wall-to-case and case-to-junction thermal resistances of 0.2 °C/(W/cm$^2$). With these conditions McDonnell Douglas [4] derived a maximum heat flux of 134 W/cm$^2$. This compares to the maximum heat flux derived in section 3.2.6 of 142 W/cm$^2$. This translates to a 5.6% difference.

However, this relatively close comparison is misleading. For these operating conditions, McDonnell Douglas reported a correlation of a mass flow rate of 329 kg/hr and a wall-to-fluid thermal resistance of 0.270 °C/(W/cm$^2$). However, for the operating conditions of a pressure drop of 45 psi (311 kPa), a coolant temperature of 0°C, and an applied heat load of 100 W/cm$^2$, this report has a correlation of a mass flow rate of 182 kg/hr and a wall-to-fluid thermal resistance of 0.232 °C/(W/cm$^2$). These diversities can be explained by revisiting the previous sections of this report. First, the thermal resistance

calculated by McDonnell Douglas is based on a linear function dependent on only the mass flow rate. However, as expained earlier in this section, the thermal resistance is not a linear function, nor is it solely dependent on the mass flow rate. Moreover, the thermal resistance is a function of the flow rate, coolant temperature, and heat load of the HFHE. Finally, the corresponding mass flow rate for the operating pressure of 311 kPa (45 psi), relates to the hydraulic performance curves obtained in section one of this chapter. McDonnell Douglas proclaims that for a mass flow rate of 329 kg/hr and a coolant temperature of 0°C, the pressure drop across the HFHE is 311 kPa (45 psi). However, as stated in Flynn et al. [4], this pressure drop across the HFHE is lower than the predicted value by Sundstrand. However, as explained in section 3.1.4, for a laminar flow regime the pressure drop across the HFHE should be greater than the pressure drop for a turbulent flow regime that is used as the analytical model used for Sundstrand's predictions. This concept is consistent with the results that at a flow rate of 182 kg/hr and a coolant temperature of 0°C, the pressure drop across the HFHE is 311 kPa (45 psi). McDonnell Douglas' hydraulic results used for their maximum heat flux calculation are not consistent with this concept.

## 3.3 Transient Thermal Performance

While the in-flight performance was modeled with steady state heat loads, the start-up and shut-down performance for the HFHE was modeled with transient heat loads. This performance is presented in the thesis by analyzing the thermal lag of the HFHE as a function of the coolant temperature, mass flow rate, and heat load. Furthermore, the thermal lag is performed by analyzing the HFHE wall temperature.

For the transient tests, the coolant temperature range was reduced to 0°C to 30°C, but still with increments of 10°C. This reduction is valid because the criterion used for analyzing the transient thermal performance, this being the wall temperature of the HFHE, is independent of the coolant temperature. However, as the coolant temperature increases so does the initial wall temperature before a heat load is applied. Therefore, for comparison between different coolant temperatures, the wall temperature must be modified. This modification consists of taking the difference between the wall temperature and the coolant temperature. This is shown in Figures 3.18 and 3.19, for the start-up model and the shut-down model, respectively. Finally, Figures 3.18 and 3.19 are for a mass flow rate of
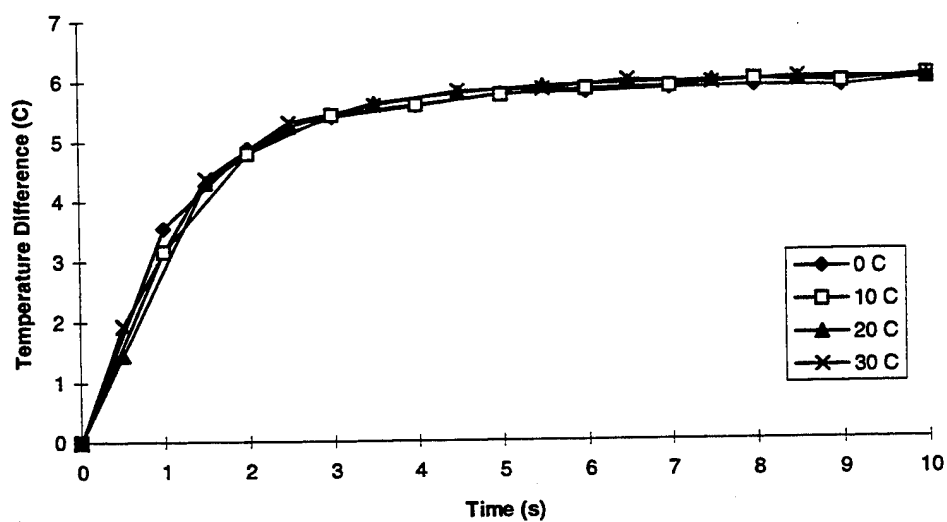
**Figure 3.18.  Thermal Lag of the HFHE During Startup as a
Function of Coolant Temperature (2.5 kg/min, 20 W).**
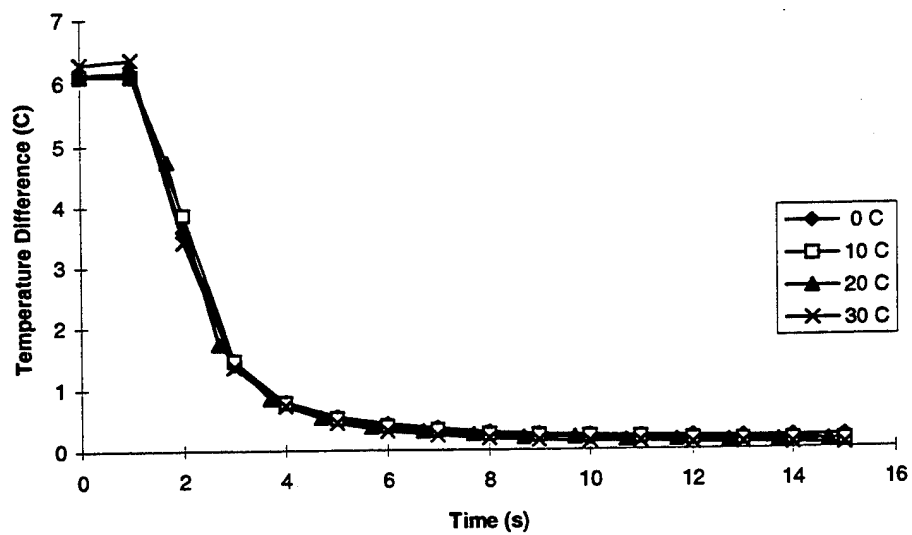
**Figure 3.19.  Thermal Lag of the HFHE during Shutdown as a Function of Coolant Temperature (2.5 kg/min, 20 W).**

2.5 kg/min, and a heat load of 20 W. In addition, the flow rate data points were the same as the flow rate data points for the last three CHICs (for example: 1.0, 1.5, 2.0, 2.5, and 3.0 kg/min for a coolant temperature of 0°C), and the heat load range was reduced to 10 W to 50 W by an increment of 10 W. This reduction of the heat load was due to the upper thermal restrictions of the MiniSystems ceramic heater. The results of the transient tests are presented into two main categories, the start-up and the shut-down models.

### 3.3.1  Performance During Start-Up

The emphasis of this study on the start-up performance of the HFHE regards the relationship of the thermal lag and the dependent parameters:  the mass flow rate, the coolant temperature, and the heat load. However, as Figures 3.18 and 3.19 show, the thermal lag is independent of the coolant temperature. As stated in Chapter II, the start-up performance was obtained by a thermal pulse for thirty seconds, or until thermal equilibrium has been reached. This pulse provides an instantaneous heat flux for the required test load. The thermal lag was then taken as the amount of time necessary for the wall temperatures to reach thermal equilibrium. Figures 3.20 through 3.24 show the
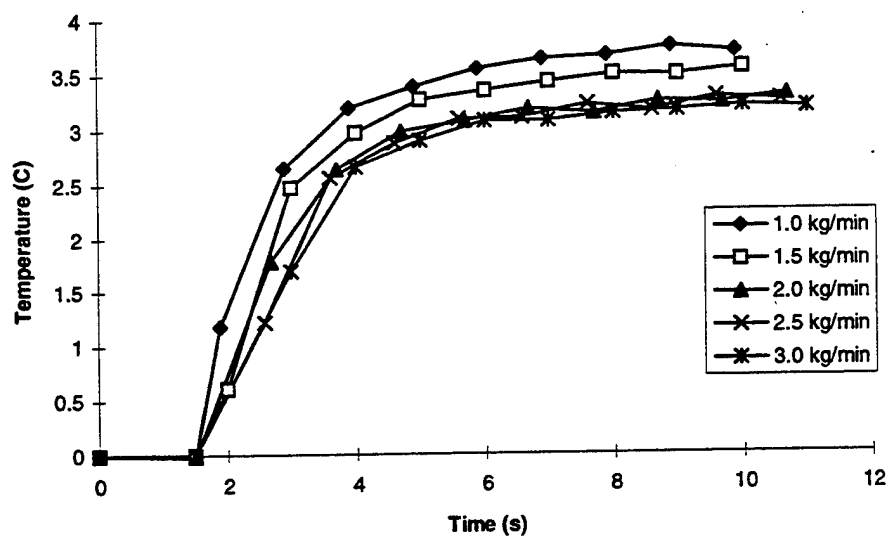
**Figure 3.20. Thermal Lag during Startup for a Heat Load of 10 W and Coolant Temperature of 0°C.**
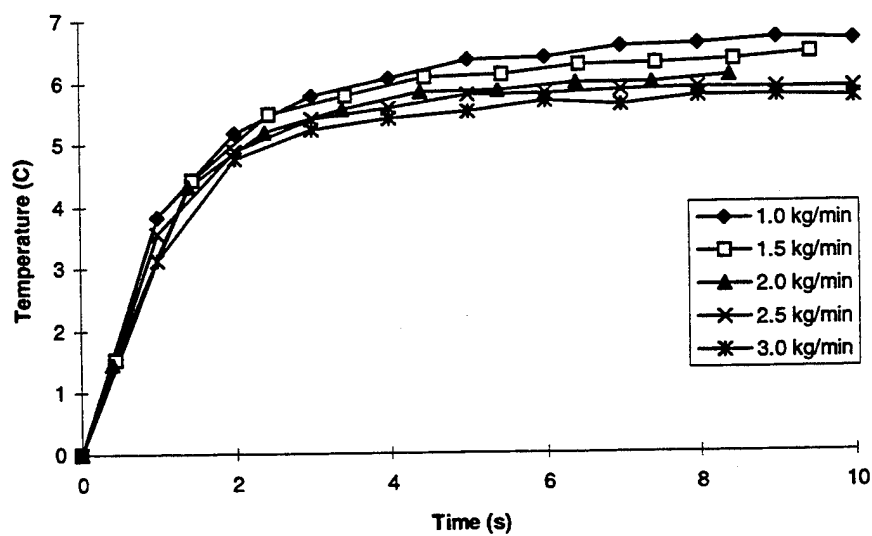
**Figure 3.21. Thermal Lag during Startup for a Heat Load of 20 W and Coolant Temperature of 0°C.**
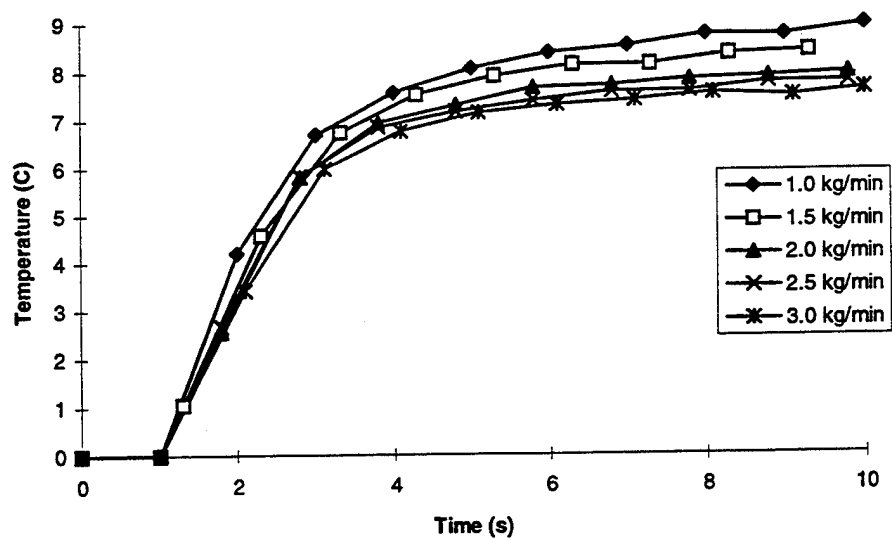
**Figure 3.22. Thermal Lag during Startup for a Heat Load of 30 W and Coolant Temperature of 0°C.**
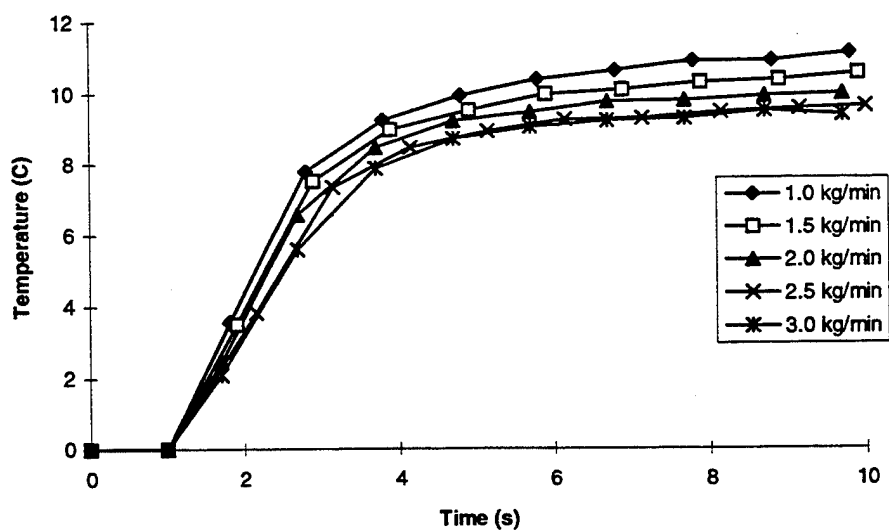
Figure 3.23. Thermal Lag during Startup for a Heat Load of 40 W and Coolant Temperature of 0°C.
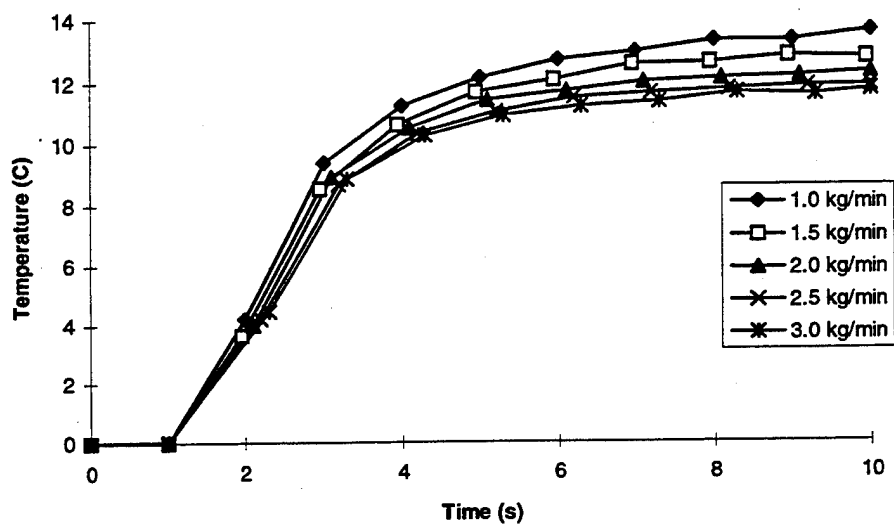
**Figure 3.24. Thermal Lag during Startup for a Heat Load of 50 W and Coolant Temperature of 0°C.**

thermal lag as a function of the mass flow rate. For each of these figures, the coolant temperature was 0°C.

As seen in the above figures, the time for the wall temperature to reach 90% of the thermal equilibrium temperature varies with both the mass flow rate and the heat load. The dependence of the lag time on these parameters are summarized in Table 3.6. As this table indicates, the trends are as follows: as the flow rate is increased, the thermal lag is decreased and as the heat load is increased, the thermal lag is increased. The minimum thermal lag is approximately 2.6 seconds and occurs at a flow rate of 3.0 kg/min and a heat load of 10 W. The maximum thermal lag is approximately 4.25 seconds and occurs at a flow rate of 1.0 kg/min and a heat load of 50 W. However, these results were expected, for as the flow rate is decreased and the heat load is increased, the temperature differential between the coolant temperature and the wall temperature, for steady-state conditions, increases. Therefore, for a constant coolant temperature, the wall temperature increases as the flow rate is decreased and the heat load is increased. Hence, the time to reach the elevated temperatures should increase as shown. The thermal performance during startup is also presented as a function of the heat load in Figures 3.25 through 3.29.

**Table 3.6.  Thermal Lag as a Function of the Heat Load and Mass Flow Rate for a Coolant Temperature of 0°C**

| Flow Rate | 1.0 kg/min | 1.5 kg/min | 2.0 kg/min | 2.5 kg/min | 3.0 kg/min |
|---|---|---|---|---|---|
| Heat Load | Thermal Lag Time | | | | |
| 10 W | 3.65 s | 3.25 s | 3.05 s | 2.75 s | 2.60 s |
| 20 W | 4.00 s | 3.40 s | 3.20 s | 3.00 s | 2.85 s |
| 30 W | 4.10 s | 3.55 s | 3.35 s | 3.25 s | 3.15 s |
| 40 W | 4.20 s | 3.80 s | 3.50 s | 3.35 s | 3.25 s |
| 50 W | 4.25 s | 3.90 s | 3.65 s | 3.50 s | 3.40 s |
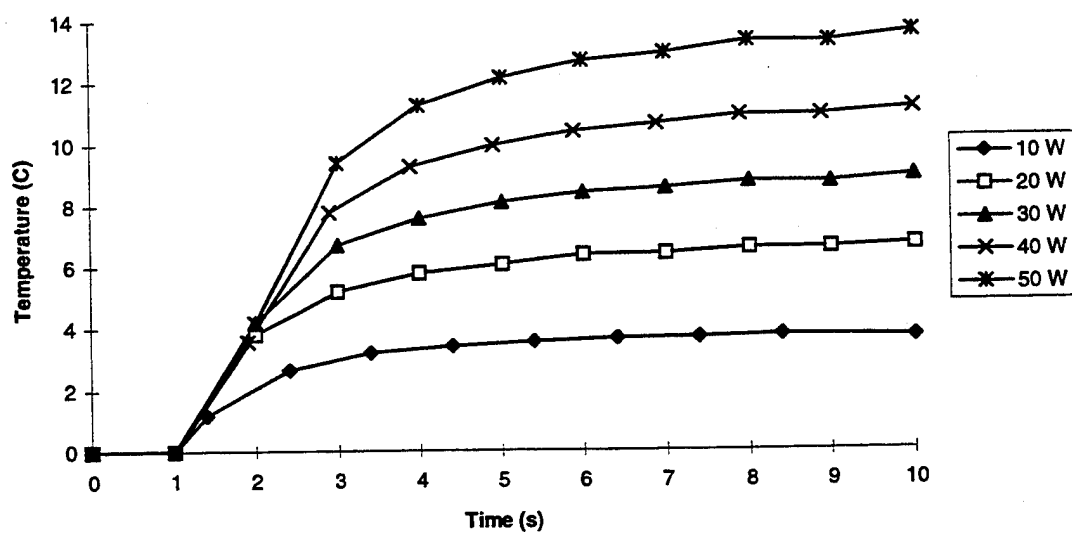
**Figure 3.25. Thermal Lag during Startup for a Flow Rate of 1.0 kg/min and Coolant Temperature of 0°C.**
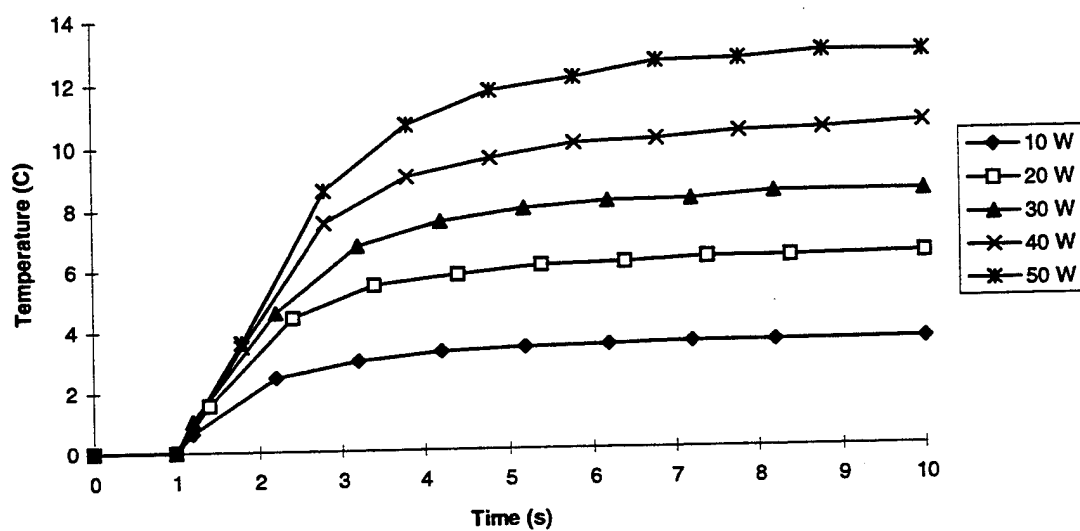
**Figure 3.26.  Thermal Lag during Startup for a Flow Rate of 1.5 kg/min and Coolant Temperature of 0°C.**
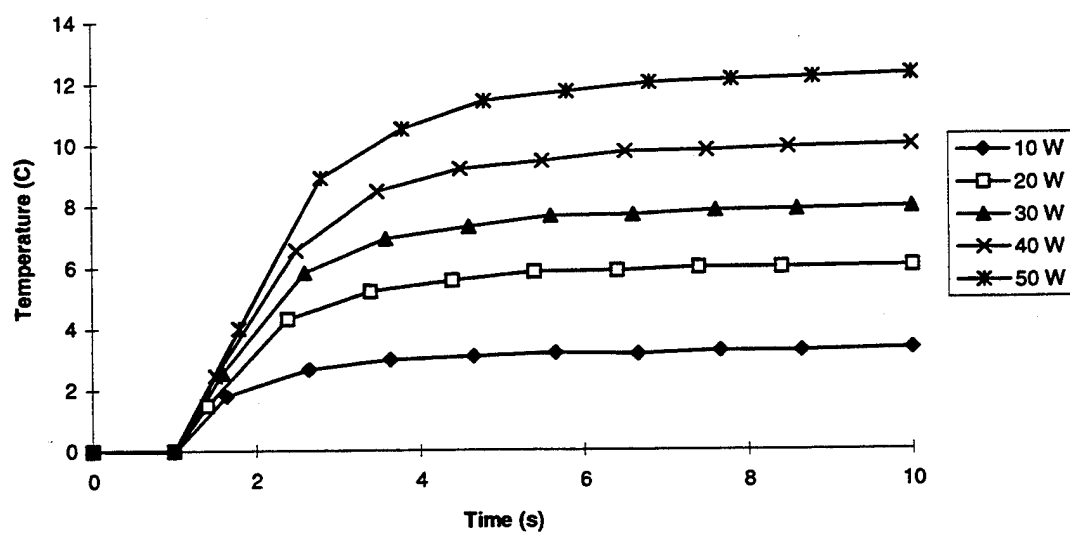
**Figure 3.27.  Thermal Lag during Startup for a Flow Rate of
2.0 kg/min and Coolant Temperature of 0°C.**
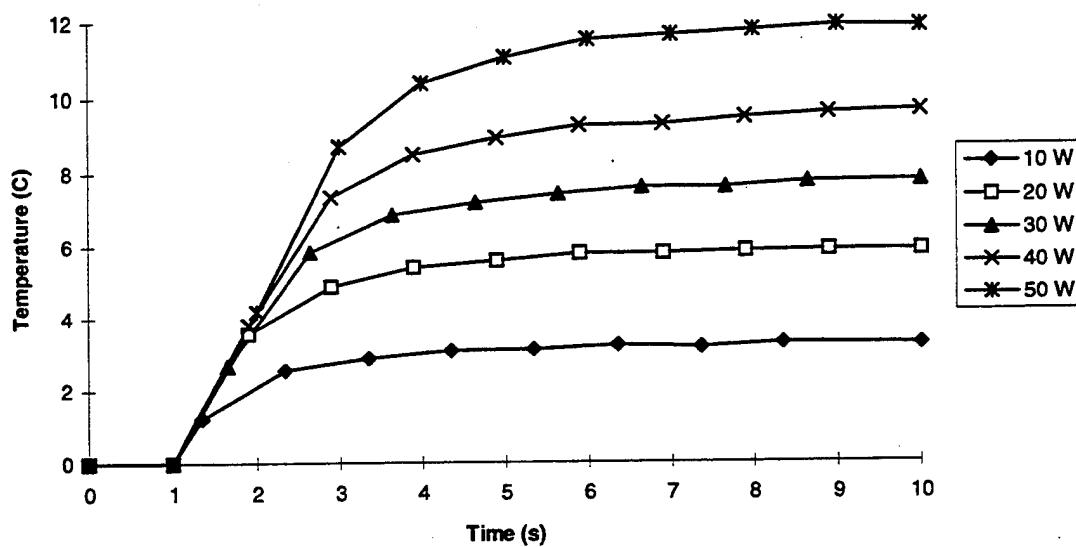
**Figure 3.28. Thermal Lag during Startup for a Flow Rate of 2.5 kg/min and Coolant Temperature of 0°C.**
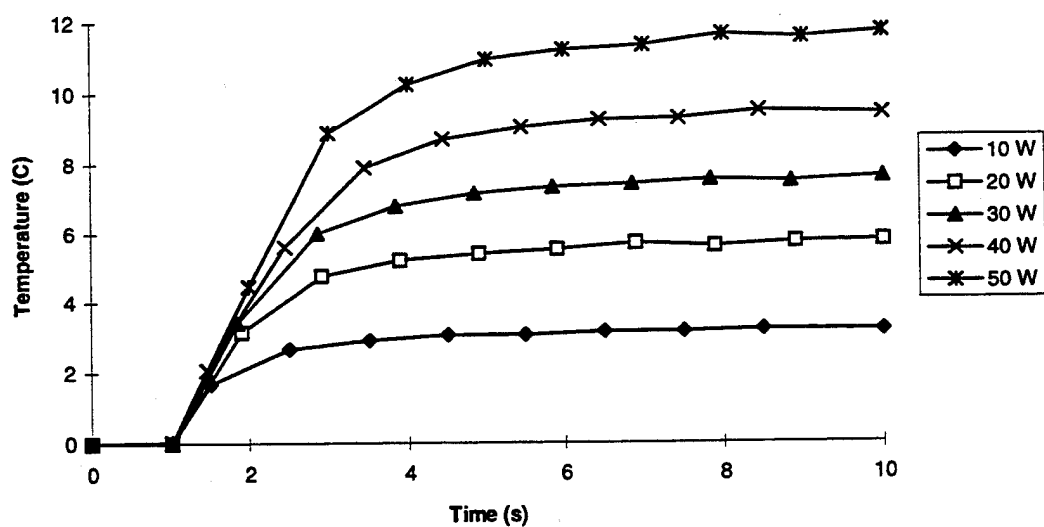
**Figure 3.29.  Thermal Lag during Startup for a Flow Rate of 3.0 kg/min and Coolant Temperature of 0°C.**

## 3.3.2  Performance During Shutdown

The modeling of the thermal performance during the shutdown stage was accomplished by allowing the wall temperature to reach thermal steady-state at a given heat load, then turning off the power to the MiniSystems ceramic heater.  This provides an abrupt end to the heat load pulse. The ranges for the shutdown modeling are retained from the startup modeling, and the time interval is thirty seconds, or until the wall temperature reaches thermal equilibrium. In addition, the presentation of the results for this modeling is retained from the modeling of the startup.  The thermal lag is presented as functions of both the mass flow rate and the heat load.  However, for this thesis the presentation of these results are condensed to only the extreme cases of the heat loads and mass flow rate, for a coolant temperature of 0°C.  This condensed version can be seen in Figures 3.30 and 3.31 for the thermal lag as a function of the flow rate, and in Figures 3.32 and 3.33 for the thermal lag as a function of the heat load.  As before, the trend for the thermal lag is as follows:  the thermal lag time increases as the flow rate decreases and the heat load increases.  The entire spectrum for the thermal lag times are presented in Table 3.7.

**Table 3.7.   Thermal Lag Times During Shutdown for a Coolant Temperature of 0°C.**

| Flow Rate | 1.0 kg/min | 1.5 kg/min | 2.0 kg/min | 2.5 kg/min | 3.0 kg/min |
|---|---|---|---|---|---|
| Heat Load | Thermal Lag Time | | | | |
| 10 W | 3.90 s | 3.80 s | 3.70 s | 3.65 s | 3.60 s |
| 20 W | 4.20 s | 4.00 s | 3.90 s | 3.80 s | 3.75 s |
| 30 W | 4.50 s | 4.20 s | 4.05 s | 3.95 s | 3.90 s |
| 40 W | 4.60 s | 4.40 s | 4.20 s | 4.10 s | 4.00 s |
| 50 W | 4.70 s | 4.50 s | 4.35 s | 4.25 s | 4.20 s |
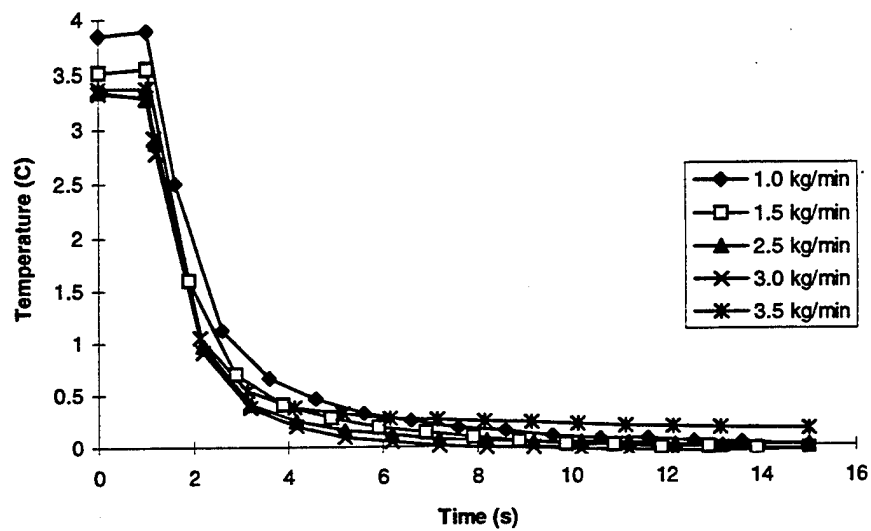
**Figure 3.30. Thermal Lag during Shutdown for a Heat Load of 10 W and Coolant Temperature of 0°C.**
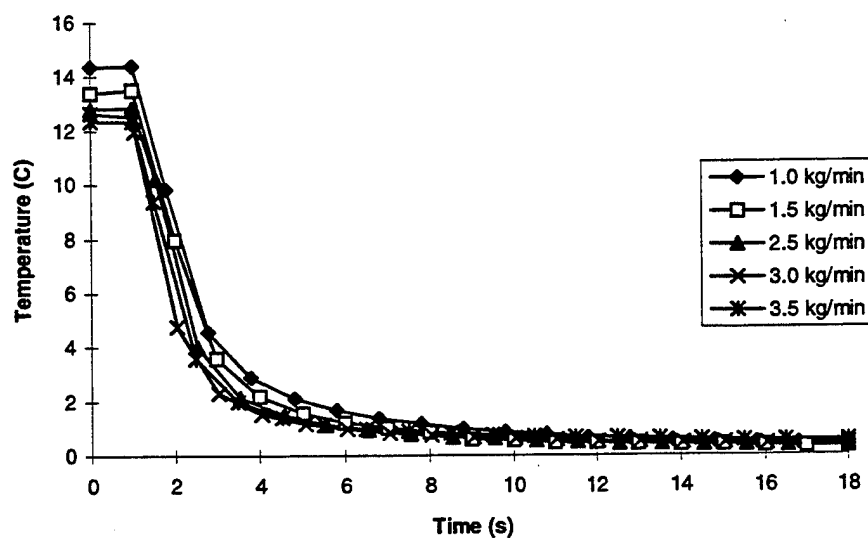
**Figure 3.31. Thermal Lag during Shutdown for a Heat Load of 20 W and Coolant Temperature of 0°C.**
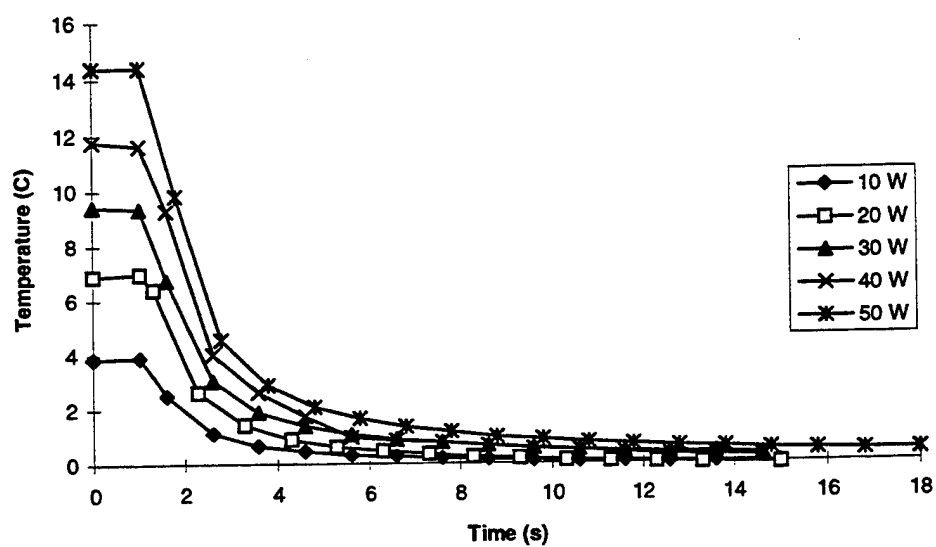
**Figure 3.32. Thermal Lag during Shutdown for a Flow Rate of 1.0 kg/min and Coolant Temperature of 0°C.**
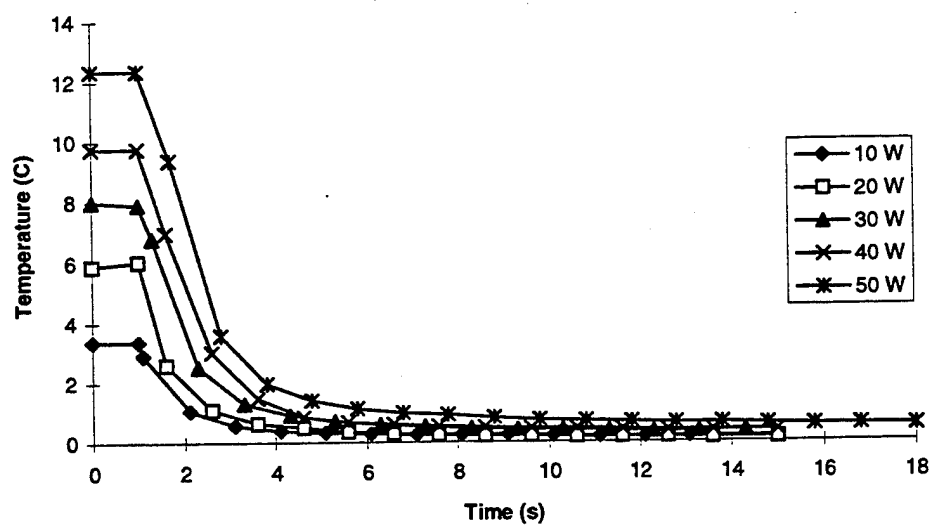
**Figure 3.33. Thermal Lag during Shutdown for a Flow Rate of 3.0 kg/min and Coolant Temperature of 0°C.**

### 3.3.3 Maximum Thermal Lag Times

As seen in Table 3.6, the maximum thermal lag time during startup approaches 4.5 seconds. In addition as seen in Table 3.7, the maximum thermal lag time during shutdown approaches 5.0 seconds. If these values were extrapolated to a heat load of 100 W and allowing for a margin of error, the maximum thermal lag time for the startup is approximately 6.0 seconds. In addition, the maximum thermal lag time during shutdown for a heat load of 100 W is approximately 7.0 seconds

### 3.3.4 Transient Performance Comparison

As the steady-state thermal tests, the only prior analysis of the transient thermal performance of the HFHE was conducted by McDonnell Douglas. For this analysis, three types of transient tests were conducted: a slow ramp to steady-state conditions, full transient testing using a slow ramp, and full transient testing using a fast ramp. However, as stated in the report by Flynn, et al. [4], none of these tests represent a transient load of any specific device. Furthermore, the results presented by McDonnell Douglas focus on both the wall temperature and the heater temperature. However, the heater temperature is dependent on the thermal resistance between the wall and the junction

(in this case, the thermal resistance of the thermal grease between the heater and the HFHE and the thermal resistance of the heater itself). Therefore, the only temperature worth noting is the wall temperature of the HFHE, as presented in this thesis. Furthermore, the abrupt pulsing of the heat load used in this thesis does reflect an actual physical characteristic. This pulsing represents the startup and shutdown of the electronic devices being cooled by the HFHE. Furthermore, the pulsing allows for all of the transient tests to approach a steady-state condition. This follows the reasoning that at startup or shutdown the electronic devices will run or remain off for a considerable length of time producing a steady-state situation. The conclusion made by McDonnell Douglas about the transient tests that "the wall temperature under the condition of increasing heat flux should always be lower than that expected under steady-state conditions" is valid. However, the addition that the wall temperature under the increasing heat flux approaches the steady-state condition should be made.

For both McDonnell Douglas and this thesis, a note should be made that the maximum thermal lag time will vary depending on the thermal resistance of the thermal grease and heat source. Because McDonnell Douglas and this

research used MiniSystems ceramic heaters, the thermal resistance of the heat source should be similar. This allows for comparison between the results.

# CHAPTER IV

## SUMMARY AND CONCLUSIONS

### 4.1 Conclusions

The goals of this thesis as set forth in Chapter 1 were successfully achieved. Construction of a versatile setup was completed, the hydraulic, steady-state thermal, and transient thermal performance of the High Flux Heat Exchanger were studied, a complete data base for all types of performance was assimilated, and performance curves encompassing all of the tests were developed. In this chapter, the accomplishment of the primary objectives set forth in Chapter I will be presented.

### 4.1.1  Experimental Apparatus

Although most of the components in the test loop have been on loan from Wright Laboratories, the setup design itself can be used for future testing of new heat exchangers that meet the SEM-E configuration. Furthermore, the experimental procedure outlined in Chapter II represents a

solid foundation for future experimentation on any high flux

heat exchanger.


## 4.1.2 Hydraulic Performance

The primary objective for the hydraulic performance was

stated as follows:  to investigate the influence of the

coolant flow rate and temperature on the pressure drop

across the inlet and the outlet of the HFHE.  In addition,

this investigation should result in a hydraulic performance

equation and corresponding performance curve with the flow

rate and temperature as the dependent variables.

The investigation of the pressure drop across the inlet

and outlet of the HFHE was completed for a coolant

temperature range of -15°C to 50°C.  Furthermore, for each

coolant temperature, the investigation covered a flow rate

range of 60 kg/hr to 240 kg/hr.  This analysis culminated in

the development of the hydraulic performance equation.  The

model for the hydraulic performance equates the pressure

drop across the HFHE to the sum of the viscous-frictional

losses and the dynamic losses.  The following performance

equation consists of the mass flow rate, kg/hr, and the

coolant temperature, K, as the inputs and yield the pressure

drop in psi. The constants $C_1$, viscous-frictional losses,

and $C_2$, dynamic losses, have values of 7354.83 and 0.428, respectively. The corresponding curve for this equation can be seen in section 3.1.2.

$$\Delta p = C_1 \left[ \left( 10^{\left( \frac{10^{9.67}}{T^{3.923}} \right)} - 0.70 \right) \times 10^{-6} \right] \dot{m}$$

$$+ C_2 \frac{\dot{m}^2}{\left( 1.36 \times 10^3 - 4.56T + 0.0157T^2 - 0.28 \times 10^{-4} T^3 + 0.174 \times 10^{-7} T^4 \right)} \quad (3.11)$$

## 4.1.2  Steady-State Thermal Performance

The objectives set forth in Chapter I for the steady-state thermal tests was to investigate the influence of the coolant flow rate and temperature on the heat flux removal capabilities of the HFHE for steady-state heat loads.  This investigation should result in a thermal performance curve and correlating equation for the necessary coolant flow rate with respect to the coolant temperature to achieve a given amount of heat flux removal (e.g.  one performance curve for 100 Watts of heat flux removal, one performance curve for 80 Watts of heat flux removal, etc.).  However, to accomplish this investigation, several thermal characteristics of the HFHE were necessary.  The characteristics included the conducted radial heat loss, the wall temperature at the

surface of each CHIC, and the thermal resistance of the
HFHE.

The simplification of applying a heat load to one CHIC
at a time is valid under the assumption that all twenty
CHICs perform identically and independently.  However, this
simplification causes an error in the net heat flux
measurement through the CHIC.  This error occurs as a
portion of the heat flux is removed radially by the
surrounding CHICs.  Therefore an analytical expression was
developed for the radial heat loss due to conduction.  This
heat loss is presented as a ratio of the heat loss per heat
load and is equivalent to an exponential decay, dependent on
the coolant temperature, the heat load applied, and the mass
flow rate.  The equation for the heat loss, at a constant
heat flux is given by the following equation.  The
coefficients for this equation are shown in Appendix F, for
each heat load examined.

$$\frac{\dot{Q}_{loss}}{\dot{Q}_{applied}} = \phi_1 + \left(\phi_2 + \phi_3 e^{(\phi_4 T)}\right) e^{\left(\left(\phi_5 + \phi_6 e^{(\phi_7 T)}\right)\dot{m}\right)} \tag{3.18}$$

The next thermal characteristic of the HFHE is the wall
temperature at the surface of the individual CHIC.  This
equation is derived by the use of the measured wall

temperature and the net heat flux through the HFHE derived from Equation (3.18). However, for the use of the wall temperature equation under normal heat load conditions (heat loads applied to all 20 CHICs at once), the applied heat load is used. This is due to the fact that the applied heat load is equivalent to the net heat load under normal heat load conditions. The wall temperature, °C, is equivalent to the sum of the fluid temperature, °C, and an exponential decay that is a function of the mass flow rate, kg/hr, and the applied heat load, W, shown in Equation (3.20).

$$T_w - T_f = \lambda_0 + \left(\lambda_1 + \lambda_2 e^{(\lambda_3 \dot{m})}\right)\dot{Q} \qquad (3.20)$$

For this equation the coefficients are as follows: $\lambda_0$ (2.25), $\lambda_1$ (0.19779), $\lambda_2$ (0.19968), and $\lambda_3$ (-0.013115). These coefficients are valid for all of the mass flow rates, coolant temperatures, and applied heat loads. The last thermal characteristic of the HFHE is its thermal resistance. This equation is developed by equating the thermal resistance, °C/(W/cm$^2$), to the difference between the wall temperature, °C, and the coolant temperature, °C, divided by the applied heat load, W.

$$R_{wf} = \frac{2.25 + \left(0.20 + 0.20e^{(-0.013\dot{m})}\right)\dot{Q}}{\dot{Q}} \qquad (3.22)$$

Using the thermal resistance equation, the steady-state thermal performance equation was developed. This equation indicates that the mass flow rate, $\dot{m}$ (kg/hr), is a logarithmic function of the wall-to-case thermal resistance, $R_{cw}$ (°C/(W/cm$^2$)), case-to-junction thermal resistance, $R_{jc}$ (°C/(W/cm$^2$)), applied heat load, $\dot{Q}$ (W), junction temperature, $T_j$ (K), and coolant temperature, $T_f$ (K).

$$\dot{m} = -76.24 \ln\left[5.01\left(\frac{-R_{cw}\dot{Q} - R_{jc}\dot{Q} - 2.25 - 0.20\dot{Q} + T_j - T_f}{\dot{Q}}\right)\right] \qquad (3.24)$$

This equation represents the *minimum* mass flow rate required to remove the given applied heat load. However, because this equation does not register the impossibility of negative flow rates, the following logical statement must be included.

IF $\dot{m}_{measured} \leq 0.0$: THEN $\dot{m}_{actual} = 0.0$

ELSE $\dot{m}_{actual} = \dot{m}_{measured}$

The steady-state thermal test investigation was completed
with the presentation of the steady-state performance
curves, shown in section 3.2.6.

## 4.1.4  Transient Thermal Performance

The third objective of this research was to investigate
the influence of the coolant flow rate and temperature on
the heat flux removal capabilities of the HFHE for transient
heat loads.  This investigation should result in graphical
presentation of the thermal lag of the HFHE.  This
presentation was for the startup and shutdown conditions of
the HFHE.  Through this investigation, it was determined
that the thermal lag of the HFHE was dependent on the heat
load applied and the mass flow rate.  However, the thermal
lag of the HFHE is independent of the coolant temperature.
Moreover, as the figures in section 3.3 indicate, the
thermal lag increases as the mass flow rate decreases and
the applied heat load increases.

## 4.1.5  Overall Performance

The last objective of this research was to develop a
guideline for the overall performance of the HFHE.  This
consisted of a performance chart and correlating equation

combining the hydraulic performance and the steady-state

performance curves.  The completion of this objective can be

seen in Figures 4.1 and 4.2.  However, another prime

directive of the overall performance not included in this

objective is the determination of the input parameter that

drives the HFHE performance.

As seen in Figure 3.12, the critical parameter for the

performance of the HFHE is the coolant temperature.  If the

coolant temperature is kept below 20°C, then the

corresponding minimum flow rate for a cooling rate of 100 W

per CHIC can be kept under 70 kg/hr.  To further show the

importance of the coolant temperature on the performance of

the HFHE, Equation (3.24), the mass flow rate as a function

of the coolant temperature for an applied heat load of 100 W

per CHIC, was substituted into Equation (3.11), the pressure

drop as a function of the flow rate and the coolant

temperature.  The result is an equation for the pressure

drop as a function of the coolant temperature for an applied

heat load of 100 W per CHIC.  This result is shown in Figure

4.1, and, as expressed earlier, if the coolant temperature

can be kept below 20°C, then the minimum pressure drop

across the HFHE needed for a cooling rate of 100 W per CHIC

is 7.2 psi.  However, the pressure drop in this equation is

the dynamic pressure drop only.  As expressed in the
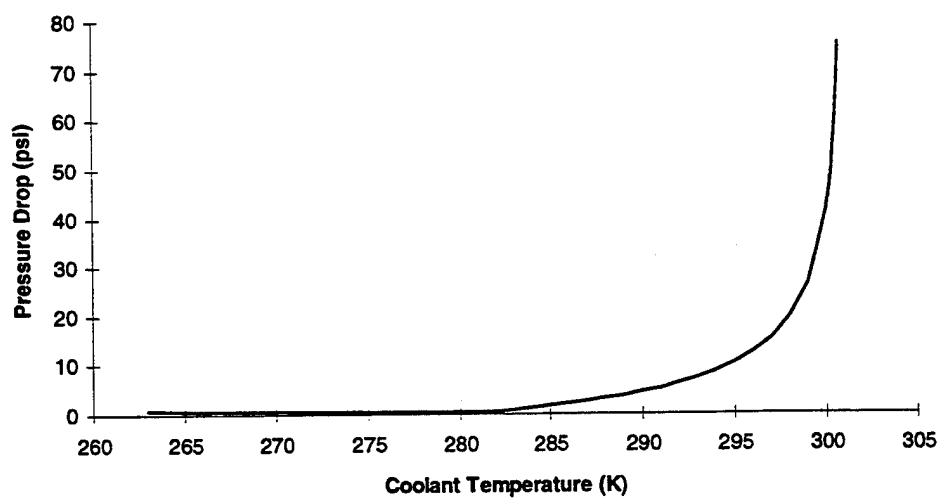
**Figure 4.1.  Dynamic Hydraulic Performance Curve for the Minimum Cooling Rate of 100 W per CHIC.**

hydraulic section of this report, as the fluid temperature decreases below 18°C, the viscosity of the fluid begins to increase exponentially. Therefore, as the coolant flow rate reaches extremely low values, <0.5 kg/hr, the Reynolds' number approaches zero. This caused the friction factor, which is inversely proportional to the flow rate, to become very large. Therefore, the pressure drop needed to initiate the flow through the HFHE will be substantially larger than the dynamic pressure drop across the HFHE when the coolant temperature is below 0°C. Hence, it is critical that the inlet temperature remain between 0°C and 20°C. In a practical sense, this can be accomplished by placing a temperature sensor in the actual electronic coolant loop. This sensor should trigger a secondary refrigeration/heater unit to maintain the coolant temperature between 0°C and 20°C. In addition, a control device should be included in the electronic coolant loop to control the flow rate as the coolant temperature varies. Finally, if the above conditions are met, a pump for the electronic coolant loop can be sized by the performance curve pressure and the pressure drop through the rest of the coolant loop.

However, the requirement for 100 W/cm$^2$ of heat flux removal represents future possibilities for electronic devices. Modern electronic devices operate at lower

temperatures and need lower heat flux removal than future expectations. Therefore, for a complete analysis of the HFHE, the overall performance curves were plotted for the complete range of heat loads, and is shown in Figure 4.2.

The curves represent the minimum pressure drop across the HFHE necessary for the removal of the correlating heat flux. However, these curves represent the dynamic pressure drop. Therefore, the pressure drop needed to initiate the flow might be slightly higher.

## 4.2  Summation

As alluded in section one of this chapter, the results of this analysis on the HFHE differ from previous experimentation. The results from this analysis are far more detailed and includes wider parameter ranges and more internal data points. In addition, for the final correlations, an increased number of dependent variables have been investigated than the previous documentations. However, the discrepencies are consistent with the factors introduced in Chapter III, a laminar flow regime instead of a turbulent flow regime and McDonnell Douglas' simplifications in the modeling of the thermal resistance of the HFHE. Because of all of these factors, it is believed that these results retained in this independent research contains more accuracy than the aforementioned results.
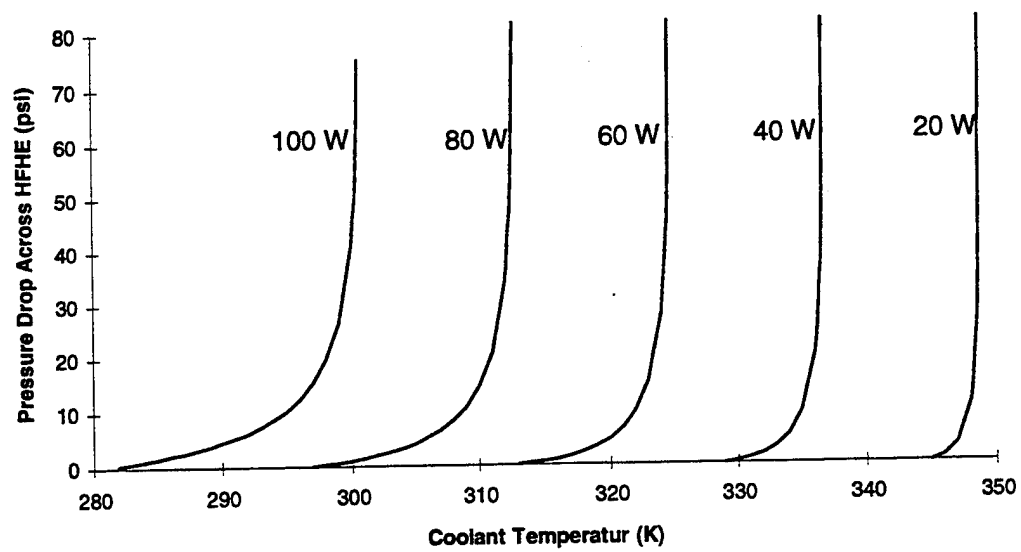
Figure 4.2. Performance Curves with Thermal Resistances of 0.2 °C/(W/cm$^2$).

REFERENCES

1.    Mackowski, M. J., "Requirements for High Flux Cooling
      of Future Avionics Systems," SAE Paper No. 912104,
      September 1991.

2.    Flynn, E. M., "Evaluation of Cooling Concepts for High
      Power Avionics Applications," SAE Paper No. 921942,
      October 1992.

3.    Bland, T. J., Niggemann, R. E., and Parekh, M. B., "A
      Compact High Intensity Cooler (CHIC)," SAE Paper No.
      831127, July 1983.

4.    Flynn, E. M., Downing, R. S., and Nguyen, D. C., "High
      Flux Heat Exchanger," Wright Laboratory Final Report
      No. WL-TR-94-2043, February 1994.

5.    Bland, T. J., Ciaccio, M. P., Downing, R. S., and
      Smith, W.G., "The Development of Advanced Cooling
      Methods for High-Power Electronics," SAE Paper No.
      901962, October 1990.

6.    Grote, M. G., Hendron, R. E., Kipp, H. W., and
      Lapinski, J. R., "Test Results of Wafer Thin Coolers at
      Heat Fluxes from 5 to 125 W/cm$^2$," SAE Paper No.
      880997, July 1988.

7.    Flynn, E. M., and Mackowski, M. J., "High Flux Heat
      Exchanger," Wright Laboratory Interim Report No. WL-
      TR-93-2027, January 1993.

8.    Gschwender, L. J., Snyder, C. E., and Conte, A. A.,
      "Polyalphaolefins as Candidate Replacements for
      Silicate Ester Dielectric Coolants in Military
      Applications," Lubrication Engineering Journal, Vol.
      41, No. 4, pp. 221-228, April 1985.

9.    Zoppoth, R. C., and Dillard, J., "PAO Report: Extended
      Testing of Polyalphaolefins as a Dielectric/Coolant
      Fluid," Texas Instruments, Defense Systems and
      Electronics Group, Dallas, Tx, July 1988.

10.   Ghajar, A. J., "Comparison of Hydraulic and Thermal
      Performances of PAO and Coolanol 25R Liquid Coolants,"
      Final Report, Summer Faculty Research Program, Wright
      Laboratory, August 1993.

11.   Flynn, E.M., Personal Communication, Summer 1994.

12. Granger, R. A., _Fluid Mechanics_. CBS College
    Publishing, New York, 1985.

13. Ghajar, A. J., Tang, W. C., and Beam, J. E.,
    "Methodology for Comparison of Hydraulic and Thermal
    Performance of Alternative Heat Transfer Fluids in
    Complex Systems," _Heat Transfer Engineering_, Vol. 16,
    No. 1, pp. 68-72, 1995.

APPENDICES

APPENDIX A


DATA MEASUREMENTS


Because of fluctuations in the output signals of the data collecting components in the test loop, an average value is used for each individual parameter. However, it must be determined how many measurements to take to get the actual average. If an insufficient number of measurements are taken, then a false reading will occur. However, an overly sufficient number of measurements will create redundancy, take up needed disk space, and prolong the data reduction procedure. Therefore, this appendix will examine the required number of data points for the hydraulic and steady-state thermal tests.


A.1  Hydraulic Tests

To examine the required number of data points needed for sufficient accuracy, 100 data points were recorded for the hydraulic tests at a coolant temperature of 10°C and a mass flow rate of 2.5 kg/min. For the hydraulic tests, the important parameters are the coolant temperature, mass flow

rate, pressure drop across the HFHE, and the density of the coolant. In addition, the room temperature was measured, because of its consistency, to portray the individual output fluctuations of the thermocouples.

For this analysis, a running average was calculated for each parameter. This average was then compared to the prior average to determine the effect of the fluctuated value of the parameter on the running average. A value of 0.0099 was selected, arbitrarily, as the largest difference possible for sufficient accuracy. The individual measurement, the running average, and the average difference can be seen for the coolant temperature and the room temperature in Table A.1 and for the pressure drop across the HFHE and the mass flow rate in Table A.2.

The density of the coolant is not measured directly and is solely dependent on the coolant temperature. Therefore, the number of measurements for a sufficient accuracy for the coolant temperature is also a sufficient number for the accuracy of the density of the coolant. As can be seen, the value of the difference between the averages never exceeds 0.001 after 13 data measurements. Therefore, to provide a small factor of safety, 15 data measurements was concluded to be sufficient for the accuracy of the overall average of the parameters.

## Table A.1. Required Measurements for Sufficient Accuracy for the Coolant and Room Temperature.

| Channel | 50 | Coolant | Temperature | 51 | Room | Temperature |
|---|---|---|---|---|---|---|
| Number of Data Points | Individual Data Point | Running Average | Difference of Averages | Individual Data Point | Running Average | Difference of Averages |
| | (°C) | (°C) | (°C) | (°C) | (°C) | (°C) |
| 1 | 9.784 | 9.784 | | 22.593 | 22.593 | |
| 2 | 9.686 | 9.735 | -0.049 | 22.511 | 22.552 | -0.041 |
| 3 | 9.981 | 9.817 | 0.082 | 22.669 | 22.591 | 0.039 |
| 4 | 9.706 | 9.78925 | -0.02775 | 22.413 | 22.5465 | -0.0445 |
| 5 | 9.733 | 9.778 | -0.01125 | 22.344 | 22.506 | -0.0405 |
| 6 | 9.961 | 9.8085 | 0.0305 | 22.49 | 22.50333 | -0.00267 |
| 7 | 9.965 | 9.830857 | 0.022357 | 22.567 | 22.51243 | 0.009095 |
| 8 | 9.828 | 9.8305 | -0.00036 | 22.418 | 22.50063 | -0.0118 |
| 9 | 9.934 | 9.842 | 0.0115 | 22.468 | 22.497 | -0.00363 |
| 10 | 10.021 | 9.8599 | 0.0179 | 22.652 | 22.5125 | 0.0155 |
| 11 | 9.91 | 9.864455 | 0.004555 | 22.338 | 22.49664 | -0.01586 |
| 12 | 10.052 | 9.880083 | 0.015629 | 22.365 | 22.48567 | -0.01097 |
| 13 | 9.782 | 9.872538 | -0.00754 | 22.312 | 22.47231 | -0.01336 |
| 14 | 9.758 | 9.864357 | -0.00818 | 22.601 | 22.4815 | 0.009192 |
| 15 | 9.879 | 9.865333 | 0.000976 | 22.56 | 22.48673 | 0.005233 |
| 16 | 9.848 | 9.86425 | -0.00108 | 22.564 | 22.49156 | 0.004829 |
| 17 | 10.011 | 9.872882 | 0.008632 | 22.626 | 22.49947 | 0.007908 |
| 18 | 9.83 | 9.8705 | -0.00238 | 22.552 | 22.50239 | 0.002918 |
| 19 | 9.998 | 9.877211 | 0.006711 | 22.584 | 22.50668 | 0.004295 |
| 20 | 10.014 | 9.88405 | 0.006839 | 22.645 | 22.5136 | 0.006916 |
| 21 | 9.814 | 9.880714 | -0.00334 | 22.465 | 22.51129 | -0.00231 |
| 22 | 10.061 | 9.888909 | 0.008195 | 22.618 | 22.51614 | 0.004851 |
| 23 | 9.748 | 9.882783 | -0.00613 | 22.545 | 22.51739 | 0.001255 |
| 24 | 9.943 | 9.885292 | 0.002509 | 22.56 | 22.51917 | 0.001775 |
| 25 | 9.802 | 9.88196 | -0.00333 | 22.263 | 22.50892 | -0.01025 |
| 26 | 9.819 | 9.879538 | -0.00242 | 22.283 | 22.50023 | -0.00869 |
| 27 | 10.019 | 9.884704 | 0.005165 | 22.535 | 22.50152 | 0.001288 |
| 28 | 10.034 | 9.890036 | 0.005332 | 22.535 | 22.50271 | 0.001196 |
| 29 | 9.873 | 9.889448 | -0.00059 | 22.577 | 22.50528 | 0.002562 |
| 30 | 9.768 | 9.8854 | -0.00405 | 22.462 | 22.50383 | -0.00144 |
| 31 | 9.677 | 9.878677 | -0.00672 | 22.256 | 22.49584 | -0.00799 |
| 32 | 9.815 | 9.876688 | -0.00199 | 22.318 | 22.49028 | -0.00556 |
| 33 | 10.107 | 9.883667 | 0.006979 | 22.59 | 22.4933 | 0.003022 |
| 34 | 10.039 | 9.888235 | 0.004569 | 22.368 | 22.48962 | -0.00369 |
| 35 | 9.926 | 9.889314 | 0.001079 | 22.529 | 22.49074 | 0.001125 |
| 36 | 9.793 | 9.886639 | -0.00268 | 22.444 | 22.48944 | -0.0013 |
| 37 | 9.714 | 9.881973 | -0.00467 | 22.265 | 22.48338 | -0.00607 |
| 38 | 9.867 | 9.881579 | -0.00039 | 22.327 | 22.47926 | -0.00412 |
| 39 | 10.008 | 9.884821 | 0.003242 | 22.494 | 22.47964 | 0.000378 |
| 40 | 9.824 | 9.8833 | -0.00152 | 22.285 | 22.47478 | -0.00487 |
| 41 | 9.691 | 9.87861 | -0.00469 | 22.242 | 22.4691 | -0.00568 |
| 42 | 10.013 | 9.88181 | 0.0032 | 22.499 | 22.46981 | 0.000712 |

Table A.1. ( cont.)

| Channel | 50 | Coolant | Temperature | 51 | Room | Temperature |
|---|---|---|---|---|---|---|
| Number of Data Points | Individual Data Point | Running Average | Difference of Averages | Individual Data Point | Running Average | Difference of Averages |
|  | (°C) | (°C) | (°C) | (°C) | (°C) | (°C) |
| 43 | 9.836 | 9.880744 | -0.00107 | 22.258 | 22.46488 | -0.00493 |
| 44 | 9.797 | 9.878841 | -0.0019 | 22.247 | 22.45993 | -0.00495 |
| 45 | 9.817 | 9.877467 | -0.00137 | 22.266 | 22.45562 | -0.00431 |
| 46 | 10.061 | 9.881457 | 0.00399 | 22.576 | 22.45824 | 0.002617 |
| 47 | 10.076 | 9.885596 | 0.004139 | 22.603 | 22.46132 | 0.00308 |
| 48 | 9.699 | 9.881708 | -0.00389 | 22.323 | 22.45844 | -0.00288 |
| 49 | 10.002 | 9.884163 | 0.002455 | 22.461 | 22.45849 | 5.23E-05 |
| 50 | 9.917 | 9.88482 | 0.000657 | 22.508 | 22.45948 | 0.00099 |
| 51 | 9.959 | 9.886275 | 0.001455 | 22.446 | 22.45922 | -0.00026 |
| 52 | 9.762 | 9.883885 | -0.00239 | 22.255 | 22.45529 | -0.00393 |
| 53 | 9.747 | 9.881302 | -0.00258 | 22.255 | 22.45151 | -0.00378 |
| 54 | 9.854 | 9.880796 | -0.00051 | 22.274 | 22.44822 | -0.00329 |
| 55 | 9.905 | 9.881236 | 0.00044 | 22.336 | 22.44618 | -0.00204 |
| 56 | 10.046 | 9.884179 | 0.002942 | 22.558 | 22.44818 | 0.001997 |
| 57 | 9.987 | 9.885982 | 0.001804 | 22.603 | 22.45089 | 0.002716 |
| 58 | 9.871 | 9.885724 | -0.00026 | 22.535 | 22.45234 | 0.00145 |
| 59 | 9.976 | 9.887254 | 0.00153 | 22.52 | 22.45349 | 0.001147 |
| 60 | 9.775 | 9.885383 | -0.00187 | 22.367 | 22.45205 | -0.00144 |
| 61 | 9.725 | 9.882754 | -0.00263 | 22.234 | 22.44848 | -0.00357 |
| 62 | 9.941 | 9.883694 | 0.000939 | 22.386 | 22.44747 | -0.00101 |
| 63 | 10.05 | 9.886333 | 0.00264 | 22.433 | 22.44724 | -0.00023 |
| 64 | 9.866 | 9.886016 | -0.00032 | 22.299 | 22.44492 | -0.00232 |
| 65 | 9.972 | 9.887338 | 0.001323 | 22.356 | 22.44355 | -0.00137 |
| 66 | 9.733 | 9.885 | -0.00234 | 22.242 | 22.4405 | -0.00305 |
| 67 | 10.05 | 9.887463 | 0.002463 | 22.406 | 22.43999 | -0.00051 |
| 68 | 9.891 | 9.887515 | 5.20E-05 | 22.437 | 22.43994 | -4.40E-05 |
| 69 | 9.843 | 9.88687 | -0.00065 | 22.246 | 22.43713 | -0.00281 |
| 70 | 10.06 | 9.889343 | 0.002473 | 22.4 | 22.4366 | -0.00053 |
| 71 | 9.989 | 9.890746 | 0.001404 | 22.533 | 22.43796 | 0.001358 |
| 72 | 9.863 | 9.890361 | -0.00039 | 22.38 | 22.43715 | -0.0008 |
| 73 | 9.743 | 9.888342 | -0.00202 | 22.266 | 22.43481 | -0.00234 |
| 74 | 9.896 | 9.888446 | 0.000103 | 22.472 | 22.43531 | 0.000503 |
| 75 | 9.715 | 9.886133 | -0.00231 | 22.236 | 22.43265 | -0.00266 |
| 76 | 9.88 | 9.886053 | -8.10E-05 | 22.358 | 22.43167 | -0.00098 |
| 77 | 10.042 | 9.888078 | 0.002025 | 22.557 | 22.4333 | 0.001628 |
| 78 | 10.116 | 9.891 | 0.002922 | 22.584 | 22.43523 | 0.001932 |
| 79 | 10.072 | 9.893291 | 0.002291 | 22.512 | 22.4362 | 0.000972 |
| 80 | 10.147 | 9.896462 | 0.003171 | 22.542 | 22.43753 | 0.001322 |
| 81 | 9.998 | 9.897716 | 0.001254 | 22.527 | 22.43863 | 0.001105 |
| 82 | 9.861 | 9.897268 | -0.00045 | 22.366 | 22.43774 | -0.00089 |
| 83 | 9.738 | 9.895349 | -0.00192 | 22.201 | 22.43489 | -0.00285 |
| 84 | 9.693 | 9.89294 | -0.00241 | 22.459 | 22.43518 | 0.000287 |
| 85 | 9.85 | 9.892435 | -0.00051 | 22.313 | 22.43374 | -0.00144 |

**Table A.1. ( cont.)**

| Channel | 50 | Coolant | Temperature | 51 | Room | Temperature |
|---------|-----|---------|-------------|-----|------|-------------|
| Number of Data Points | Individual Data Point | Running Average | Difference of Averages | Individual Data Point | Running Average | Difference of Averages |
| | (°C) | (°C) | (°C) | (°C) | (°C) | (°C) |
| 86 | 9.85 | 9.891942 | -0.00049 | 22.313 | 22.43234 | -0.0014 |
| 87 | 9.728 | 9.890057 | -0.00188 | 22.248 | 22.43022 | -0.00212 |
| 88 | 9.881 | 9.889955 | -0.0001 | 22.325 | 22.42902 | -0.0012 |
| 89 | 9.802 | 9.888966 | -0.00099 | 22.236 | 22.42685 | -0.00217 |
| 90 | 9.802 | 9.888 | -0.00097 | 22.248 | 22.42487 | -0.00199 |
| 91 | 9.924 | 9.888396 | 0.000396 | 22.34 | 22.42393 | -0.00093 |
| 92 | 9.889 | 9.888402 | 6.57E-06 | 22.52 | 22.42498 | 0.001044 |
| 93 | 10.07 | 9.890355 | 0.001953 | 22.596 | 22.42682 | 0.001839 |
| 94 | 9.906 | 9.890521 | 0.000166 | 22.44 | 22.42696 | 0.00014 |
| 95 | 10.054 | 9.892242 | 0.001721 | 22.554 | 22.42829 | 0.001337 |
| 96 | 9.941 | 9.89275 | 0.000508 | 22.616 | 22.43025 | 0.001955 |
| 97 | 9.926 | 9.893093 | 0.000343 | 22.589 | 22.43189 | 0.001637 |
| 98 | 9.706 | 9.891184 | -0.00191 | 22.471 | 22.43229 | 0.000399 |
| 99 | 10.005 | 9.892333 | 0.00115 | 22.605 | 22.43403 | 0.001745 |
| 100 | 9.725 | 9.89066 | -0.00167 | 22.363 | 22.43332 | -0.00071 |

**Table A.2. Required Measurements for Sufficient Accuracy for the Pressure Drop and Mass Flow Rate.**

| Channel | 55 Pressure Drop | | | 61 Mass Flow Rate | | |
|---|---|---|---|---|---|---|
| Number of Data Points | Individual Data Point | Running Average | Difference of Averages | Individual Data Point | Running Average | Difference of Averages |
| | (psi) | (psi) | (psi) | (kg/min)) | (kg/min) | (kg/min) |
| 1 | 26.073 | 26.073 | | 2.486 | 2.486 | |
| 2 | 26.313 | 26.193 | 0.12 | 2.449 | 2.4675 | -0.0185 |
| 3 | 25.932 | 26.106 | -0.087 | 2.514 | 2.483 | 0.0155 |
| 4 | 25.821 | 26.03475 | -0.07125 | 2.464 | 2.47825 | -0.00475 |
| 5 | 26.036 | 26.035 | 0.00025 | 2.379 | 2.4584 | -0.01985 |
| 6 | 25.991 | 26.02767 | -0.00733 | 2.534 | 2.471 | 0.0126 |
| 7 | 26.222 | 26.05543 | 0.027762 | 2.511 | 2.476714 | 0.005714 |
| 8 | 26.111 | 26.06238 | 0.006946 | 2.473 | 2.47625 | -0.00046 |
| 9 | 25.968 | 26.05189 | -0.01049 | 2.496 | 2.478444 | 0.002194 |
| 10 | 25.837 | 26.0304 | -0.02149 | 2.31 | 2.4616 | -0.01684 |
| 11 | 26.215 | 26.04718 | 0.016782 | 2.559 | 2.470455 | 0.008855 |
| 12 | 26.158 | 26.05642 | 0.009235 | 2.537 | 2.476 | 0.005545 |
| 13 | 26.628 | 26.10038 | 0.043968 | 2.467 | 2.475308 | -0.00069 |
| 14 | 26.092 | 26.09979 | -0.0006 | 2.414 | 2.470929 | -0.00438 |
| 15 | 26.023 | 26.09467 | -0.00512 | 2.472 | 2.471 | 7.14E-05 |
| 16 | 25.957 | 26.08606 | -0.0086 | 2.366 | 2.464438 | -0.00656 |
| 17 | 26.108 | 26.08735 | 0.00129 | 2.563 | 2.470235 | 0.005798 |
| 18 | 26.165 | 26.09167 | 0.004314 | 2.515 | 2.472722 | 0.002487 |
| 19 | 26.221 | 26.09848 | 0.006807 | 2.452 | 2.471632 | -0.00109 |
| 20 | 26.244 | 26.11075 | 0.007013 | 2.512 | 2.47365 | 0.002018 |
| 21 | 26.08 | 26.10929 | -0.00146 | 2.386 | 2.469476 | -0.00417 |
| 22 | 26.031 | 26.10573 | -0.00356 | 2.47 | 2.4695 | 2.38E-05 |
| 23 | 26.08 | 26.10461 | -0.00112 | 2.448 | 2.468565 | -0.00093 |
| 24 | 25.892 | 26.09575 | -0.00886 | 2.444 | 2.467542 | -0.00102 |
| 25 | 26.078 | 26.05592 | 0.00092 | 2.471 | 2.46768 | 0.000138 |
| 26 | 26.114 | 26.05815 | 0.002234 | 2.331 | 2.462423 | -0.00526 |
| 27 | 26.139 | 26.05956 | 0.00141 | 2.485 | 2.463259 | 0.000836 |
| 28 | 25.188 | 26.06139 | -0.00177 | 2.343 | 2.458964 | -0.00429 |
| 29 | 26.079 | 26.05234 | 0.000952 | 2.439 | 2.458276 | -0.00069 |
| 30 | 26.209 | 26.05757 | 0.005222 | 2.361 | 2.455033 | -0.00324 |
| 31 | 26.102 | 26.059 | 0.001433 | 2.436 | 2.454419 | -0.00061 |
| 32 | 26.375 | 26.06825 | 0.00925 | 2.439 | 2.453938 | -0.00048 |
| 33 | 25.993 | 26.07567 | -0.00258 | 2.397 | 2.452212 | -0.00173 |
| 34 | 26.134 | 26.07738 | 0.001716 | 2.407 | 2.450882 | -0.00133 |
| 35 | 26.061 | 26.07691 | -0.00047 | 2.489 | 2.451971 | 0.001089 |
| 36 | 26.255 | 26.08186 | 0.004947 | 2.396 | 2.450417 | -0.00155 |
| 37 | 26.313 | 26.08811 | 0.006247 | 2.555 | 2.453243 | 0.002827 |
| 38 | 26.322 | 26.09426 | 0.006155 | 2.426 | 2.452526 | -0.00072 |
| 39 | 26.193 | 26.09679 | 0.002532 | 2.492 | 2.453538 | 0.001012 |
| 40 | 26.142 | 26.09793 | 0.00113 | 2.512 | 2.455 | 0.001462 |
| 41 | 26.025 | 26.09615 | -0.00178 | 2.545 | 2.457195 | 0.002195 |
| 42 | 26.189 | 26.09836 | 0.002211 | 2.417 | 2.456238 | -0.00096 |

Table A.2. ( cont.)

| Channel | 55 Pressure Drop | | | 61 Mass Flow Rate | | |
|---|---|---|---|---|---|---|
| Number of Data Points | Individual Data Point | Running Average | Difference of Averages | Individual Data Point | Running Average | Difference of Averages |
| | (psi) | (psi) | (psi) | (kg/min) | (kg/min) | (kg/min) |
| 43 | 26.212 | 26.101 | 0.002643 | 2.394 | 2.454791 | -0.00145 |
| 44 | 26.309 | 26.10573 | 0.004727 | 2.517 | 2.456205 | 0.001414 |
| 45 | 25.888 | 26.10089 | -0.00484 | 2.466 | 2.456422 | 0.000218 |
| 46 | 26.03 | 26.09935 | -0.00154 | 2.545 | 2.458348 | 0.001926 |
| 47 | 26.109 | 26.09955 | 0.000205 | 2.555 | 2.460404 | 0.002056 |
| 48 | 26.32 | 26.10415 | 0.004593 | 2.337 | 2.457833 | -0.00257 |
| 49 | 26.213 | 26.10637 | 0.002222 | 2.532 | 2.459347 | 0.001514 |
| 50 | 26.201 | 26.10826 | 0.001893 | 2.477 | 2.4597 | 0.000353 |
| 51 | 26.008 | 26.10629 | -0.00197 | 2.53 | 2.461078 | 0.001378 |
| 52 | 26.067 | 26.10554 | -0.00076 | 2.516 | 2.462135 | 0.001056 |
| 53 | 26.044 | 26.10438 | -0.00116 | 2.424 | 2.461415 | -0.00072 |
| 54 | 26.003 | 26.1025 | -0.00188 | 2.538 | 2.462833 | 0.001418 |
| 55 | 26.059 | 26.10171 | -0.00079 | 2.507 | 2.463636 | 0.000803 |
| 56 | 26.265 | 26.10463 | 0.002916 | 2.47 | 2.46375 | 0.000114 |
| 57 | 26.316 | 26.10833 | 0.003708 | 2.52 | 2.464737 | 0.000987 |
| 58 | 26.148 | 26.10902 | 0.000684 | 2.556 | 2.46631 | 0.001574 |
| 59 | 26.106 | 26.10897 | -5.10E-05 | 2.567 | 2.468017 | 0.001707 |
| 60 | 24.608 | 26.08395 | -0.02502 | 2.45 | 2.467717 | -0.0003 |
| 61 | 26.035 | 26.08315 | -0.0008 | 2.506 | 2.468344 | 0.000628 |
| 62 | 26.185 | 26.08479 | 0.001643 | 2.282 | 2.465339 | -0.00301 |
| 63 | 26.091 | 26.08489 | 9.86E-05 | 2.529 | 2.466349 | 0.00101 |
| 64 | 26.305 | 26.08833 | 0.003439 | 2.412 | 2.4655 | -0.00085 |
| 65 | 26.391 | 26.09298 | 0.004656 | 2.449 | 2.465246 | -0.00025 |
| 66 | 25.132 | 26.07842 | -0.01456 | 2.488 | 2.465591 | 0.000345 |
| 67 | 26 | 26.07725 | -0.00117 | 2.51 | 2.466254 | 0.000663 |
| 68 | 26.056 | 26.07694 | -0.00031 | 2.528 | 2.467162 | 0.000908 |
| 69 | 26.14 | 26.07786 | 0.000914 | 2.519 | 2.467913 | 0.000751 |
| 70 | 26.003 | 26.07679 | -0.00107 | 2.488 | 2.4682 | 0.000287 |
| 71 | 26.035 | 26.0762 | -0.00059 | 2.497 | 2.468606 | 0.000406 |
| 72 | 25.904 | 26.07381 | -0.00239 | 2.544 | 2.469653 | 0.001047 |
| 73 | 26.203 | 26.07558 | 0.00177 | 2.547 | 2.470712 | 0.00106 |
| 74 | 26.176 | 26.07693 | 0.001357 | 2.574 | 2.472108 | 0.001396 |
| 75 | 26.411 | 26.08139 | 0.004454 | 2.488 | 2.47232 | 0.000212 |
| 76 | 26.301 | 26.08428 | 0.00289 | 2.407 | 2.471461 | -0.00086 |
| 77 | 26.617 | 26.09119 | 0.006918 | 2.361 | 2.470026 | -0.00143 |
| 78 | 25.915 | 26.08894 | -0.00226 | 2.519 | 2.470654 | 0.000628 |
| 79 | 26.187 | 26.09018 | 0.001241 | 2.491 | 2.470911 | 0.000258 |
| 80 | 26.124 | 26.0906 | 0.000423 | 2.397 | 2.469988 | -0.00092 |
| 81 | 26.167 | 26.09154 | 0.000943 | 2.442 | 2.469642 | -0.00035 |
| 82 | 26.099 | 26.09163 | 9.09E-05 | 2.384 | 2.468598 | -0.00104 |
| 83 | 26.132 | 26.09212 | 0.000486 | 2.471 | 2.468627 | 2.89E-05 |
| 84 | 26.039 | 26.09149 | -0.00063 | 2.468 | 2.468619 | -7.50E-06 |
| 85 | 26.288 | 26.0938 | 0.002312 | 2.457 | 2.468482 | -0.00014 |

**Table A.2. ( cont.)**

| Channel | 55 PressureDrop | | | 61 Mass Flow Rate | | |
|---|---|---|---|---|---|---|
| Number of Data Points | Individual Data Point | Running Average | Difference of Averages | Individual Data Point | Running Average | Difference of Averages |
| | (psi) | (psi) | (psi) | (kg/min) | (kg/min) | (kg/min) |
| 86 | 26.609 | 26.09979 | 0.005991 | 2.496 | 2.468802 | 0.00032 |
| 87 | 25.988 | 26.09851 | -0.00128 | 2.51 | 2.469276 | 0.000474 |
| 88 | 26.105 | 26.09858 | 7.38E-05 | 2.535 | 2.470023 | 0.000747 |
| 89 | 26.064 | 26.09819 | -0.00039 | 2.479 | 2.470124 | 0.000101 |
| 90 | 26.132 | 26.09857 | 0.000376 | 2.472 | 2.470144 | 2.08E-05 |
| 91 | 26.428 | 26.10219 | 0.00362 | 2.496 | 2.470429 | 0.000284 |
| 92 | 25.956 | 26.1006 | -0.00159 | 2.525 | 2.471022 | 0.000593 |
| 93 | 25.915 | 26.0986 | -0.002 | 2.474 | 2.471054 | 3.20E-05 |
| 94 | 26.321 | 26.10097 | 0.002366 | 2.539 | 2.471777 | 0.000723 |
| 95 | 26.001 | 26.09992 | -0.00105 | 2.529 | 2.472379 | 0.000602 |
| 96 | 26.106 | 26.09998 | 6.34E-05 | 2.506 | 2.472729 | 0.00035 |
| 97 | 26.252 | 26.10155 | 0.001567 | 2.553 | 2.473557 | 0.000828 |
| 98 | 26.291 | 26.10348 | 0.001933 | 2.513 | 2.473959 | 0.000402 |
| 99 | 26.25 | 26.10496 | 0.00148 | 2.435 | 2.473566 | -0.00039 |
| 100 | 26.005 | 26.10396 | -0.001 | 2.339 | 2.47222 | -0.00135 |

## A.2  Steady-State Thermal Tests

After the thermal system has reached steady-state, an average may be used to represent each parameter's value. However, even though the system is steady state, some fluctuations may occur in the output of the data collecting apparatus.  Therefore, an analysis, similar to that of the hydraulic tests, was performed to calculate the minimum number of measurements needed to reach sufficient accuracy for the parameters' values.  However, because the hydraulic tests showed that 15 data measurements were sufficient, only 30 data measurements were included into the thermal analysis (instead of 100 measurements that were used for the hydraulic tests).  For the steady state test, the important parameters include:  the surface temperatures, the coolant temperature, the mass flow rate, the density of the coolant, and the voltage and current inputted into the system. Instead of including 12 surface temperatures, the embedded temperature was selected to represent all of the surface temperatures.  This is valid because all of the surface temperature thermocouples yielded similar fluctuations in their output.  Furthermore, the voltage and current were lumped into one category, the power inputted into the system.  This is valid because the power consists of the product of the voltage and current outputs and is the actual parameter used in the presentation of the results.  Finally,

the density of the coolant was not included into the analysis of the required measurements due to the same reasoning as stated in section A.1.

For the analysis of the required measurements for the steady-state thermal tests, 30 data measurements were taken for CHIC A, see Figure 1.1, at a coolant temperature of 40°C, mass flow rate of 3.75 kg/min, and a heat load of 20 W. The actual analysis for the required measurements is identical to the analysis performed for the hydraulic test. This includes calculating a running average, and the amount each data measurement affects the average. This amount is represented by the difference in the running average to its prior value. Finally, an error value of 0.0099 was selected, arbitrarily, as the maximum difference in the running average for sufficient accuracy in the presentation of the data. This analysis can be seen in Table A.3, for the embedded temperature and the coolant temperature, and in Table A.4, for the mass flow rate and the power input. As seen in these tables, the difference in the averages does not exceed 0.001 after the 13 measurement. Therefore, for sufficient accuracy, including a small safety factor, 15 data measurements was selected for each thermal test run.

**Table A.3.  Required Measurement for Thermal Accuracy for the Embedded and Coolant Temperature**

| Channel | 11 Embedded Temperature | | | 50 Coolant Temperature | | |
|---|---|---|---|---|---|---|
| Data Number | Individual Data Point | Running Average | Difference of Averages | Individual Data Point | Running Average | Difference of Averages |
| | (°C) | (°C) | (°C) | (°C) | (°C) | (°C) |
| 1 | 48.745 | 48.745 | | 39.826 | 39.826 | |
| 2 | 48.735 | 48.74 | -0.005 | 39.76 | 39.793 | -0.033 |
| 3 | 48.743 | 48.741 | 0.001 | 39.771 | 39.78567 | -0.00733 |
| 4 | 48.747 | 48.7425 | 0.0015 | 39.791 | 39.787 | 0.001333 |
| 5 | 48.755 | 48.745 | 0.0025 | 39.879 | 39.8054 | 0.0184 |
| 6 | 48.749 | 48.74567 | 0.000667 | 39.998 | 39.8375 | 0.0321 |
| 7 | 48.739 | 48.74471 | -0.00095 | 39.987 | 39.85886 | 0.021357 |
| 8 | 48.738 | 48.74388 | -0.00084 | 39.969 | 39.87263 | 0.013768 |
| 9 | 48.767 | 48.74644 | 0.002569 | 39.815 | 39.86622 | -0.0064 |
| 10 | 48.76784 | 48.74858 | 0.002139 | 39.808 | 39.8604 | -0.00582 |
| 11 | 48.784 | 48.7518 | 0.00322 | 39.812 | 39.856 | -0.0044 |
| 12 | 48.78186 | 48.75431 | 0.002505 | 39.871 | 39.85725 | 0.00125 |
| 13 | 48.77864 | 48.75618 | 0.001872 | 40.011 | 39.86908 | 0.011827 |
| 14 | 48.876 | 48.76474 | 0.008559 | 39.978 | 39.87686 | 0.00778 |
| 15 | 48.77 | 48.76509 | 0.000351 | 40.024 | 39.89333 | 0.009333 |
| 16 | 48.76144 | 48.76486 | -0.00023 | 39.877 | 39.89231 | -0.00102 |
| 17 | 48.76109 | 48.76464 | -0.00022 | 39.891 | 39.89224 | -7.70E-05 |
| 18 | 48.861 | 48.76999 | 0.005353 | 39.965 | 39.89628 | 0.004042 |
| 19 | 48.757 | 48.76931 | -0.00068 | 40.07 | 39.90542 | 0.009143 |
| 20 | 48.75165 | 48.76843 | -0.00088 | 40.028 | 39.91155 | 0.006129 |
| 21 | 48.854 | 48.7725 | 0.004075 | 40.111 | 39.92105 | 0.009498 |
| 22 | 48.758 | 48.77184 | -0.00066 | 40.031 | 39.93059 | 0.009543 |
| 23 | 48.75393 | 48.77106 | -0.00078 | 39.942 | 39.93109 | 0.0005 |
| 24 | 48.861 | 48.77481 | 0.003747 | 40.139 | 39.93975 | 0.00866 |
| 25 | 48.86178 | 48.77829 | 0.003479 | 40.088 | 39.94568 | 0.00593 |
| 26 | 48.85803 | 48.78136 | 0.003067 | 40.014 | 39.94831 | 0.00263 |
| 27 | 48.85455 | 48.78407 | 0.002711 | 39.912 | 39.94696 | -0.00135 |
| 28 | 48.799 | 48.7846 | 0.000533 | 39.941 | 39.94675 | -0.00021 |
| 29 | 48.79629 | 48.785 | 0.000403 | 40.055 | 39.95048 | 0.00373 |
| 30 | 48.882 | 48.78824 | 0.003233 | 40.104 | 39.9556 | 0.00512 |

**Table A.4.  Required Measurement for Thermal Accuracy for the Mass Flow Rate and Power Input**

| Channel | 61    Mass Flow Rate | | | 82    Power Input | | |
|---|---|---|---|---|---|---|
| Number of Data Points | Individual Data Point | Running Average | Difference of Averages | Individual Data Point | Running Average | Difference of Averages |
| | (kg/min) | (kg/min) | (kg/min) | (W) | (W) | (W) |
| 1 | 3.725 | 3.725 | | 19.522 | 19.522 | |
| 2 | 3.716 | 3.7205 | -0.0045 | 19.535 | 19.5285 | 0.0065 |
| 3 | 3.8 | 3.747 | 0.0265 | 19.718 | 19.59167 | 0.063167 |
| 4 | 3.741 | 3.7455 | -0.0015 | 19.718 | 19.62325 | 0.031583 |
| 5 | 3.77 | 3.7504 | 0.0049 | 19.723 | 19.6432 | 0.01995 |
| 6 | 3.693 | 3.740833 | -0.00957 | 19.723 | 19.6565 | 0.0133 |
| 7 | 3.738 | 3.740429 | -0.0004 | 19.543 | 19.64029 | -0.01621 |
| 8 | 3.728 | 3.738875 | -0.00155 | 19.543 | 19.62813 | -0.01216 |
| 9 | 3.679 | 3.732222 | -0.00665 | 19.547 | 19.61911 | -0.00901 |
| 10 | 3.641 | 3.7231 | -0.00912 | 19.732 | 19.6304 | 0.011289 |
| 11 | 3.704 | 3.721364 | -0.00174 | 19.727 | 19.63918 | 0.008782 |
| 12 | 3.791 | 3.727167 | 0.005803 | 19.757 | 19.649 | 0.009818 |
| 13 | 3.664 | 3.722308 | -0.00486 | 19.753 | 19.657 | 0.008 |
| 14 | 3.71 | 3.721429 | -0.00088 | 19.77 | 19.66507 | 0.008071 |
| 15 | 3.741 | 3.722733 | 0.001305 | 19.782 | 19.67287 | 0.007795 |
| 16 | 3.735 | 3.7235 | 0.000767 | 19.778 | 19.67944 | 0.006571 |
| 17 | 3.661 | 3.719824 | -0.00368 | 19.774 | 19.685 | 0.005562 |
| 18 | 3.773 | 3.722778 | 0.002954 | 19.778 | 19.69017 | 0.005167 |
| 19 | 3.717 | 3.722474 | -0.0003 | 19.782 | 19.695 | 0.004833 |
| 20 | 3.783 | 3.7255 | 0.003026 | 19.791 | 19.6998 | 0.0048 |
| 21 | 3.767 | 3.727476 | 0.001976 | 19.778 | 19.70352 | 0.003724 |
| 22 | 3.744 | 3.728227 | 0.000751 | 19.778 | 19.70691 | 0.003385 |
| 23 | 3.735 | 3.728522 | 0.000294 | 19.766 | 19.70948 | 0.002569 |
| 24 | 3.776 | 3.7305 | 0.001978 | 19.539 | 19.70238 | -0.0071 |
| 25 | 3.742 | 3.73096 | 0.00046 | 19.539 | 19.69584 | -0.00653 |
| 26 | 3.686 | 3.729231 | -0.00173 | 19.535 | 19.68965 | -0.00619 |
| 27 | 3.715 | 3.728704 | -0.00053 | 19.535 | 19.68393 | -0.00573 |
| 28 | 3.628 | 3.725107 | -0.0036 | 19.718 | 19.68514 | 0.001217 |
| 29 | 3.776 | 3.726862 | 0.001755 | 19.535 | 19.67997 | -0.00518 |
| 30 | 3.676 | 3.725167 | -0.0017 | 19.493 | 19.67373 | -0.00623 |

APPENDIX B


PLATE STACKING FOR THE HFHE

In this appendix, a listing of the individual copper

laminates and their corresponding diagrams are presented.


## B.1  Stacking Order

The HFHE consists of eight individual laminates.  Plate

A, the target plate, is the surface that the jets impinge

upon.  Plate B, the target spacer, provides a y-direction

for the jets, see Figure 1.2.  Plate C, the orifice plate,

and plate C*, the orifice plate flipped over, are for

creating the jets.  Plate D, the spacer plate, is a plate

that lies in between the C plates to provide some depth to

the jets.  Plate E, the spacer/manifold divider plate, is

similar to plate D and provides the same function.  However,

Plate E does not include a channel opening for the exiting

fluid from the HFHE.  Plate F, the distributor plate,

creates a uniform flow throughout the CHIC, and plate G

which is the back cover for the CHIC.  This particular

stacking represents the number four model of the HFHE

developed by McDonnell Douglas [4]. This stacking differs from the model used by McDonnell Douglas in that it contains an orifice plate that has large openings, 0.010 in, as well as orifice plates that contain the usual small openings, 0.008 in. The large orifice plate, located on the target side of the manifold divider, provides a short circuit flow path. The stacking order can be seen in Table B.1.

## B.2   Plate Diagrams

Each laminate consists of copper plates 0.038 or 0.010 cm (0.015 or 0.004 inches) in thickness. These plates were assembled by hydrogen diffusion. This bonding creates one sheet of copper 0.467 cm (0.184 inches) thick. The individual laminates can be seen in Figures B.1 through B.8.

**Table B.1.  CHIC Plate Stacking Order, Unit #4**

| Plate Number | Plate Type | Description | Thickness | |
|---|---|---|---|---|
| | | | cm | in |
| 1 | A | Target Plate | 0.038 | 0.015 |
| 2 | A | Target Plate | 0.038 | 0.015 |
| 3 | B | Target Spacer | 0.038 | 0.015 |
| 4 | C | Orifice | 0.010 | 0.004 |
| 5 | D | Spacer | 0.010 | 0.004 |
| 6 | C* big | Orifice (Flipped) | 0.010 | 0.004 |
| 7 | D | Spacer | 0.010 | 0.004 |
| 8 | C | Orifice | 0.010 | 0.004 |
| 9 | E | Spacer/Manifold | 0.038 | 0.004 |
| 10 | C* small | Orifice (Flipped) | 0.010 | 0.004 |
| 11 | D | Spacer | 0.010 | 0.004 |
| 12 | C | Orifice | 0.010 | 0.004 |
| 13 | D | Spacer | 0.010 | 0.004 |
| 14 | C* small | Orifice (Flipped) | 0.010 | 0.004 |
| 15 | D | Spacer | 0.010 | 0.004 |
| 16 | C | Orifice | 0.010 | 0.004 |
| 17 | D | Spacer | 0.010 | 0.004 |
| 18 | C* small | Orifice (Flipped) | 0.010 | 0.004 |
| 19 | D | Spacer | 0.010 | 0.004 |
| 20 | C | Orifice | 0.010 | 0.004 |
| 21 | F | Distributor | 0.038 | 0.015 |
| 22 | F | Distributor | 0.038 | 0.015 |
| 23 | F | Distributor | 0.038 | 0.015 |
| 24 | G | Back Cover | 0.038 | 0.015 |
| 25 | G | Back Cover | 0.038 | 0.015 |
| | | TOTAL | 0.467 | 0.184 |
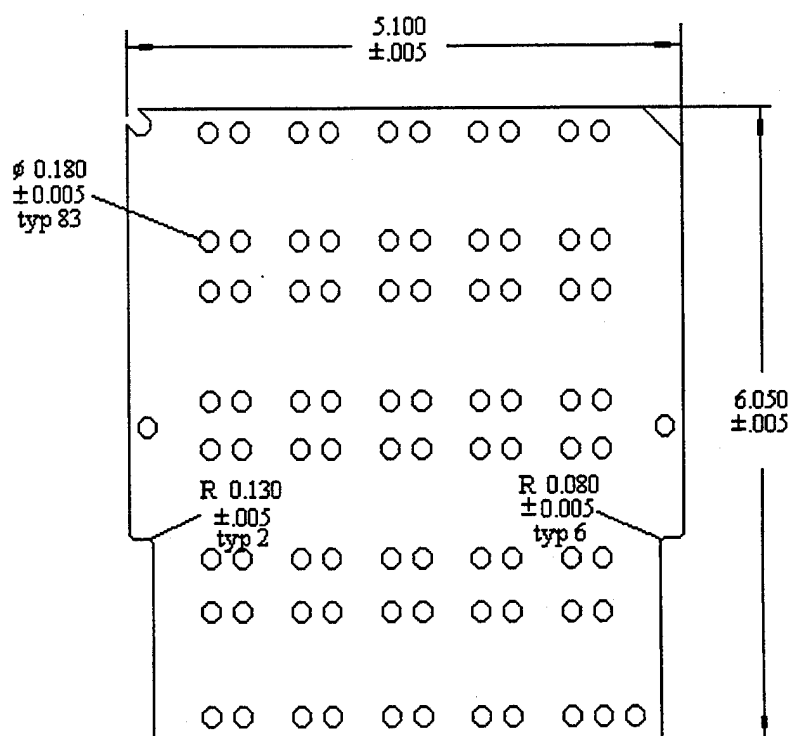
**Figure B.1. Plate "A", Target Plate. (units in inches)**
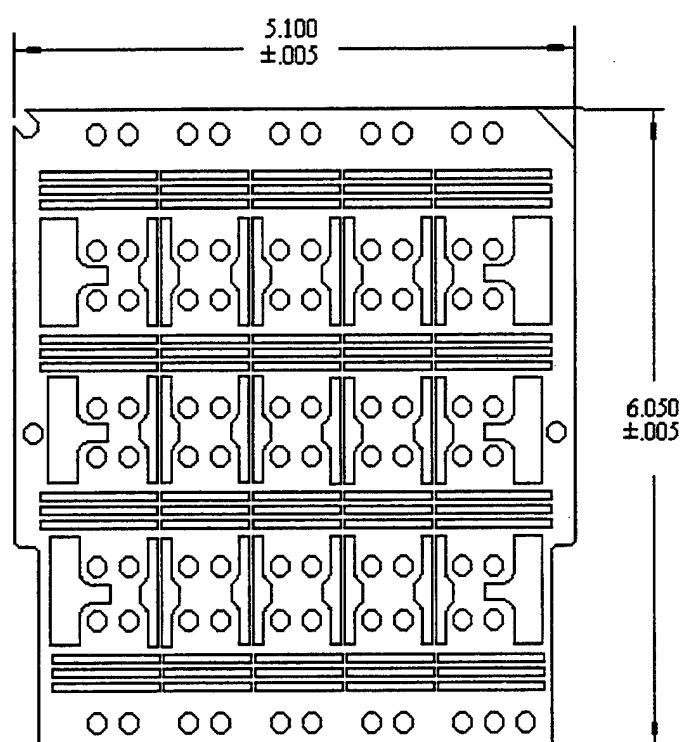
**Figure B.2. Plate "B", Target Spacer. (units in inches)**
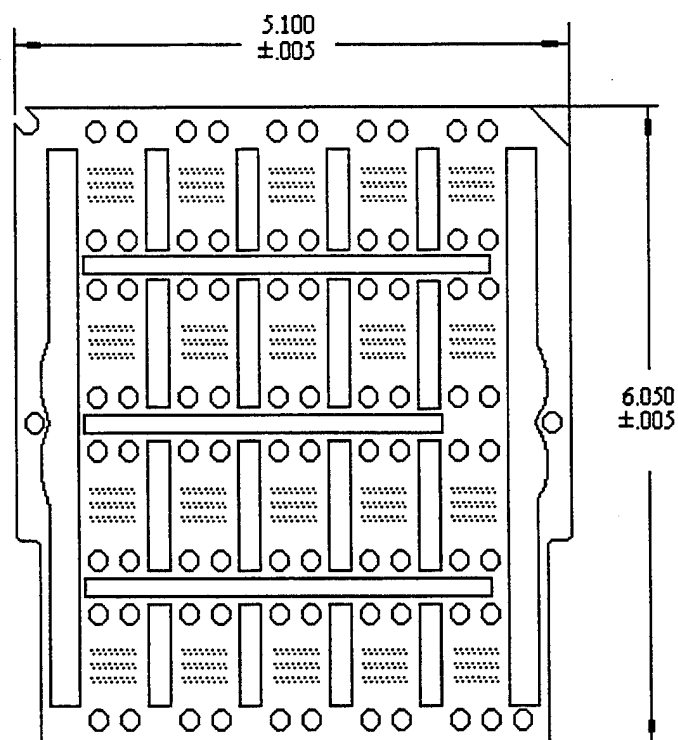
**Figure B.3. Plate "C", Orifice Plate. (units in inches)**
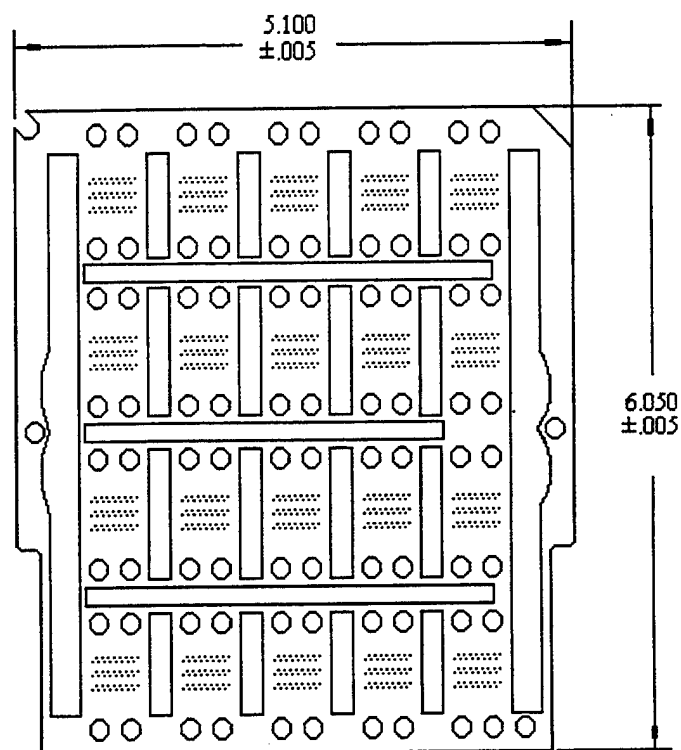
**Figure B.4.** Plate "C*", Orifice Plate, Orifices Staggered Relative to Plate "C". (units in inches)
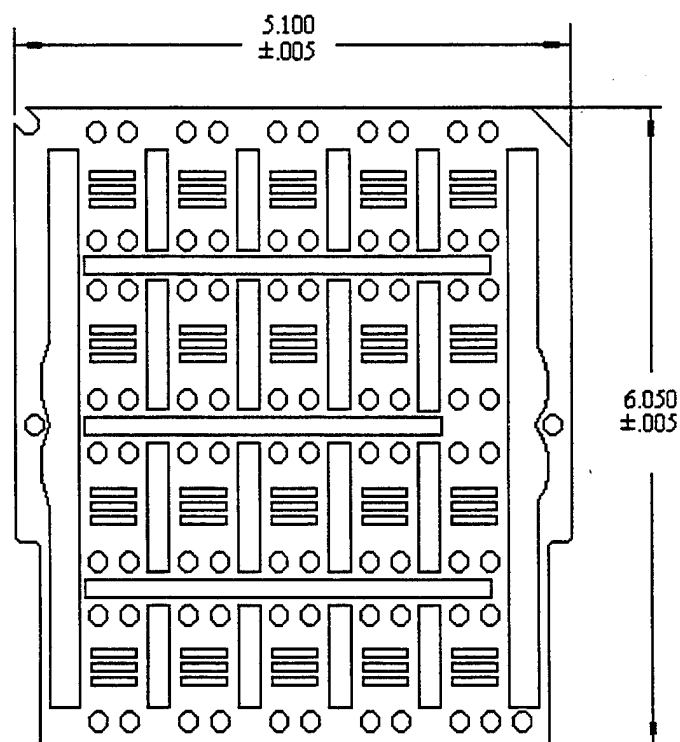
**Figure B.5. Plate "D", Spacer Plate. (units in inches)**
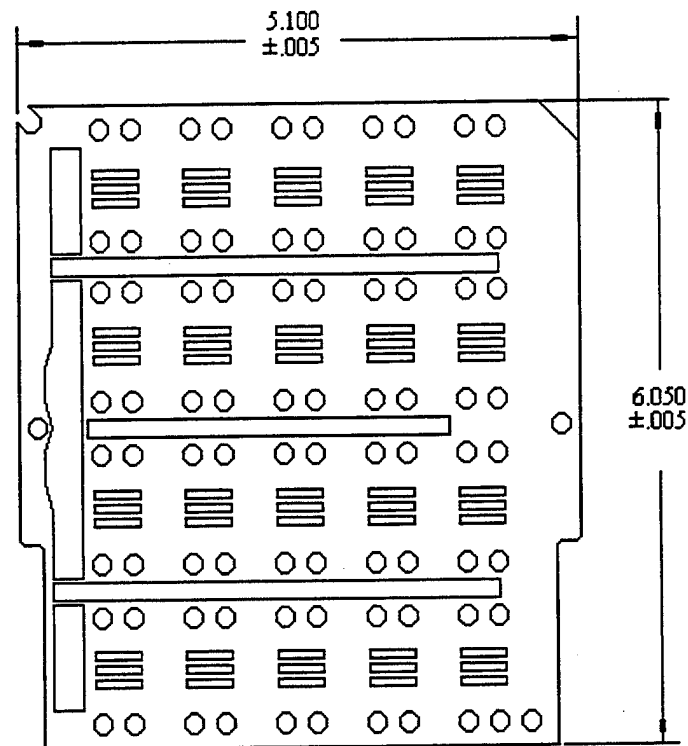
**Figure B.6. Plate "E", Spacer/Manifold Divider Plate. (units in inches)**
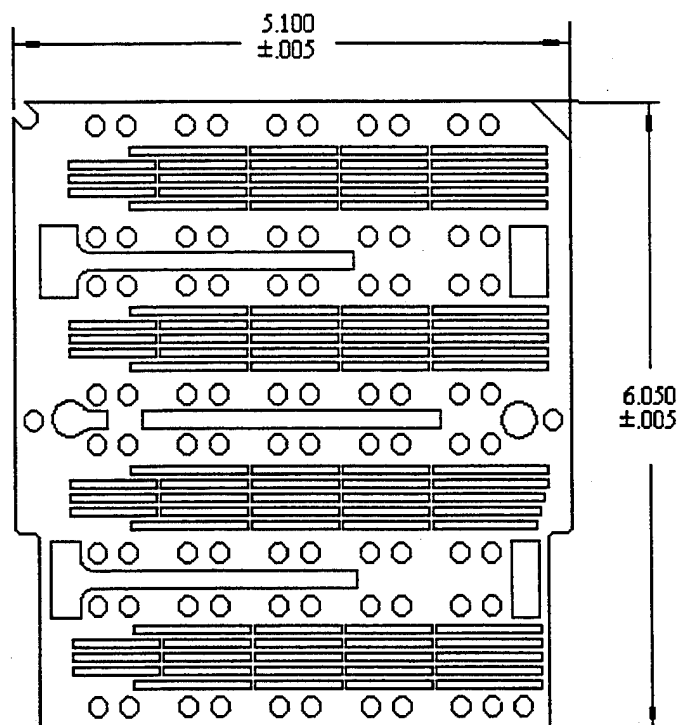
**Figure B.7.  Plate "F", Distributor Plate. (units in inches)**
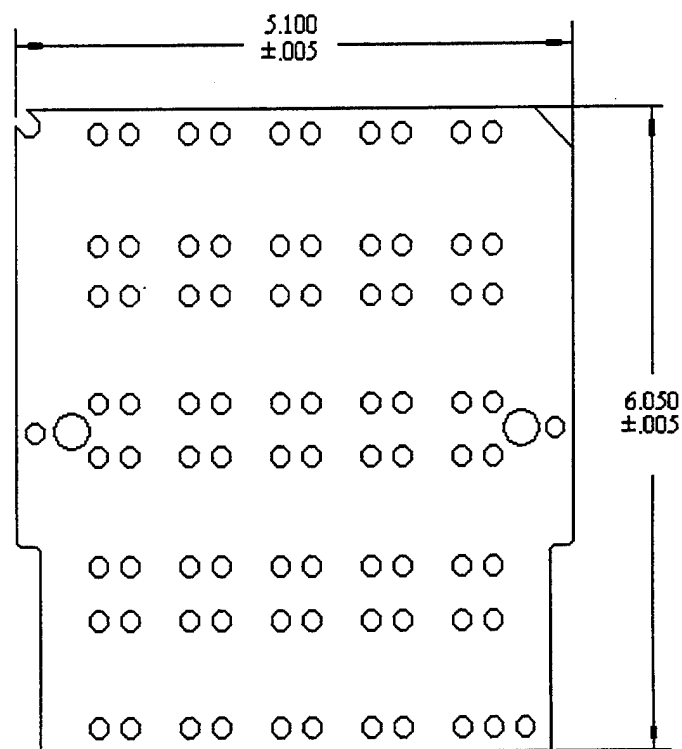
**Figure B.8.  Plate "G", Back Cover.  (units in inches)**

APPENDIX C


THERMOCOUPLE CALIBRATION RESULTS


In this appendix, the results of the thermocouple

calibration are presented.  This presentation includes an

example calibration curve, the calibration data, and the

curve fit equation.  In addition, the curve fit equation

includes the standard deviation and maximum error.  As

explained in Chapter II, the thermocouples were calibrated

with the use of the cold temperature bath over the range of

-20°C to 60°C at an increment of 10°C.  However, due to the

limited size of the reservoir of the temperature bath, it

was not possible to calibrate all of the thermocouples at

the same time.  Therefore, the thermocouples were divided

into the following sections:  the surface thermocouples 0

through 8, the surface thermocouples 11 through 15, and the

heat flux amplifier thermocouples.  The amplifier

thermocouple section also includes the thermocouple probes,

which measure the coolant temperature at the inlet and

outlet of the HFHE.  As can be seen by Tables C.1 and C.2,

the calibration data for each of the thermocouples are very similar.

## C.1  Surface Thermocouples 0 - 8

These surface thermocouples are for the temperature profile in the y-direction used in the calculation of the radial heat loss due to conduction.  In addition, these thermocouples were used to measure the heater temperature and the wall temperature of the HFHE.  An example of the calibration curve for the surface thermocouples is shown in Figure C.1.  In addition, the calibration data and the curve fit equations for these thermocouples are shown in Table C.1 and Table C.2, respectively.  Furthermore, the maximum error for each thermocouple occurs at 20°C.

## C.2  Surface Thermocouples 11-15

These surface thermocouples are for the temperature profile in the x-direction used in the calculation of the radial heat loss due to conduction.  An example of the calibration curve for the surface thermocouples is shown in Figure C.2.  In addition, the calibration data and the curve fit equations for these thermocouples are shown in Table C.3 and Table C.4, respectively.  All of the maximum errors occurred at 10°C or 60°C.
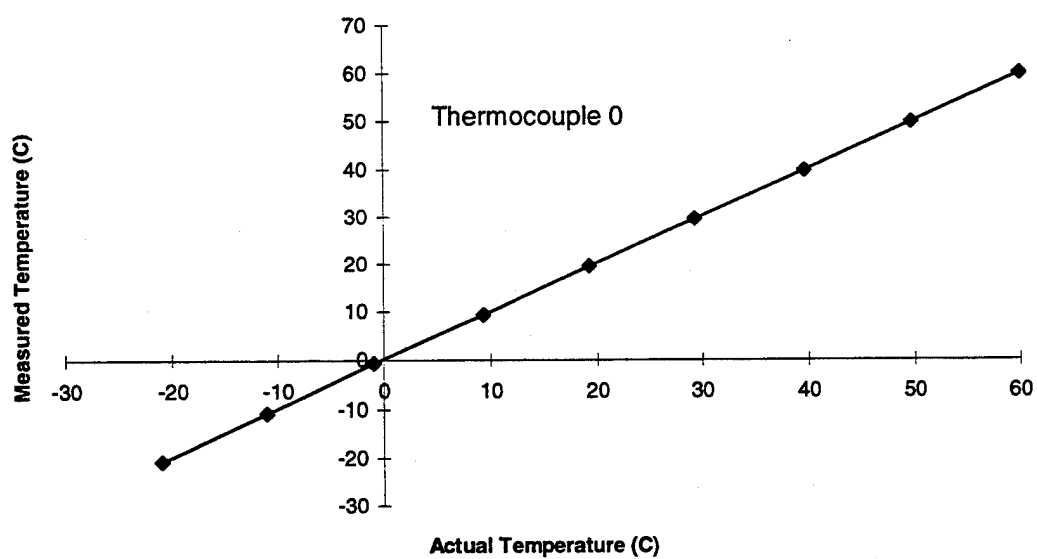
Figure C.1.   Example Calibration Curve for the Surface
Thermocouple 0.

**Table C.1.  Calibration Data for the Surface
Thermocouples 0-8.**

| Thermo-couple Number | Surface Temp. (C) | Surface Temp. (C) | Surface Temp. (C) | Surface Temp. (C) | Surface Temp. (C) | Surface Temp. (C) | Surface Temp. (C) | Surface Temp. (C) | Surface Temp. (C) |
|---|---|---|---|---|---|---|---|---|---|
| Actual | -21.020 | -11.020 | -0.916 | 9.217 | 19.230 | 29.300 | 39.617 | 49.680 | 59.990 |
| 0 | -20.788 | -10.735 | -0.631 | 9.406 | 19.549 | 29.546 | 39.789 | 49.961 | 60.099 |
| 1 | -20.769 | -10.706 | -0.639 | 9.449 | 19.579 | 29.582 | 39.822 | 49.968 | 60.156 |
| 2 | -20.680 | -10.663 | -0.565 | 9.486 | 19.637 | 29.629 | 39.868 | 50.032 | 60.168 |
| 3 | -20.630 | -10.584 | -0.503 | 9.565 | 19.713 | 29.705 | 39.932 | 50.088 | 60.228 |
| 4 | -20.611 | -10.553 | -0.479 | 9.599 | 19.708 | 29.729 | 39.954 | 50.125 | 60.244 |
| 5 | -20.518 | -10.497 | -0.451 | 9.660 | 19.776 | 29.780 | 40.005 | 50.170 | 60.315 |
| 6 | -20.559 | -10.520 | -0.444 | 9.682 | 19.765 | 29.797 | 40.031 | 50.204 | 60.340 |
| 7 | -20.517 | -10.487 | -0.451 | 9.700 | 19.815 | 29.846 | 40.058 | 50.231 | 60.383 |
| 8 | -20.438 | -10.436 | -0.420 | 9.741 | 19.859 | 29.869 | 40.085 | 50.255 | 60.398 |

**Table C.2.  Curve Fit Equations for the Surface Thermocouples 0-8.**

| Thermcouple Number | Y=mx + b | | Standard Deviation | Maximum Error |
|---|---|---|---|---|
| | Slope (m) | Intercept (b) | | |
| 0 | 1.0011 | -0.257 | 0.06 | 0.101 |
| 1 | 1.0009 | -0.2794 | 0.052 | 0.103 |
| 2 | 1.0013 | -0.3409 | 0.06 | 0.109 |
| 3 | 1.0014 | -0.4089 | 0.062 | 0.117 |
| 4 | 1.0014 | -0.4318 | 0.06 | -0.1 |
| 5 | 1.0015 | -0.4927 | 0.056 | 0.1 |
| 6 | 1.0008 | -0.4834 | 0.055 | -0.09 |
| 7 | 1.0006 | -0.5121 | 0.059 | 0.102 |
| 8 | 1.0012 | -0.5615 | 0.061 | 0.109 |
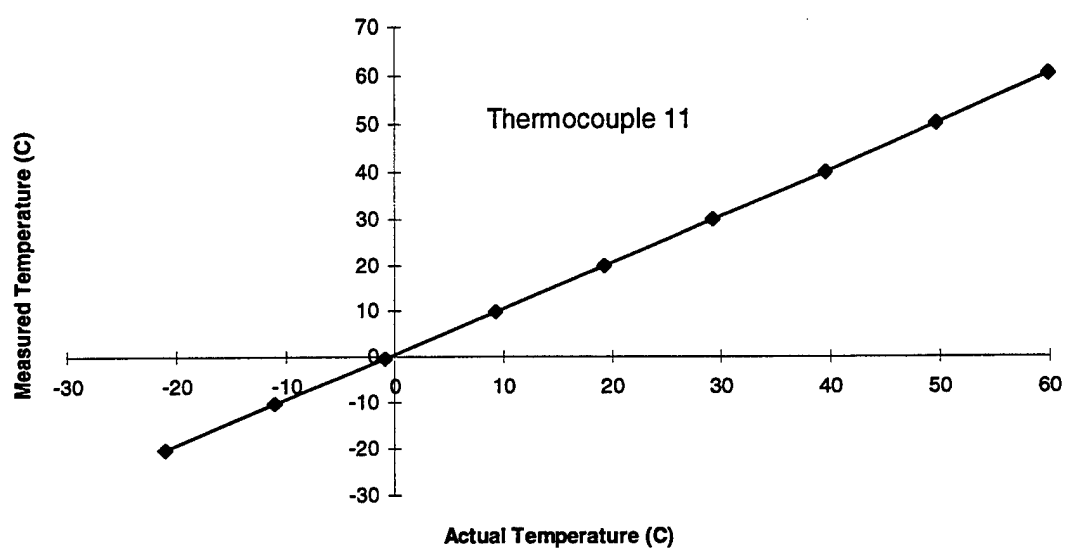
Figure C.2.  Calibration Curve for Thermocouple 11.

**Table C.3. Calibration Data for the Surface Thermocouples 11-15.**

| Thermo-couple Number | Surface Temp. (C) | Surface Temp. (C) | Surface Temp. (C) | Surface Temp. (C) | Surface Temp. (C) | Surface Temp. (C) | Surface Temp. (C) | Surface Temp. (C) | Surface Temp. (C) |
|---|---|---|---|---|---|---|---|---|---|
| Actual | -21.0611 | -10.9833 | -0.91111 | 9.217172 | 19.23333 | 29.30556 | 39.47222 | 49.63333 | 59.89444 |
| 11 | -20.1028 | -10.1508 | -0.45 | 9.8261 | 19.81027 | 29.81 | 39.95558 | 50.06856 | 60.3622 |
| 12 | -20.2484 | -10.3112 | -0.41667 | 9.8037 | 19.80445 | 29.8424 | 40.12 | 50.14444 | 60.3971 |
| 13 | -20.3948 | -10.2855 | -0.58333 | 9.8139 | 19.83818 | 29.8538 | 40.05392 | 50.19256 | 60.4822 |
| 14 | -20.4642 | -10.2799 | -0.35 | 9.8632 | 19.87618 | 29.8843 | 40.07 | 50.18544 | 60.4702 |
| 15 | -20.2952 | -10.2002 | -0.3148 | 9.744 | 19.811 | 29.388 | 39.589 | 49.781 | 60.069 |

**Table C.4.  Curve Fit Equations for the Surface Thermocouples 11-15.**

| Thermcouple Number | Y=mx + b | | Standard Deviation | Maximum Error |
| | Slope (m) | Intercept (b) | | |
|---|---|---|---|---|
| 11 | 1.005306 | -0.69768 | 0.104541 | -0.23896 |
| 12 | 1.002414 | -0.64086 | 0.074716 | -0.14742 |
| 13 | 1.00043 | -0.58305 | 0.097719 | -0.25552 |
| 14 | 1.000876 | -0.62354 | 0.040109 | 0.070888 |
| 15 | 1.009418 | -0.60484 | 0.118078 | -0.11521 |

## C.3  Amplifier Thermocouples

These surface thermocouples are for the temperature profile of the heat flux amplifier used in the approximation of the wall temperature of the HFHE.  In addition, these thermocouples include the two thermocouple probes used to measure the coolant temperature at the inlet and outlet of the HFHE.  The number for the thermocouple probes for the inlet and outlet of the HFHE are thermocouple 50 and 51, respectively.  An example of the calibration curve for the amplifier thermocouples is shown in Figure C.3.  In addition, the calibration data and the curve fit equations for these thermocouples are shown in Table C.5 and Table C.6, respectively.  As can be seen from these tables, the maximum error occurs at 20°C for all of the thermocouples except for thermocouples 27 and 45 which contain maximum errors at 50°C.
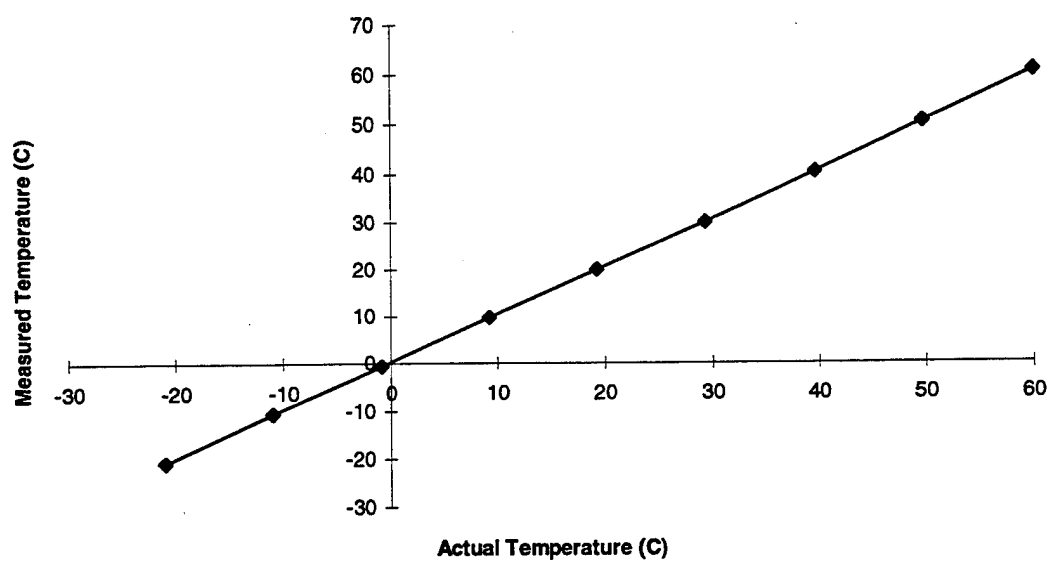
**Figure C.3. Calibration Curve for Thermocouple 51.**

**Table C.5. Calibration Data for the Amplifier Thermocouples**

| Thermo-couple Number | Surface Temp. (C) | Surface Temp. (C) | Surface Temp. (C) | Surface Temp. (C) | Surface Temp. (C) | Surface Temp. (C) | Surface Temp. (C) | Surface Temp. (C) | Surface Temp. (C) |
|---|---|---|---|---|---|---|---|---|---|
| Actual | -21.02 | -11.02 | -0.916 | 9.217 | 19.23 | 29.3 | 39.617 | 49.68 | 59.99 |
| 22 | -20.558 | -10.54 | -0.544 | 9.512 | 19.623 | 29.59 | 39.778 | 49.935 | 60.087 |
| 24 | -20.423 | -10.43 | -0.461 | 9.624 | 19.726 | 29.69 | 39.867 | 50.022 | 60.163 |
| 25 | -20.446 | -10.457 | -0.489 | 9.622 | 19.739 | 29.707 | 39.894 | 50.052 | 60.195 |
| 27 | -20.406 | -10.424 | -0.465 | 9.678 | 19.789 | 29.764 | 39.953 | 50.114 | 60.259 |
| 30 | -20.256 | -10.299 | -0.374 | 9.829 | 19.936 | 29.912 | 40.096 | 50.252 | 60.389 |
| 32 | -20.277 | -10.33 | -0.4 | 9.799 | 19.915 | 29.886 | 40.073 | 50.231 | 60.368 |
| 33 | -20.274 | -10.328 | -0.394 | 9.814 | 19.924 | 29.894 | 40.084 | 50.244 | 60.381 |
| 35 | -20.275 | -10.322 | -0.388 | 9.814 | 19.926 | 29.902 | 40.087 | 50.247 | 60.393 |
| 38 | -20.327 | -10.38 | -0.443 | 9.763 | 19.871 | 29.842 | 40.035 | 50.198 | 60.337 |
| 40 | -20.595 | -10.568 | -0.554 | 9.462 | 19.559 | 29.535 | 39.72 | 49.873 | 60.036 |
| 41 | -20.509 | -10.488 | -0.49 | 9.542 | 19.644 | 29.61 | 39.79 | 49.948 | 60.1 |
| 43 | -20.388 | -10.383 | -0.404 | 9.678 | 19.774 | 29.741 | 39.926 | 50.078 | 60.23 |
| 45 | -20.384 | -10.392 | -0.419 | 9.697 | 19.802 | 29.778 | 39.974 | 50.142 | 60.3 |
| 50 | -20.45 | -10.49 | -0.43 | 9.862 | 19.923 | 29.998 | 40.202 | 50.125 | 60.542 |
| 51 | -20.686 | -10.637 | -0.532 | 9.782 | 19.909 | 30.018 | 40.271 | 50.488 | 60.751 |

**Table C.4. Curve Fit Equations for the Amplifier Thermocouples**

| Thermcouple Number | Y=mx + b | | Standard Deviation | Maximum Error |
|---|---|---|---|---|
| | Slope (m) | Intercept (b) | | |
| 22 | 1.0042 | -0.395 | 0.056 | 0.098 |
| 24 | 1.0047 | -0.5048 | 0.058 | 0.102 |
| 25 | 1.0039 | -0.4923 | 0.061 | 0.11 |
| 27 | 1.0035 | -0.5333 | 0.063 | 0.11 |
| 30 | 1.0034 | -0.6677 | 0.073 | 0.122 |
| 32 | 1.0033 | -0.6419 | 0.074 | 0.125 |
| 33 | 1.0032 | -0.6482 | 0.073 | 0.125 |
| 35 | 1.0031 | -0.6509 | 0.072 | 0.123 |
| 38 | 1.0031 | -0.5967 | 0.072 | 0.122 |
| 40 | 1.0047 | -0.3571 | 0.054 | 0.08 |
| 41 | 1.0048 | -0.4359 | 0.056 | 0.089 |
| 43 | 1.0045 | -0.5525 | 0.055 | 0.097 |
| 45 | 1.0034 | -0.5595 | 0.058 | 0.097 |
| 50 | 1.0001 | -0.5807 | 0.092 | 0.104 |
| 51 | 0.994 | -0.4675 | 0.062 | 0.105 |

APPENDIX D


DATA REDUCTION PROCESS


In this appendix, a step by step process of the data reduction is presented. This presentation begins with the output data file from the Fluke data logger for the steady-state thermal tests on CHIC B, see Figure 1.1. This output file is then reduced into an intermediate file listed as BT6F12P2 by the data reduction program, LAB. LAB is a self written FORTRAN program specifically for the reduction of the output file of the Fluke data logger. In addition, the data reduction program inputs the averaged value for all of the parameters into a summary file. Each summary file contains the output information over the entire ranges of flow rates and heat loads for a given coolant temperature. An example summary file is given for the coolant temperature of 30°C. Finally, in this appendix, the self-constructed data reduction program, LAB, is presented by its' source code.

## D.1  Fluke Output Data File

The following data file is an example of the output file

from the Fluke data logger.  This particular output file is

for a coolant temperature of 30°C, flow rate of 3.75 kg/min,

and a heat load of 40 W.

```
Data File BT6F12P2
***********************************************************
BEGIN SCAN GROUP 1    12 JUL 95   14:49:53
HYD. TESTS

C   1 BORDER BARRIER    35.171 C
C   2 BORDER BARRIER    34.246 C
C   3 BORDER BARRIER    33.586 C
C   4 BORDER BARRIER    32.658 C
C   5 BORDER BARRIER    30.796 C
C   6 BORDER BARRIER    39.496 C
C   7 BORDER BARRIER    30.867 C
C   8 BORDER BARRIER    30.879 C
C  11 BARRIER HTR       31.006 C
C  12 BARRIER HTR       35.423 C
C  13 BARRIER HTR       33.978 C
C  14 BARRIER HTR       33.433 C
C  15 BARRIER HTR       32.292 C
C  22 AMPLIFIER         50.832 C
C  24 AMPLIFIER         51.308 C
C  27 AMPLIFIER         50.274 C
C  30 AMPLIFIER         53.598 C
C  38 AMPLIFIER         55.690 C
C  40 AMPLIFIER         54.435 C
C  41 AMPLIFIER         55.297 C
C  45 AMPLIFIER         65.143 C
C  50 HFHE TC IN        29.912 C
C  52 TEMP OUT          30.273 C
C  55 PRESSURE IN       41.744 PSIG
C  61 PAO FLOWRATE       3.687 KG/MIN
C  62 PAO DENSITY       0.7854 KG/L
C  80 VAC IN            28.30 VAC IN
C  81 AMP IN             1.413 AMP
C  82 WATTS IN          39.994 W

END SCAN GROUP 1      12 JUL 95   14:49:56


BEGIN SCAN GROUP 1    12 JUL 95   14:50:03
```

HYD. TESTS

```
C    1 BORDER BARRIER     35.034 C
C    2 BORDER BARRIER     34.206 C
C    3 BORDER BARRIER     33.564 C
C    4 BORDER BARRIER     32.621 C
C    5 BORDER BARRIER     30.745 C
C    6 BORDER BARRIER     39.445 C
C    7 BORDER BARRIER     30.813 C
C    8 BORDER BARRIER     30.827 C
C   11 BARRIER HTR        30.984 C
C   12 BARRIER HTR        35.328 C
C   13 BARRIER HTR        33.941 C
C   14 BARRIER HTR        33.394 C
C   15 BARRIER HTR        32.267 C
C   22 AMPLIFIER          50.667 C
C   24 AMPLIFIER          51.225 C
C   27 AMPLIFIER          50.166 C
C   30 AMPLIFIER          53.777 C
C   38 AMPLIFIER          55.950 C
C   40 AMPLIFIER          54.427 C
C   41 AMPLIFIER          55.277 C
C   45 AMPLIFIER          64.938 C
C   50 HFHE TC IN         30.040 C
C   52 TEMP OUT           30.499 C
C   55 PRESSURE IN        41.857 PSIG
C   61 PAO FLOWRATE        3.755 KG/MIN
C   62 PAO DENSITY        0.7853 KG/L
C   80 VAC IN             28.32 VAC IN
C   81 AMP IN              1.413 AMP
C   82 WATTS IN           40.028 W
```

END SCAN GROUP 1     12 JUL 95  14:50:06


BEGIN SCAN GROUP 1   12 JUL 95  14:50:13
HYD. TESTS

```
C    1 BORDER BARRIER     35.010 C
C    2 BORDER BARRIER     34.196 C
C    3 BORDER BARRIER     33.595 C
C    4 BORDER BARRIER     32.611 C
C    5 BORDER BARRIER     30.749 C
C    6 BORDER BARRIER     39.450 C
C    7 BORDER BARRIER     30.832 C
C    8 BORDER BARRIER     30.817 C
C   11 BARRIER HTR        30.989 C
C   12 BARRIER HTR        35.277 C
C   13 BARRIER HTR        33.946 C
C   14 BARRIER HTR        33.386 C
```

```
C   15 BARRIER HTR        32.260 C
C   22 AMPLIFIER          50.659 C
C   24 AMPLIFIER          51.214 C
C   27 AMPLIFIER          50.061 C
C   30 AMPLIFIER          53.616 C
C   38 AMPLIFIER          55.708 C
C   40 AMPLIFIER          54.459 C
C   41 AMPLIFIER          55.428 C
C   45 AMPLIFIER          64.969 C
C   50 HFHE TC IN         29.783 C
C   52 TEMP OUT           30.385 C
C   55 PRESSURE IN        41.613 PSIG
C   61 PAO FLOWRATE        3.701 KG/MIN
C   62 PAO DENSITY        0.7855 KG/L
C   80 VAC IN             28.34 VAC IN
C   81 AMP IN              1.413 AMP
C   82 WATTS IN           40.047 W
```

END SCAN GROUP 1      12 JUL 95   14:50:16


BEGIN SCAN GROUP 1    12 JUL 95   14:50:23
HYD. TESTS

```
C    1 BORDER BARRIER     35.136 C
C    2 BORDER BARRIER     34.210 C
C    3 BORDER BARRIER     33.539 C
C    4 BORDER BARRIER     32.611 C
C    5 BORDER BARRIER     30.719 C
C    6 BORDER BARRIER     39.421 C
C    7 BORDER BARRIER     30.805 C
C    8 BORDER BARRIER     30.805 C
C   11 BARRIER HTR        30.944 C
C   12 BARRIER HTR        35.362 C
C   13 BARRIER HTR        33.919 C
C   14 BARRIER HTR        33.357 C
C   15 BARRIER HTR        32.216 C
C   22 AMPLIFIER          50.729 C
C   24 AMPLIFIER          51.247 C
C   27 AMPLIFIER          50.267 C
C   30 AMPLIFIER          53.578 C
C   38 AMPLIFIER          55.777 C
C   40 AMPLIFIER          54.381 C
C   41 AMPLIFIER          55.110 C
C   45 AMPLIFIER          64.984 C
C   50 HFHE TC IN         30.071 C
C   52 TEMP OUT           30.348 C
C   55 PRESSURE IN        41.755 PSIG
C   61 PAO FLOWRATE        3.746 KG/MIN
C   62 PAO DENSITY        0.7852 KG/L
```

```
C   80 VAC IN              28.32 VAC IN
C   81 AMP IN              1.413 AMP
C   82 WATTS IN            40.028 W

END SCAN GROUP 1       12 JUL 95  14:50:26


BEGIN SCAN GROUP 1     12 JUL 95  14:50:33
HYD. TESTS

C    1 BORDER BARRIER     34.876 C
C    2 BORDER BARRIER     34.132 C
C    3 BORDER BARRIER     33.573 C
C    4 BORDER BARRIER     32.545 C
C    5 BORDER BARRIER     30.668 C
C    6 BORDER BARRIER     39.370 C
C    7 BORDER BARRIER     30.739 C
C    8 BORDER BARRIER     30.753 C
C   11 BARRIER HTR        30.907 C
C   12 BARRIER HTR        35.296 C
C   13 BARRIER HTR        33.882 C
C   14 BARRIER HTR        33.320 C
C   15 BARRIER HTR        32.193 C
C   22 AMPLIFIER          50.679 C
C   24 AMPLIFIER          51.169 C
C   27 AMPLIFIER          50.012 C
C   30 AMPLIFIER          53.636 C
C   38 AMPLIFIER          55.702 C
C   40 AMPLIFIER          54.420 C
C   41 AMPLIFIER          55.392 C
C   45 AMPLIFIER          64.931 C
C   50 HFHE TC IN         29.791 C
C   52 TEMP OUT           30.379 C
C   55 PRESSURE IN        41.515 PSIG
C   61 PAO FLOWRATE        3.723 KG/MIN
C   62 PAO DENSITY        0.7854 KG/L
C   80 VAC IN             28.33 VAC IN
C   81 AMP IN             1.413 AMP
C   82 WATTS IN           40.034 W

END SCAN GROUP 1       12 JUL 95  14:50:36


BEGIN SCAN GROUP 1     12 JUL 95  14:50:43
HYD. TESTS

C    1 BORDER BARRIER     35.070 C
C    2 BORDER BARRIER     34.159 C
C    3 BORDER BARRIER     33.458 C
C    4 BORDER BARRIER     32.574 C
```

```
C    5  BORDER BARRIER      30.694 C
C    6  BORDER BARRIER      39.399 C
C    7  BORDER BARRIER      30.753 C
C    8  BORDER BARRIER      30.765 C
C   11  BARRIER HTR         30.926 C
C   12  BARRIER HTR         35.258 C
C   13  BARRIER HTR         33.898 C
C   14  BARRIER HTR         33.350 C
C   15  BARRIER HTR         32.209 C
C   22  AMPLIFIER           50.639 C
C   24  AMPLIFIER           51.197 C
C   27  AMPLIFIER           50.135 C
C   30  AMPLIFIER           53.528 C
C   38  AMPLIFIER           55.620 C
C   40  AMPLIFIER           54.371 C
C   41  AMPLIFIER           55.261 C
C   45  AMPLIFIER           65.016 C
C   50  HFHE TC IN          29.773 C
C   52  TEMP OUT            30.247 C
C   55  PRESSURE IN         41.820 PSIG
C   61  PAO FLOWRATE         3.761 KG/MIN
C   62  PAO DENSITY          0.7855 KG/L
C   80  VAC IN              28.32 VAC IN
C   81  AMP IN               1.422 AMP
C   82  WATTS IN            40.263 W

END SCAN GROUP 1      12 JUL 95   14:50:46


BEGIN SCAN GROUP 1    12 JUL 95   14:50:53
HYD. TESTS

C    1  BORDER BARRIER      35.006 C
C    2  BORDER BARRIER      34.136 C
C    3  BORDER BARRIER      33.506 C
C    4  BORDER BARRIER      32.548 C
C    5  BORDER BARRIER      30.671 C
C    6  BORDER BARRIER      39.359 C
C    7  BORDER BARRIER      30.769 C
C    8  BORDER BARRIER      30.757 C
C   11  BARRIER HTR         30.896 C
C   12  BARRIER HTR         35.285 C
C   13  BARRIER HTR         33.871 C
C   14  BARRIER HTR         33.309 C
C   15  BARRIER HTR         32.182 C
C   22  AMPLIFIER           50.639 C
C   24  AMPLIFIER           51.169 C
C   27  AMPLIFIER           50.149 C
C   30  AMPLIFIER           53.654 C
C   38  AMPLIFIER           55.867 C
```

```
C  40 AMPLIFIER        54.385 C
C  41 AMPLIFIER        55.140 C
C  45 AMPLIFIER        64.869 C
C  50 HFHE TC IN       30.038 C
C  52 TEMP OUT         30.413 C
C  55 PRESSURE IN      42.029 PSIG
C  61 PAO FLOWRATE      3.744 KG/MIN
C  62 PAO DENSITY      0.7853 KG/L
C  80 VAC IN            28.32 VAC IN
C  81 AMP IN            1.413 AMP
C  82 WATTS IN         40.028 W

END SCAN GROUP 1     12 JUL 95  14:50:56


BEGIN SCAN GROUP 1   12 JUL 95  14:51:03
HYD. TESTS

C   1 BORDER BARRIER   34.869 C
C   2 BORDER BARRIER   34.111 C
C   3 BORDER BARRIER   33.537 C
C   4 BORDER BARRIER   32.538 C
C   5 BORDER BARRIER   30.676 C
C   6 BORDER BARRIER   39.378 C
C   7 BORDER BARRIER   30.732 C
C   8 BORDER BARRIER   30.747 C
C  11 BARRIER HTR      30.901 C
C  12 BARRIER HTR      35.263 C
C  13 BARRIER HTR      33.876 C
C  14 BARRIER HTR      33.313 C
C  15 BARRIER HTR      32.187 C
C  22 AMPLIFIER        50.621 C
C  24 AMPLIFIER        51.122 C
C  27 AMPLIFIER        49.994 C
C  30 AMPLIFIER        53.643 C
C  38 AMPLIFIER        55.724 C
C  40 AMPLIFIER        54.429 C
C  41 AMPLIFIER        55.347 C
C  45 AMPLIFIER        64.848 C
C  50 HFHE TC IN       29.785 C
C  52 TEMP OUT         30.376 C
C  55 PRESSURE IN      41.896 PSIG
C  61 PAO FLOWRATE      3.746 KG/MIN
C  62 PAO DENSITY      0.7855 KG/L
C  80 VAC IN            28.31 VAC IN
C  81 AMP IN            1.413 AMP
C  82 WATTS IN         40.014 W

END SCAN GROUP 1     12 JUL 95  14:51:06
```

```
BEGIN SCAN GROUP 1    12 JUL 95  14:51:13
HYD. TESTS

C    1 BORDER BARRIER    35.041 C
C    2 BORDER BARRIER    34.130 C
C    3 BORDER BARRIER    33.444 C
C    4 BORDER BARRIER    32.542 C
C    5 BORDER BARRIER    30.665 C
C    6 BORDER BARRIER    39.382 C
C    7 BORDER BARRIER    30.707 C
C    8 BORDER BARRIER    30.736 C
C   11 BARRIER HTR       30.893 C
C   12 BARRIER HTR       35.238 C
C   13 BARRIER HTR       33.865 C
C   14 BARRIER HTR       33.303 C
C   15 BARRIER HTR       32.176 C
C   22 AMPLIFIER         50.593 C
C   24 AMPLIFIER         51.165 C
C   27 AMPLIFIER         50.171 C
C   30 AMPLIFIER         53.496 C
C   38 AMPLIFIER         55.628 C
C   40 AMPLIFIER         54.321 C
C   41 AMPLIFIER         55.065 C
C   45 AMPLIFIER         64.939 C
C   50 HFHE TC IN        29.973 C
C   52 TEMP OUT          30.261 C
C   55 PRESSURE IN       41.818 PSIG
C   61 PAO FLOWRATE       3.821 KG/MIN
C   62 PAO DENSITY       0.7853 KG/L
C   80 VAC IN            28.33 VAC IN
C   81 AMP IN             1.413 AMP
C   82 WATTS IN          40.034 W

END SCAN GROUP 1     12 JUL 95  14:51:16


BEGIN SCAN GROUP 1    12 JUL 95  14:51:23
HYD. TESTS

C    1 BORDER BARRIER    34.788 C
C    2 BORDER BARRIER    34.059 C
C    3 BORDER BARRIER    33.486 C
C    4 BORDER BARRIER    32.471 C
C    5 BORDER BARRIER    30.582 C
C    6 BORDER BARRIER    39.300 C
C    7 BORDER BARRIER    30.665 C
C    8 BORDER BARRIER    30.665 C
C   11 BARRIER HTR       30.834 C
C   12 BARRIER HTR       35.182 C
```

```
C   13  BARRIER HTR      33.795 C
C   14  BARRIER HTR      33.247 C
C   15  BARRIER HTR      32.120 C
C   22  AMPLIFIER        50.543 C
C   24  AMPLIFIER        51.058 C
C   27  AMPLIFIER        49.916 C
C   30  AMPLIFIER        53.608 C
C   38  AMPLIFIER        55.714 C
C   40  AMPLIFIER        54.361 C
C   41  AMPLIFIER        55.279 C
C   45  AMPLIFIER        64.767 C
C   50  HFHE TC IN       29.770 C
C   52  TEMP OUT         30.331 C
C   55  PRESSURE IN      41.820 PSIG
C   61  PAO FLOWRATE      3.797 KG/MIN
C   62  PAO DENSITY      0.7855 KG/L
C   80  VAC IN           28.33 VAC IN
C   81  AMP IN            1.413 AMP
C   82  WATTS IN         40.034 W

END SCAN GROUP 1      12 JUL 95  14:51:26

BEGIN SCAN GROUP 1    12 JUL 95  14:51:33
HYD. TESTS

C    1  BORDER BARRIER   34.919 C
C    2  BORDER BARRIER   34.034 C
C    3  BORDER BARRIER   33.378 C
C    4  BORDER BARRIER   32.449 C
C    5  BORDER BARRIER   30.587 C
C    6  BORDER BARRIER   39.276 C
C    7  BORDER BARRIER   30.655 C
C    8  BORDER BARRIER   30.655 C
C   11  BARRIER HTR      30.827 C
C   12  BARRIER HTR      35.201 C
C   13  BARRIER HTR      33.784 C
C   14  BARRIER HTR      33.237 C
C   15  BARRIER HTR      32.110 C
C   22  AMPLIFIER        50.587 C
C   24  AMPLIFIER        51.051 C
C   27  AMPLIFIER        49.906 C
C   30  AMPLIFIER        53.505 C
C   38  AMPLIFIER        55.597 C
C   40  AMPLIFIER        54.369 C
C   41  AMPLIFIER        55.288 C
C   45  AMPLIFIER        64.790 C
C   50  HFHE TC IN       29.691 C
C   52  TEMP OUT         30.308 C
C   55  PRESSURE IN      41.805 PSIG
C   61  PAO FLOWRATE      3.789 KG/MIN
```

```
C  62 PAO DENSITY        0.7855 KG/L
C  80 VAC IN              28.31 VAC IN
C  81 AMP IN              1.413 AMP
C  82 WATTS IN           40.008 W

END SCAN GROUP 1      12 JUL 95   14:51:36

BEGIN SCAN GROUP 1    12 JUL 95   14:51:43
HYD. TESTS

C   1 BORDER BARRIER    35.008 C
C   2 BORDER BARRIER    34.067 C
C   3 BORDER BARRIER    33.411 C
C   4 BORDER BARRIER    32.479 C
C   5 BORDER BARRIER    30.602 C
C   6 BORDER BARRIER    39.308 C
C   7 BORDER BARRIER    30.703 C
C   8 BORDER BARRIER    30.688 C
C  11 BARRIER HTR       30.842 C
C  12 BARRIER HTR       35.204 C
C  13 BARRIER HTR       33.803 C
C  14 BARRIER HTR       33.255 C
C  15 BARRIER HTR       32.113 C
C  22 AMPLIFIER         50.587 C
C  24 AMPLIFIER         51.131 C
C  27 AMPLIFIER         50.140 C
C  30 AMPLIFIER         53.408 C
C  38 AMPLIFIER         55.543 C
C  40 AMPLIFIER         54.290 C
C  41 AMPLIFIER         55.059 C
C  45 AMPLIFIER         64.962 C
C  50 HFHE TC IN        29.842 C
C  52 TEMP OUT          30.175 C
C  55 PRESSURE IN       41.819 PSIG
C  61 PAO FLOWRATE       3.716 KG/MIN
C  62 PAO DENSITY        0.7854 KG/L
C  80 VAC IN             28.32 VAC IN
C  81 AMP IN             1.422 AMP
C  82 WATTS IN          40.256 W

END SCAN GROUP 1      12 JUL 95   14:51:46

BEGIN SCAN GROUP 1    12 JUL 95   14:51:53
HYD. TESTS

C   1 BORDER BARRIER    34.882 C
C   2 BORDER BARRIER    34.067 C
C   3 BORDER BARRIER    33.479 C
C   4 BORDER BARRIER    32.479 C
C   5 BORDER BARRIER    30.632 C
```

```
C    6  BORDER BARRIER    39.320 C
C    7  BORDER BARRIER    30.729 C
C    8  BORDER BARRIER    30.703 C
C   11  BARRIER HTR       30.872 C
C   12  BARRIER HTR       35.216 C
C   13  BARRIER HTR       33.817 C
C   14  BARRIER HTR       33.270 C
C   15  BARRIER HTR       32.158 C
C   22  AMPLIFIER         50.537 C
C   24  AMPLIFIER         51.109 C
C   27  AMPLIFIER         50.115 C
C   30  AMPLIFIER         53.577 C
C   38  AMPLIFIER         55.776 C
C   40  AMPLIFIER         54.290 C
C   41  AMPLIFIER         55.005 C
C   45  AMPLIFIER         64.828 C
C   50  HFHE TC IN        30.021 C
C   52  TEMP OUT          30.328 C
C   55  PRESSURE IN       41.793 PSIG
C   61  PAO FLOWRATE       3.842 KG/MIN
C   62  PAO DENSITY       0.7853 KG/L
C   80  VAC IN            28.30 VAC IN
C   81  AMP IN             1.413 AMP
C   82  WATTS IN          40.001 W

END SCAN GROUP 1      12 JUL 95   14:51:56

BEGIN SCAN GROUP 1    12 JUL 95   14:52:03
HYD. TESTS

C    1  BORDER BARRIER    34.786 C
C    2  BORDER BARRIER    34.042 C
C    3  BORDER BARRIER    33.483 C
C    4  BORDER BARRIER    32.472 C
C    5  BORDER BARRIER    30.607 C
C    6  BORDER BARRIER    39.269 C
C    7  BORDER BARRIER    30.678 C
C    8  BORDER BARRIER    30.692 C
C   11  BARRIER HTR       30.846 C
C   12  BARRIER HTR       35.194 C
C   13  BARRIER HTR       33.792 C
C   14  BARRIER HTR       33.245 C
C   15  BARRIER HTR       32.118 C
C   22  AMPLIFIER         50.541 C
C   24  AMPLIFIER         51.031 C
C   27  AMPLIFIER         49.903 C
C   30  AMPLIFIER         53.553 C
C   38  AMPLIFIER         55.645 C
C   40  AMPLIFIER         54.387 C
C   41  AMPLIFIER         55.277 C
```

```
C  45  AMPLIFIER        64.793 C
C  50  HFHE TC IN       29.680 C
C  52  TEMP OUT         30.340 C
C  55  PRESSURE IN      41.968 PSIG
C  61  PAO FLOWRATE      3.776 KG/MIN
C  62  PAO DENSITY      0.7855 KG/L
C  80  VAC IN           28.31 VAC IN
C  81  AMP IN            1.413 AMP
C  82  WATTS IN         40.008 W

END SCAN GROUP 1      12 JUL 95   14:52:06

BEGIN SCAN GROUP 1    12 JUL 95   14:52:13
HYD. TESTS

C   1  BORDER BARRIER   34.987 C
C   2  BORDER BARRIER   34.062 C
C   3  BORDER BARRIER   33.390 C
C   4  BORDER BARRIER   32.462 C
C   5  BORDER BARRIER   30.584 C
C   6  BORDER BARRIER   39.288 C
C   7  BORDER BARRIER   30.682 C
C   8  BORDER BARRIER   30.655 C
C  11  BARRIER HTR      30.809 C
C  12  BARRIER HTR      35.169 C
C  13  BARRIER HTR      33.770 C
C  14  BARRIER HTR      33.208 C
C  15  BARRIER HTR      32.096 C
C  22  AMPLIFIER        50.531 C
C  24  AMPLIFIER        51.089 C
C  27  AMPLIFIER        50.109 C
C  30  AMPLIFIER        53.395 C
C  38  AMPLIFIER        55.595 C
C  40  AMPLIFIER        54.298 C
C  41  AMPLIFIER        54.959 C
C  45  AMPLIFIER        64.889 C
C  50  HFHE TC IN       29.956 C
C  52  TEMP OUT         30.230 C
C  55  PRESSURE IN      41.822 PSIG
C  61  PAO FLOWRATE      3.672 KG/MIN
C  62  PAO DENSITY      0.7853 KG/L
C  80  VAC IN           28.32 VAC IN
C  81  AMP IN            1.413 AMP
C  82  WATTS IN         40.021 W

END SCAN GROUP 1      12 JUL 95   14:52:16

STOPPED SCANNING      12 JUL 95   14:52:17
*********************************************************************************
```

## D.2  Output File

The following file shows the output file from the data

reduction program, LAB.  This particular file is for the

coolant temperature of 30°C, flow rate of 3.75 kg/min, and a

heat load of 40 W.  This file shows the individual data

points for all 15 measurements.

```
******************************************************************
12 JUL 95
    1 BORDER BARRIER      35.171   35.034   35.010   35.136   34.876   35.070
35.006   34.869   35.041   34.788   34.919   35.008   34.882   34.786   34.987
    2 BORDER BARRIER      34.246   34.206   34.196   34.210   34.132   34.159
34.136   34.111   34.130   34.059   34.034   34.067   34.067   34.042   34.062
    3 BORDER BARRIER      33.586   33.564   33.595   33.539   33.573   33.458
33.506   33.537   33.444   33.486   33.378   33.411   33.479   33.483   33.390
    4 BORDER BARRIER      32.658   32.621   32.611   32.611   32.545   32.574
32.548   32.538   32.542   32.471   32.449   32.479   32.479   32.472   32.462
    5 BORDER BARRIER      30.796   30.745   30.749   30.719   30.668   30.694
30.671   30.676   30.665   30.582   30.587   30.602   30.632   30.607   30.584
    6 BORDER BARRIER      39.496   39.445   39.450   39.421   39.370   39.399
39.359   39.378   39.382   39.300   39.276   39.308   39.320   39.269   39.288
    7 BORDER BARRIER      30.867   30.813   30.832   30.805   30.739   30.753
30.769   30.732   30.707   30.665   30.655   30.703   30.729   30.678   30.682
    8 BORDER BARRIER      30.879   30.827   30.817   30.805   30.753   30.765
30.757   30.747   30.736   30.665   30.655   30.688   30.703   30.692   30.655
   11 BARRIER HTR         31.006   30.984   30.989   30.944   30.907   30.926
30.896   30.901   30.893   30.834   30.827   30.842   30.872   30.846   30.809
   12 BARRIER HTR         35.423   35.328   35.277   35.362   35.296   35.258
35.285   35.263   35.238   35.182   35.201   35.204   35.216   35.194   35.169
   13 BARRIER HTR         33.978   33.941   33.946   33.919   33.882   33.898
33.871   33.876   33.865   33.795   33.784   33.803   33.817   33.792   33.770
   14 BARRIER HTR         33.433   33.394   33.386   33.357   33.320   33.350
33.309   33.313   33.303   33.247   33.237   33.255   33.270   33.245   33.208
   15 BARRIER HTR         32.292   32.267   32.260   32.216   32.193   32.209
32.182   32.187   32.176   32.120   32.110   32.113   32.158   32.118   32.096
   22 AMPLIFIER           50.832   50.667   50.659   50.729   50.679   50.639
50.639   50.621   50.593   50.543   50.587   50.587   50.537   50.541   50.531
   24 AMPLIFIER           51.308   51.225   51.214   51.247   51.169   51.197
51.169   51.122   51.165   51.058   51.051   51.131   51.109   51.031   51.089
   27 AMPLIFIER           50.274   50.166   50.061   50.267   50.012   50.135
50.149   49.994   50.171   49.916   49.906   50.140   50.115   49.903   50.109
   30 AMPLIFIER           53.598   53.777   53.616   53.578   53.636   53.528
53.654   53.643   53.496   53.608   53.505   53.408   53.577   53.553   53.395
   38 AMPLIFIER           55.690   55.950   55.708   55.777   55.702   55.620
55.867   55.724   55.628   55.714   55.597   55.543   55.776   55.645   55.595
   40 AMPLIFIER           54.435   54.427   54.459   54.381   54.420   54.371
54.385   54.429   54.321   54.361   54.369   54.290   54.290   54.387   54.298
```

```
   41 AMPLIFIER         55.297  55.277  55.428  55.110  55.392  55.261
55.140  55.347  55.065  55.279  55.288  55.059  55.005  55.277  54.959
   45 AMPLIFIER         65.143  64.938  64.969  64.984  64.931  65.016
64.869  64.848  64.939  64.767  64.790  64.962  64.828  64.793  64.889
   50 HFHE TC IN        29.912  30.040  29.783  30.071  29.791  29.773
30.038  29.785  29.973  29.770  29.691  29.842  30.021  29.680  29.956
   52 TEMP OUT          30.273  30.499  30.385  30.348  30.379  30.247
30.413  30.376  30.261  30.331  30.308  30.175  30.328  30.340  30.230
   55 PRESSURE IN       41.744  41.857  41.613  41.755  41.515  41.820
42.029  41.896  41.818  41.820  41.805  41.819  41.793  41.968  41.822
   61 PAO FLOWRATE       3.687   3.755   3.701   3.746   3.723   3.761
 3.744   3.746   3.821   3.797   3.789   3.716   3.842   3.776   3.672
   62 PAO DENSITY        0.785   0.785   0.785   0.785   0.785   0.785
 0.785   0.785   0.785   0.785   0.785   0.785   0.785   0.785   0.785
   80 VAC IN            28.300  28.320  28.340  28.320  28.330  28.320
28.320  28.310  28.330  28.330  28.310  28.320  28.300  28.310  28.320
   81 AMP IN             1.413   1.413   1.413   1.413   1.413   1.422
 1.413   1.413   1.413   1.413   1.413   1.422   1.413   1.413   1.413
   82 WATTS IN          39.994  40.028  40.047  40.028  40.034  40.263
40.028  40.014  40.034  40.034  40.008  40.256  40.001  40.008  40.021
**********************************************************************
```

## D.3   Summary File

The following file is the summary file consisting of the averaged values of the 15 measurments for the entire range of flow rates and heat loads for a given temperature. This particular file represents the averaged values for a coolant temperature of 30°C.  The summary file is obtained one line at a time by the data reduction program.  For this particular summary program the averaged values are presented in the following form:

```
Flow Rate &
Heat Load        c 1          c 2          c 3          c 4          c 5
c 6          c 7          c 8          c 11         c 12         c 13
c 15         c 22         c 24         c 27         c 30         c 38
c 40         c 41         c 45         c 50         c 52
c 55         c 61         c 80         c 81         c 82
```

Where the channels represent the following:

| | |
|---|---|
| c  1 - c 15 | Surface Temperatures (°C) |
| c 22 - c 45 | Amplifier Temperatures (°C) |
| c 50 & c 52 | Coolant Inlet and Outlet Temperatures (°C) |
| c 55 | Pressure Drop across the HFHE (psi) |
| c 61 | Mass Flow Rate (kg/min) |
| c 80 | Voltage (V) |
| c 81 | Current (A) |
| c 82 | Input Power (W) |

File BT6

\* \* \* \* \* \* \* \* \* \* \* \* \* \* \* \* \* \* \* \* \* \* \* \* \* \* \* \* \* \* \* \* \* \* \* \* \* \* \* \* \* \* \* \* \* \* \* \* \* \* \* \* \* \*

```
f7p1            33.923        33.444        33.097        32.475        31.274
36.633      31.338        31.348        31.474        34.284        33.461
33.146      32.420        43.150        43.485        42.883        44.955
46.120      44.884        45.795        51.371        30.011        30.416
23.410       2.730         0.785        21.424         0.931        19.940
f9p1            34.002        33.524        33.173        32.578        31.416
36.686      31.490        31.498        31.622        34.357        33.543
33.227      32.518        43.233        43.549        42.954        44.999
46.182      44.878        45.806        51.423        30.125        30.515
27.165       2.979         0.785        21.489         0.930        19.983
f10p1           33.812        33.341        33.011        32.435        31.327
36.455      31.397        31.403        31.529        34.159        33.350
33.041      32.364        42.966        43.281        42.690        44.713
45.886      44.680        45.523        51.113        30.046        30.389
32.251       3.250         0.785        21.396         0.927        19.842
f11p1           33.668        33.201        32.857        32.303        31.217
36.315      31.279        31.294        31.418        34.009        33.205
32.904      32.231        42.832        43.178        42.564        44.622
45.797      44.453        45.453        51.040        29.936        30.300
35.817       3.458         0.785        21.400         0.927        19.846
f12p1           33.529        33.065        32.729        32.168        31.105
36.174      31.171        31.181        31.300        33.857        33.047
32.747      32.077        42.777        43.102        42.494        44.544
45.732      44.652        45.383        51.046        29.880        30.236
40.433       3.690         0.785        21.449         0.931        19.972
f12p1           33.738        33.293        32.975        32.416        31.387
36.378      31.458        31.460        31.586        34.070        33.267
32.966      32.325        43.015        43.324        42.725        44.762
45.962      44.824        45.590        51.261        30.162        30.502
46.638       4.034         0.785        21.465         0.933        20.020
f1p2            37.558        36.603        35.812        34.385        31.350
42.589      31.459        31.440        31.585        38.148        36.592
35.925      34.399        53.834        54.427        53.295        56.789
58.906      56.158        58.334        67.928        29.877        31.019
3.364        1.062         0.785        28.332         1.399        39.622
f2p2            37.132        36.189        35.398        34.102        31.277
42.053      31.371        31.359        31.511        37.694        36.160
35.515      34.041        53.195        53.730        52.675        56.151
58.257      55.786        57.717        67.308        29.982        30.906
5.240        1.292         0.785        28.290         1.401        39.629
f3p2            36.694        35.796        35.053        33.837        31.253
41.427      31.348        31.337        31.494        37.194        35.720
35.104      33.708        52.393        52.907        51.898        55.321
57.396      55.205        56.871        66.307        30.065        30.838
7.981        1.516         0.785        28.121         1.389        39.066
f4p2            36.290        35.417        34.716        33.531        31.092
40.938      31.186        31.170        31.338        36.775        35.335
34.734      33.385        51.818        52.320        51.311        54.694
56.750      54.647        56.224        65.607        29.900        30.570
9.947        1.727         0.785        28.135         1.391        39.149
f5p2            36.360        35.469        34.773        33.612        31.252
40.990      31.351        31.332        31.495        36.783        35.333
34.732      33.400        52.071        52.557        51.528        54.996
57.094      55.041        56.559        66.081        30.172        30.801
13.129       2.000         0.785        28.192         1.401        39.478
f6p2            36.077        35.222        34.542        33.424        31.165
40.675      31.262        31.251        31.409        36.504        35.062
34.473      33.181        51.787        52.308        51.271        54.708
56.820      54.864        56.266        65.819        30.147        30.692
16.215       2.239         0.785        28.191         1.403        39.551
f7p2            35.755        34.895        34.230        33.161        31.001
40.279      31.098        31.085        31.247        36.141        34.719
34.140      32.886        51.346        51.853        50.834        54.251
56.346      54.618        55.824        65.364        30.045        30.545
20.180       2.555         0.785        28.154         1.393        39.212



f8p2            35.584        34.742        34.091        33.033        30.934
40.130      31.028        31.013        31.178        35.964        34.541
```

| | | | | | |
|---|---|---|---|---|---|
| 33.966 | 32.731 | 51.328 | 51.840 | 50.799 | 54.269 |
| 56.386 | 54.677 | 55.861 | 65.497 | 29.989 | 30.475 |
| 23.839 | 2.804 | 0.785 | 28.337 | 1.415 | 40.098 |
| f9p2 | 35.510 | 34.654 | 34.004 | 32.982 | 30.959 |
| 39.977 | 31.042 | 31.039 | 31.198 | 35.838 | 34.424 |
| 33.853 | 32.662 | 51.171 | 51.694 | 50.647 | 54.114 |
| 56.227 | 54.596 | 55.718 | 65.358 | 30.026 | 30.496 |
| 28.482 | 3.059 | 0.785 | 28.347 | 1.412 | 40.034 |
| f10p2 | 35.338 | 34.520 | 33.892 | 32.891 | 30.924 |
| 39.787 | 31.012 | 31.005 | 31.169 | 35.687 | 34.288 |
| 33.729 | 32.561 | 50.935 | 51.449 | 50.397 | 53.882 |
| 55.997 | 54.431 | 55.472 | 65.054 | 30.061 | 30.506 |
| 32.305 | 3.250 | 0.785 | 28.247 | 1.403 | 39.628 |
| f11p2 | 35.337 | 34.504 | 33.876 | 32.902 | 30.996 |
| 39.733 | 31.079 | 31.075 | 31.233 | 35.644 | 34.257 |
| 33.711 | 32.562 | 50.873 | 51.400 | 50.364 | 53.803 |
| 55.912 | 54.432 | 55.401 | 65.008 | 30.087 | 30.519 |
| 36.281 | 3.462 | 0.785 | 28.346 | 1.410 | 39.974 |
| f12p2 | 35.042 | 34.201 | 33.577 | 32.613 | 30.735 |
| 39.444 | 30.818 | 30.816 | 30.971 | 35.334 | 33.937 |
| 33.385 | 32.253 | 50.718 | 51.245 | 50.182 | 53.666 |
| 55.798 | 54.436 | 55.301 | 65.011 | 29.932 | 30.382 |
| 41.696 | 3.766 | 0.785 | 28.337 | 1.415 | 40.100 |
| f1p3 | 40.349 | 38.986 | 37.812 | 35.816 | 31.474 |
| 47.364 | 31.594 | 31.549 | 31.724 | 41.092 | 38.901 |
| 37.949 | 35.788 | 63.152 | 63.800 | 62.362 | 67.158 |
| 70.208 | 66.275 | 69.504 | 82.994 | 29.898 | 31.408 |
| 2.855 | 0.945 | 0.785 | 33.985 | 1.799 | 61.135 |
| f2p3 | 39.690 | 38.330 | 37.173 | 35.298 | 31.213 |
| 46.554 | 31.321 | 31.288 | 31.466 | 40.316 | 38.153 |
| 37.215 | 35.120 | 62.396 | 63.067 | 61.604 | 66.461 |
| 69.501 | 65.821 | 68.837 | 82.350 | 29.876 | 31.155 |
| 4.649 | 1.213 | 0.785 | 34.061 | 1.807 | 61.542 |
| f3p3 | 38.903 | 37.583 | 36.496 | 34.747 | 31.027 |
| 45.536 | 31.135 | 31.107 | 31.287 | 39.430 | 37.321 |
| 36.415 | 34.435 | 61.324 | 61.995 | 60.530 | 65.371 |
| 68.383 | 65.017 | 67.749 | 81.178 | 29.923 | 30.932 |
| 8.031 | 1.513 | 0.785 | 33.932 | 1.798 | 61.014 |
| f4p3 | 38.575 | 37.282 | 36.230 | 34.531 | 30.980 |
| 45.136 | 31.084 | 31.056 | 31.246 | 39.073 | 36.969 |
| 36.080 | 34.155 | 60.944 | 61.673 | 60.215 | 64.997 |
| 68.055 | 64.840 | 67.375 | 80.933 | 29.977 | 30.834 |
| 10.473 | 1.768 | 0.785 | 33.908 | 1.789 | 60.669 |
| f5p3 | 38.270 | 37.004 | 35.982 | 34.308 | 30.876 |
| 44.831 | 30.978 | 30.953 | 31.141 | 38.752 | 36.661 |
| 35.782 | 33.888 | 60.721 | 61.423 | 59.944 | 64.801 |
| 67.841 | 64.635 | 67.199 | 80.750 | 29.923 | 30.743 |
| 12.653 | 1.933 | 0.785 | 33.995 | 1.798 | 61.130 |
| f6p3 | 37.936 | 36.651 | 35.617 | 34.056 | 30.820 |
| 44.310 | 30.920 | 30.895 | 31.082 | 38.297 | 36.238 |
| 35.376 | 33.559 | 60.206 | 60.904 | 59.418 | 64.249 |
| 67.279 | 64.280 | 66.649 | 80.210 | 29.925 | 30.647 |
| 16.798 | 2.272 | 0.785 | 33.897 | 1.797 | 60.922 |
| f7p3 | 37.843 | 36.540 | 35.517 | 34.006 | 30.874 |
| 44.144 | 30.971 | 30.946 | 31.134 | 38.155 | 36.099 |
| 35.247 | 33.467 | 60.095 | 60.802 | 59.300 | 64.144 |
| 67.166 | 64.284 | 66.558 | 80.163 | 29.975 | 30.642 |
| 19.969 | 2.481 | 0.785 | 33.909 | 1.794 | 60.847 |
| f8p3 | 37.608 | 36.373 | 35.412 | 33.893 | 30.877 |
| 43.919 | 30.983 | 30.952 | 31.139 | 37.956 | 35.914 |
| 35.074 | 33.336 | 59.914 | 60.625 | 59.145 | 63.979 |
| 67.049 | 64.108 | 66.380 | 80.012 | 30.059 | 30.681 |
| 23.583 | 2.747 | 0.785 | 34.021 | 1.801 | 61.267 |
| f9p3 | 37.394 | 36.166 | 35.216 | 33.741 | 30.813 |
| 43.653 | 30.908 | 30.888 | 31.075 | 37.721 | 35.696 |
| 34.876 | 33.168 | 59.604 | 60.307 | 58.813 | 63.692 |
| 66.724 | 63.896 | 66.081 | 79.649 | 29.979 | 30.595 |
| 26.475 | 2.943 | 0.785 | 33.994 | 1.796 | 61.064 |
| f10p3 | 37.065 | 35.850 | 34.921 | 33.492 | 30.681 |
| 43.262 | 30.781 | 30.759 | 30.946 | 37.356 | 35.350 |
| 34.540 | 32.890 | 59.283 | 59.976 | 58.471 | 63.351 |

| | | | | | |
|---|---|---|---|---|---|
| 66.380 | 63.634 | 65.760 | 79.351 | 29.875 | 30.463 |
| 32.891 | 3.283 | 0.785 | 33.953 | 1.792 | 60.842 |
| f11p3 | 37.024 | 35.808 | 34.870 | 33.500 | 30.772 |
| 43.179 | 30.856 | 30.847 | 31.029 | 37.284 | 35.306 |
| 34.505 | 32.891 | 59.148 | 59.867 | 58.376 | 63.203 |
| 66.234 | 64.018 | 65.595 | 79.218 | 29.946 | 30.507 |
| 36.789 | 3.506 | 0.785 | 33.889 | 1.784 | 60.472 |
| f13p3 | 36.891 | 35.711 | 34.826 | 33.487 | 30.913 |
| 43.024 | 31.001 | 30.993 | 31.175 | 37.173 | 35.193 |
| 34.410 | 32.871 | 59.039 | 59.746 | 58.245 | 63.122 |
| 66.164 | 63.685 | 65.522 | 79.092 | 30.002 | 30.558 |
| 46.953 | 4.057 | 0.785 | 34.065 | 1.793 | 61.097 |
| f3p4 | 41.394 | 39.688 | 38.276 | 36.021 | 31.210 |
| 49.798 | 31.330 | 31.284 | 31.499 | 42.014 | 39.290 |
| 38.121 | 35.578 | 69.875 | 70.756 | 68.855 | 74.995 |
| 78.890 | 74.315 | 78.128 | 95.303 | 29.925 | 31.238 |
| 7.350 | 1.469 | 0.785 | 38.618 | 2.092 | 80.789 |
| f4p4 | 40.958 | 39.314 | 37.960 | 35.769 | 31.204 |
| 49.289 | 31.330 | 31.284 | 31.494 | 41.495 | 38.842 |
| 37.682 | 35.213 | 69.441 | 70.201 | 68.427 | 74.606 |
| 78.499 | 74.104 | 77.762 | 94.988 | 30.113 | 31.270 |
| 10.084 | 1.733 | 0.785 | 38.707 | 2.089 | 80.828 |
| f5p4 | 40.515 | 38.883 | 37.565 | 35.440 | 31.078 |
| 48.741 | 31.214 | 31.153 | 31.369 | 41.042 | 38.347 |
| 37.210 | 34.805 | 68.968 | 69.990 | 68.018 | 74.161 |
| 78.124 | 73.976 | 77.313 | 94.737 | 30.180 | 31.154 |
| 13.100 | 1.960 | 0.785 | 38.802 | 2.091 | 81.115 |
| f6p4 | 39.888 | 38.304 | 37.030 | 34.974 | 30.797 |
| 48.009 | 30.917 | 30.869 | 31.086 | 40.370 | 37.728 |
| 36.616 | 34.274 | 68.199 | 69.104 | 67.234 | 73.355 |
| 77.311 | 73.398 | 76.528 | 93.856 | 30.034 | 30.953 |
| 16.311 | 2.227 | 0.785 | 38.598 | 2.085 | 80.453 |
| f7p4 | 39.374 | 37.783 | 36.528 | 34.562 | 30.587 |
| 47.329 | 30.711 | 30.661 | 30.879 | 39.774 | 37.153 |
| 36.061 | 33.798 | 67.436 | 68.393 | 66.526 | 72.561 |
| 76.501 | 72.891 | 75.717 | 93.146 | 29.863 | 30.632 |
| 20.463 | 2.529 | 0.785 | 38.656 | 2.088 | 80.703 |
| f8p4 | 39.197 | 37.638 | 36.406 | 34.458 | 30.585 |
| 47.197 | 30.704 | 30.659 | 30.874 | 39.599 | 36.975 |
| 35.888 | 33.660 | 67.496 | 68.403 | 66.498 | 72.694 |
| 76.637 | 73.035 | 75.899 | 93.339 | 29.842 | 30.632 |
| 23.912 | 2.759 | 0.785 | 38.785 | 2.094 | 81.203 |
| f9p4 | 39.139 | 37.612 | 36.424 | 34.532 | 30.826 |
| 47.048 | 30.945 | 30.899 | 31.118 | 39.516 | 36.933 |
| 35.863 | 33.706 | 67.295 | 68.216 | 66.305 | 72.489 |
| 76.428 | 73.075 | 75.691 | 93.123 | 30.128 | 30.854 |
| 28.858 | 3.057 | 0.785 | 38.774 | 2.096 | 81.242 |
| f11p4 | 38.596 | 37.056 | 35.861 | 34.065 | 30.532 |
| 46.368 | 30.640 | 30.603 | 30.819 | 38.849 | 36.319 |
| 35.268 | 33.189 | 66.701 | 67.618 | 65.680 | 71.925 |
| 75.848 | 72.755 | 75.142 | 92.615 | 29.938 | 30.651 |
| 37.274 | 3.497 | 0.785 | 38.720 | 2.094 | 81.083 |
| f12p4 | 38.316 | 36.828 | 35.691 | 33.916 | 30.498 |
| 46.069 | 30.613 | 30.578 | 30.795 | 38.622 | 36.100 |
| 35.064 | 33.040 | 66.277 | 67.228 | 65.315 | 71.469 |
| 75.414 | 72.484 | 74.667 | 92.160 | 29.935 | 30.569 |
| 41.997 | 3.776 | 0.785 | 38.769 | 2.093 | 81.116 |
| f13p4 | 38.375 | 36.857 | 35.700 | 33.974 | 30.625 |
| 46.055 | 30.734 | 30.703 | 30.914 | 38.609 | 36.108 |
| 35.076 | 33.079 | 66.298 | 67.241 | 65.315 | 71.508 |
| 75.446 | 72.511 | 74.713 | 92.178 | 30.025 | 30.670 |
| 46.062 | 3.985 | 0.785 | 38.772 | 2.090 | 81.008 |
| f5p5 | 42.486 | 40.480 | 38.852 | 36.258 | 30.926 |
| 52.551 | 31.065 | 31.000 | 31.246 | 43.067 | 39.769 |
| 38.359 | 35.417 | 77.421 | 78.557 | 76.235 | 83.770 |
| 88.661 | 83.542 | 87.751 | 109.110 | 29.910 | 31.097 |
| 13.648 | 2.001 | 0.785 | 43.410 | 2.350 | 102.020 |
| f7p5 | 41.519 | 39.565 | 38.018 | 35.591 | 30.692 |
| 51.278 | 30.832 | 30.768 | 31.019 | 41.961 | 38.737 |
| 37.383 | 34.608 | 76.029 | 76.992 | 74.853 | 82.362 |
| 87.215 | 82.515 | 86.346 | 107.578 | 29.909 | 30.907 |
| 20.195 | 2.519 | 0.785 | 43.286 | 2.343 | 101.410 |

```
f9p5            41.057        39.121        37.616        35.326        30.742
50.625        30.858        30.817        31.060        41.390        38.215
36.896        34.250        75.424        76.581        74.233        81.739
86.577        82.088        85.706       106.979        29.976        30.836
27.852         2.990         0.785        43.146         2.340       100.963
f10p5           40.840        38.880        37.369        35.147        30.708
50.315        30.819        30.778        31.017        41.080        37.932
36.626        34.040        75.207        76.308        73.996        81.567
86.400        82.032        85.559       106.820        29.940        30.803
32.405         3.208         0.785        43.244         2.342       101.279
f11p5           40.261        38.418        37.014        34.783        30.491
49.770        30.625        30.563        30.808        40.606        37.484
36.191        33.677        74.637        75.734        73.442        80.973
85.810        81.741        84.942       106.153        29.897        30.700
37.227         3.496         0.785        43.214         2.343       101.250
f12p5           40.199        38.363        36.958        34.787        30.607
49.629        30.720        30.678        30.923        40.524        37.403
36.127        33.659        74.462        75.697        73.308        80.735
85.663        81.399        84.674       106.036        30.083        30.758
41.720         3.707         0.785        43.110         2.340       100.884
f13p5           40.190        38.297        36.871        34.773        30.703
49.504        30.812        30.775        31.014        40.405        37.310
36.050        33.628        74.381        75.499        73.133        80.691
85.505        81.350        84.671       105.942        30.056        30.777
46.661         4.026         0.785        43.233         2.344       101.327
```

* * * * * * * * * * * * * * * * * * * * * * * * * * * * * * * * * * * * * * * * * * * * * * * * * * * * * * * * * *

## D.4  Data Reduction Program

The following program represents the data reduction

program LAB.  This program contains one input, the data

output file of the Fluke data logger, and two outputs, the

data output file and the summary file.

```
*****************************************************************

PROGRAM LAB
*     This is a data conversion program for Mike Cutbirth
*     written 7/1/95
        REAL X1(30,30),SD(30),AVGFILE(30)
        CHARACTER
C*1,A(5)*50,A1(2,30)*15,FILNM1*10,FILNM2*10
        CHARACTER FILNM3*10,IDNEW*10,IDOLD*10
        INTEGER Y(30)
        PRINT*,'ENTER THE FILENAME OF THE DATA FILE        '
        READ*, FILNM1
        OPEN (UNIT=8,FILE=FILNM1,STATUS='OLD')
        PRINT*,'ENTER THE FILENAME OF THE NEW DATA FILE  '
        READ*, FILNM2
        OPEN (UNIT=9,FILE=FILNM2,STATUS='UNKNOWN')
*************************************************************
*         THIS BLOCK READS IN THE FIRST DATA SET            *
*************************************************************
*
*
        DO 10, I=1,5
                READ (8,100) A(I)
   10   CONTINUE
        J=1
        DO 20, I=1,30
                READ (8,110) C,Y(I),A1(1,I),X1(J,I),A1(2,I)
                IF(C.NE."C") THEN
                        K=I-1
                        GOTO 21
                ENDIF
   20   CONTINUE
   21   CONTINUE
*
****************************************************************
*
*  THIS BLOCK CHECKS TO SEE IF ADDITIONAL DATA SETS
*
*    EXISTS AND READS THEM
*
```

```
************************************************************
*
*
*
        DO 40, J=2,30
        I=1
        DO 23, M=1,15
        READ(8,125,ERR=22) C,X1(J,I)
 22     CONTINUE
        IF(C.EQ."S") GOTO 50
        IF(C.EQ."C") GOTO 25
 23     CONTINUE
 25     CONTINUE
        DO 30, I=2,K
                READ(8,130) X1(J,I)
 30     CONTINUE
 40     CONTINUE
 50     CONTINUE
*
*************************************************************
****
*   THIS BLOCK PRINT THE DATA IN THE NEW FORMAT
*
*************************************************************
****
*
*
        K1=J-1
        WRITE(9,135) A(3)
        DO 60, I=1,K
                WRITE(9,140) Y(I),A1(1,I),(X1(K2,I),K2=1,K1)
 60     CONTINUE
        CLOSE(8)
*
*************************************************************
***
*   THIS BLOCK CALCULATES AND PRINTS THE AVERAGES AND RMS
*
*************************************************************
***
*
*
*       WRITE(9,*)
C       WRITE(9,*) '        RMS AND AVERAGES  '
        DO 80, I=1,K
        X2=0.0
        DO 70, J=1,K1
                X2=X2+X1(J,I)
 70     CONTINUE
        X2AVG=X2/REAL(K1)
```

```
               AVGFILE(I)=X2AVG
               DO 72, J=1,K1
                     SD(J)=SQRT((X1(J,I)-X2AVG)**2)
     72      CONTINUE
C              WRITE(9,140) Y(I),A1(1,I),(SD(J),J=1,K1)
C              WRITE(9,150) X2AVG
C              WRITE(9,*)
     80      CONTINUE
             PRINT*, '   DATA CONVERSION COMPLETED   '
             CLOSE(9)
*************************************************************
*
*         THIS BLOCK PRINTS AVERAGES IN A DIFFERENT FILE
*         AFTER PREVIOUS RUNS
*************************************************************
**

             PRINT*
             PRINT*,'    ENTER FILENAME FOR ACCUM. AVERAGE FILE'
             PRINT*
             READ*, FILNM3
             PRINT*, '   ENTER INDENTIFIER NAME FOR THIS RUN'
             PRINT*
             READ*, IDNEW
             OPEN(UNIT=10, FILE=FILNM3, STATUS='UNKNOWN')
             DO 90, I=1,150
                     READ(10,160,END=91) IDOLD, AVGOLD
     90      CONTINUE
     91      CONTINUE
             WRITE(10,170) IDNEW,(AVGFILE(J),J=1,K)
             CLOSE(10)
*************************************************************
**
*
    100      FORMAT(19X,A12)
    110      FORMAT(A1,1X,I3,1X,A15,1X,E7.3,1X,A7)
    120      FORMAT(A1)
    125      FORMAT(A1,21X,E7.3)
    130      FORMAT(22X,E7.3)
    135      FORMAT(6X,A12)
    140      FORMAT(1X,I3,1X,A15,1X,30F8.3)
    150      FORMAT(1X,'AVERAGE = ',F15.3)
    160      FORMAT(A10,F15.3)
    170      FORMAT(A10,30F15.3)
             END
*************************************************************
```

APPENDIX E


UNCERTAINTY ANALYSIS


To fully evaluate the equations that were developed
from curve fitting the experimental data, such as the radial
heat loss due to conduction equation and the temperature
difference between the wall and fluid, a least squares
analysis was performed on the deviation between the
experimental data and the curve fitted data for each
equation. However, this analysis does not apply for
equations developed by using previous equations instead of
experimental data. Examples of these equations include the
thermal resistance equation and the thermal performance
equation. It is assumed that the uncertainty of these
equations are the sum of the uncertainties of these
equations used for their development. For example, the
uncertainty of the thermal resistance is the equivalent of
the uncertainty of the wall temperature equation.
Furthermore, the uncertainty of the thermal performance
equation is the sum of the uncertainty for the thermal
resistance equation and the hydraulic performance equation.

## E.1 Uncertainty for the Heat Loss Equation

A least squares analysis was performed for the radial heat loss equation, seen in Equation (3.18). This analysis is described in section 2.2.3. The experimental data can be seen in Appendix F.

$$\frac{\dot{Q}_{loss}}{\dot{Q}_{applied}} = \phi_1 + \left(\phi_2 + \phi_3 e^{(\phi_4 T)}\right) e^{\left(\left(\phi_5 + \phi_6 e^{(\phi_7 T)}\right)\dot{m}\right)}$$  (3.18)

However, the coefficients, $\phi$, are dependent on the applied heat load. Therefore, for this least squares analysis, the equation for each applied heat load must evaluated. The results of this analysis is presented using the standard deviation of the curve fitted data, shown in the heat loss per heat applied and in percentage of the deviation to the experimental data. In addition, the maximum error and the corresponding flow rate are presented. These results are shown in Table E.1, for the standard deviation, and Table E.2, for the maximum errors. As can be seen from these tables, the standard deviation of the error of the curve fit is less than 1.0% for each heat load. Furthermore, the maximum error is less 0.002 $\dot{Q}_{loss} / \dot{Q}_{applied}$.

**Table E.1   Uncertainties for the Heat Loss Equation.**

|        | -10°C   | 0°C     | 10°C    | 20°C    | 30°C    | 40°C    |
|--------|---------|---------|---------|---------|---------|---------|
|        | Standard | Deviation | in W/W | | | |
| 20 W   | 0.00100 | 0.00034 | 0.00047 | 0.00073 | 0.00050 | 0.00074 |
| 40 W   | 0.00085 | 0.00066 | 0.00054 | 0.00121 | 0.00037 | 0.00119 |
| 60 W   | 0.00066 | 0.00077 | 0.00054 | 0.00097 | 0.00100 | 0.00055 |
| 80 W   | 0.00096 | 0.00055 | 0.00055 | 0.00064 | 0.00060 |         |
| 100 W  | 0.00035 | 0.00047 | 0.00082 | 0.00046 |         |         |
|        | Standard | Deviation | in % | | | |
| 20 W   | 0.503   | 0.147   | 0.205   | 0.372   | 0.277   | 0.407   |
| 40 W   | 0.498   | 0.283   | 0.271   | 0.623   | 0.188   | 0.683   |
| 60 W   | 0.377   | 0.392   | 0.298   | 0.539   | 0.576   | 0.322   |
| 80 W   | 0.594   | 0.273   | 0.256   | 0.330   | 0.341   |         |
| 100 W  | 0.218   | 0.272   | 0.450   | 0.251   |         |         |

**Table E.2   Maximum Error for the Heat Loss Equation.**

|        |            |        | -10°C   | 0°C     | 10°C    | 20°C    | 30°C    | 40°C    |
|--------|------------|--------|---------|---------|---------|---------|---------|---------|
| 20 W   | max. error |        | -0.0016 | -0.0008 | -0.0009 | 0.0010  | -0.0005 | -0.0008 |
|        | @flow rate | kg/hr  | 60      | 90      | 75      | 60      | 240     | 225     |
| 40 W   | max. error |        | -0.0012 | 0.0011  | 0.0011  | -0.0018 | -0.0007 | 0.0018  |
|        | @flow rate | kg/hr  | 120     | 75      | 240     | 195     | 120     | 180     |
| 60 W   | max. error |        | 0.0013  | 0.0014  | -0.0010 | 0.0019  | 0.0015  | 0.0008  |
|        | @flow rate | kg/hr  | 180     | 60      | 60      | 240     | 195     | 195     |
| 80 W   | max. error |        | 0.0013  | 0.0012  | -0.0015 | -0.0012 | -0.0013 |         |
|        | @flow rate | kg/hr  | 150     | 60      | 240     | 240     | 240     |         |
| 100 W  | max. error |        | 0.0005  | 0.0007  | -0.0015 | 0.0008  |         |         |
|        | @flow rate | kg/hr  | 180     | 90      | 75      | 105     |         |         |

E.2  Uncertainty for the Temperature Difference Equation

A least squares analysis was performed for the radial heat loss equation, seen in Equation (3.20).

$$T_w - T_f = \lambda_0 + \left(\lambda_1 + \lambda_2 e^{(\lambda_3 \dot{m})}\right)\dot{Q} \tag{3.20}$$

The constants $\lambda_n$ are independent of the flow rate, heat load, and fluid temperature and have the following values: $\lambda_0$ (2.25), $\lambda_1$ (0.19779), $\lambda_2$ (0.19968), and $\lambda_3$ (-0.013115). In addition, the mass flow rate is in kg/hr, and the heat load is in W/cm$^2$. The experimental data for this equation can be seen in Table E.3. The results of this analysis is presented using the standard deviation of the curve fitted data, shown in the heat loss per heat applied and in percentage of the deviation to the experimental data. In addition, the maximum error and the corresponding flow rate are presented. These results are shown in Table E.4, for the standard deviation and the maximum errors. As can be seen from these tables, the standard deviation of the error of the curve fit is less than 4.3% for each heat load. Furthermore, the maximum error is less 10.44%. However, this large maximum error occurs for the heat load of 20 W, at which the temperature difference is relatively small.

**Table E.3   Data for the Temperature Difference Equation.**

| Heat Load | 20 W | | | 40 W | | | 60 W | | |
|---|---|---|---|---|---|---|---|---|---|
| Flow Rate | Net Heat Load | $T_w-T_f$ (Actual) | $T_w-T_f$ (fitted) | Net Heat Load | $T_w-T_f$ (Actual) | $T_w-T_f$ (fitted) | Net Heat Load | $T_w-T_f$ (Actual) | $T_w-T_f$ (fitted) |
| kg/hr | W | °C (K) | °C (K) | W | °C (K) | °C (K) | W | °C (K) | °C (K) |
| 60 | 15.719 | 6.615 | 6.788 | 32.180 | 11.620 | 11.540 | 48.764 | 16.487 | 16.328 |
| 75 | 15.892 | 6.218 | 6.580 | 32.445 | 11.025 | 11.090 | 49.097 | 15.817 | 15.627 |
| 90 | 16.059 | 5.845 | 6.411 | 32.718 | 10.595 | 10.728 | 49.486 | 15.216 | 15.073 |
| 105 | 16.211 | 5.680 | 6.273 | 32.851 | 10.174 | 10.403 | 49.822 | 14.841 | 14.614 |
| 120 | 16.219 | 6.187 | 6.129 | 33.128 | 9.827 | 10.173 | 49.898 | 14.431 | 14.184 |
| 135 | 16.366 | 6.095 | 6.043 | 33.344 | 9.599 | 9.978 | 50.183 | 14.096 | 13.881 |
| 150 | 16.410 | 6.094 | 5.954 | 33.497 | 9.384 | 9.810 | 50.561 | 13.908 | 13.662 |
| 165 | 16.505 | 5.993 | 5.893 | 33.628 | 9.2443 | 9.672 | 50.701 | 13.744 | 13.441 |
| 180 | 16.615 | 5.916 | 5.849 | 33.653 | 9.230 | 9.540 | 50.754 | 13.888 | 13.245 |
| 195 | 16.378 | 5.863 | 5.743 | 33.434 | 9.275 | 9.380 | 50.672 | 13.745 | 13.056 |
| 210 | 16.462 | 5.797 | 5.715 | 33.602 | 9.186 | 9.323 | 50.719 | 13.633 | 12.926 |
| 225 | 16.533 | 5.717 | 5.693 | 33.717 | 8.982 | 9.271 | 50.879 | 13.489 | 12.844 |
| 240 | 16.559 | 5.649 | 5.667 | 33.766 | 8.762 | 9.218 | 50.826 | 13.265 | 12.739 |

**Table E.3 (cont.)**

| Heat Load | 80 W | | | 100 W | | | | | |
|---|---|---|---|---|---|---|---|---|---|
| Flow Rate | Net Heat Load | $T_w-T_f$ (Actual) | $T_w-T_f$ (fitted) | Net Heat Load | $T_w-T_f$ (Actual) | $T_w-T_f$ (fitted) | | | |
| kg/hr | W | °C (K) | °C (K) | W | °C (K) | °C (K) | | | |
| 60 | 65.822 | 21.146 | 21.252 | 82.480 | 25.786 | 11.540 | | | |
| 75 | 66.334 | 20.406 | 20.324 | 83.017 | 25.009 | 11.090 | | | |
| 90 | 66.850 | 19.484 | 19.573 | 83.517 | 24.030 | 10.728 | | | |
| 105 | 67.093 | 18.788 | 18.901 | 83.981 | 23.130 | 10.403 | | | |
| 120 | 67.413 | 18.369 | 18.374 | 84.409 | 22.401 | 10.173 | | | |
| 135 | 67.732 | 17.899 | 17.949 | 84.801 | 21.952 | 9.978 | | | |
| 150 | 67.935 | 17.564 | 17.584 | 85.157 | 21.528 | 9.810 | | | |
| 165 | 68.115 | 17.329 | 17.285 | 85.476 | 21.210 | 9.672 | | | |
| 180 | 68.389 | 17.113 | 17.065 | 85.760 | 20.973 | 9.540 | | | |
| 195 | 68.263 | 16.658 | 16.808 | 86.007 | 20.697 | 9.380 | | | |
| 210 | 68.362 | 16.415 | 16.641 | 86.218 | 20.321 | 9.323 | | | |
| 225 | 68.515 | 16.295 | 16.517 | 86.393 | 20.102 | 9.271 | | | |
| 240 | 68.516 | 16.220 | 16.389 | 86.532 | 19.931 | 9.218 | | | |

**Table E.4  Uncertainties for the Temperature Difference Equation.**

|  |  | 20 W | 40 W | 60 W | 80 W | 100 W |
|---|---|---|---|---|---|---|
| Standard | °C | .262 | .295 | .435 | .123 | .130 |
| Deviation | % | 4.29 | 2.90 | 2.93 | 0.66 | 0.57 |
| Maximum | °C | -0.593 | -0.456 | 0.707 | -0.226 | -0.177 |
| Error | % | -10.44 | -5.21 | 5.22 | 1.37 | 0.89 |
| @ Flow Rate | kg/hr | 105 | 240 | 210 | 210 | 240 |

APPENDIX F


RADIAL CONDUCTED HEAT LOSS


The raw data, the curve fit coefficients, and the curve fits for the radial heat loss due to conduction are presented in this appendix. This data represents the heat loss due to the simplification of applying a heat load to one CHIC at a time. Futhermore, the radial heat loss is presented as a function of the mass flow rate and coolant temperature for various applied heat loads. The analytical model for the radial heat loss is presented as a ratio of the heat loss to the applied heat load and is equivalent to an exponential decay function with the coolant temperature and the mass flow rate as the dependent variables. However, the coefficients shown in the following equation are dependent on the applied heat load, and shown in Table F.1.

$$\frac{\dot{Q}_{loss}}{\dot{Q}_{applied}} = \phi_1 + \left(\phi_2 + \phi_3 e^{(\phi_4 T)}\right) e^{\left(\left(\phi_5 + \phi_6 e^{(\phi_7 T)}\right)\dot{m}\right)}$$

Furthermore, Figures F.1 through F.5 show the curve fits for the various equations. Finally, the raw data for these curves is presented in Tables F.2 through F.6.

**Table F.1. Curve Fit Coefficients for the Radial Heat Loss**

| Applied Heat Load | Curve Fit Coefficients | | | | | | |
|---|---|---|---|---|---|---|---|
| | $\phi_1$ | $\phi_2$ | $\phi_3$ | $\phi_4$ | $\phi_5$ | $\phi_6$ | $\phi_7$ |
| 20 W | 0.143 | 0.290 | -0.621 | -0.0050 | -0.0048 | -0.612 | -0.0180 |
| 40 W | 0.134 | 0.280 | -0.470 | -0.0035 | -0.0048 | -0.489 | -0.0177 |
| 60 W | 0.128 | 0.265 | -0.376 | -0.0029 | -0.0052 | -0.419 | -0.0173 |
| 80 W | 0.125 | 0.189 | -0.253 | -0.0032 | -0.0035 | -0.121 | -0.0116 |
| 100 W | 0.119 | 0.119 | -0.786 | -0.0011 | -0.0047 | -0.377 | -0.0170 |
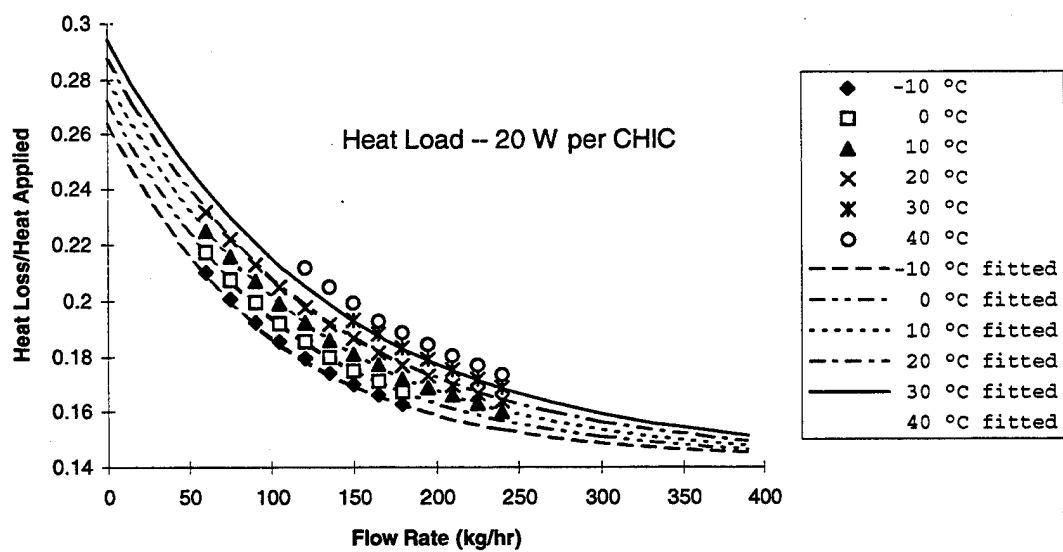
**Figure F.1. Radial Heat Loss Due to Conduction Heat Transfer for an Applied Heat Load of 20 W.**
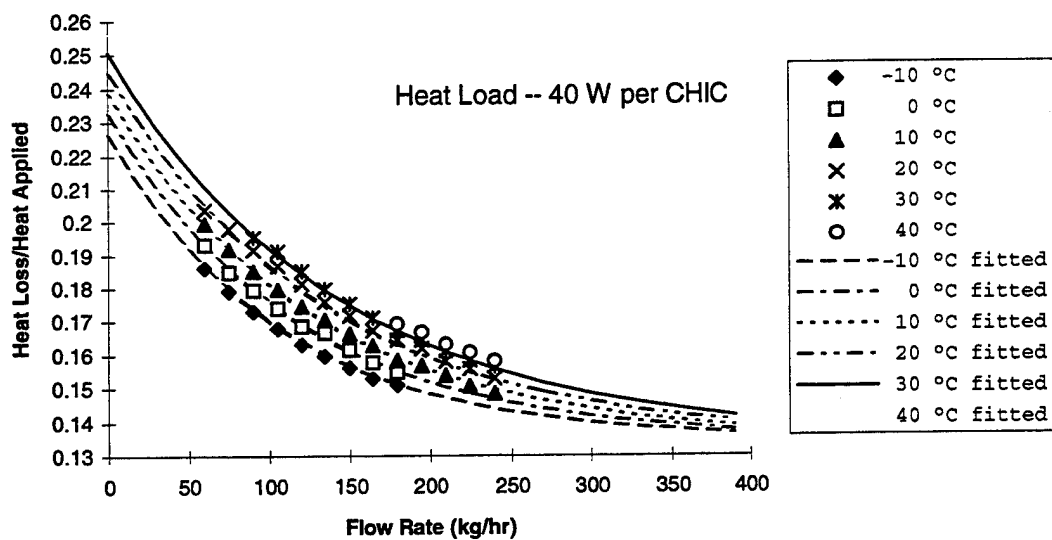
**Figure F.2. Radial Heat Loss Due to Conduction Heat Transfer for an Applied Heat Load of 40 W.**

Figure F.3. Radial Heat Loss Due to Conduction Heat Transfer for an Applied Heat Load of 60 W.
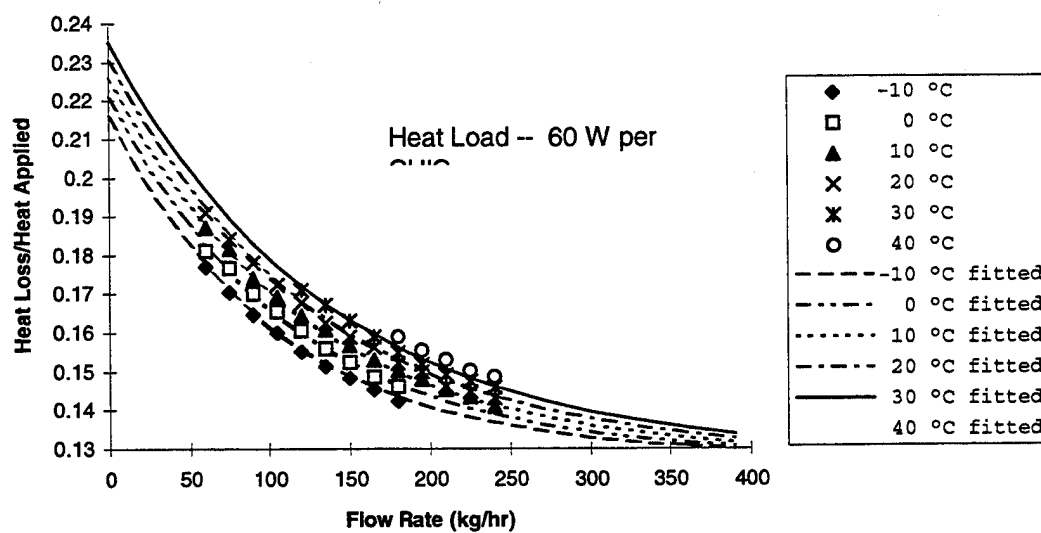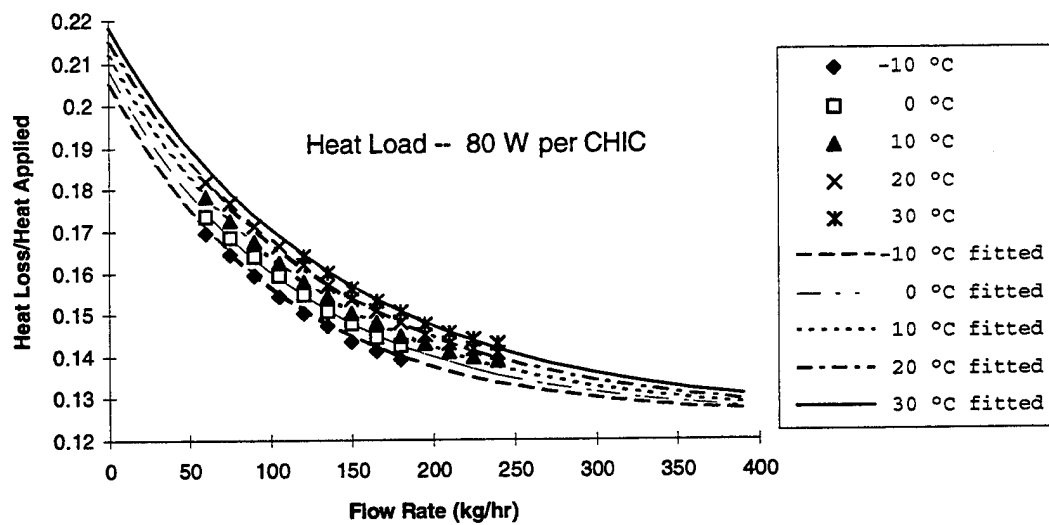
**Figure F.4. Radial Heat Loss Due to Conduction Heat Transfer for an Applied Heat Load of 80 W.**
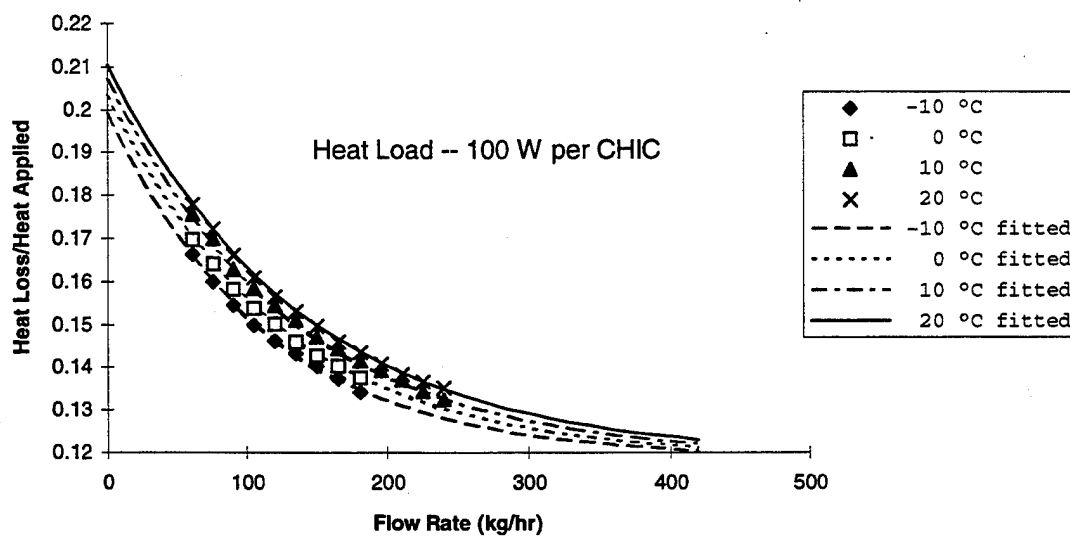
Figure F.5.   Radial Heat Loss Due to Conduction Heat
Transfer for an Applied Heat Load of 100 W.

**Table F.2. Curve Fit Data for the Radial Heat Loss for an Applied Heat Load of 20 W.**

| Heat Loss /Heat Applied | | | | | | |
|---|---|---|---|---|---|---|
| Flow Rate | Coolant   Temperature | | | | | |
| kg/hr | -10°C | 0°C | 10°C | 20°C | 30°C | 40°C |
| 60 | 0.210 | 0.217 | 0.225 | 0.232 | | |
| 75 | 0.201 | 0.208 | 0.216 | 0.222 | | |
| 90 | 0.193 | 0.200 | 0.207 | 0.213 | | |
| 105 | 0.186 | 0.192 | 0.199 | 0.205 | | |
| 120 | 0.179 | 0.186 | 0.193 | 0.198 | | |
| 135 | 0.174 | 0.180 | 0.186 | 0.192 | | |
| 150 | 0.170 | 0.175 | 0.181 | 0.187 | 0.193 | 0.199 |
| 165 | 0.166 | 0.171 | 0.177 | 0.181 | 0.188 | 0.193 |
| 180 | 0.163 | 0.167 | 0.172 | 0.177 | 0.183 | 0.189 |
| 195 | | | 0.169 | 0.173 | 0.179 | 0.184 |
| 210 | | | 0.166 | 0.169 | 0.175 | 0.180 |
| 225 | | | 0.163 | 0.167 | 0.172 | 0.177 |
| 240 | | | 0.160 | 0.164 | 0.169 | 0.173 |

**Table F.3.   Curve Fit Data for the Radial Heat Loss for an Applied Heat Load of 40 W.**

| Heat Loss /Heat Applied | | | | | | |
|---|---|---|---|---|---|---|
| Flow Rate | Coolant    Temperature | | | | | |
| kg/hr | -10°C | 0°C | 10°C | 20°C | 30°C | 40°C |
| 60 | 0.186 | 0.193 | 0.199 | 0.204 | | |
| 75 | 0.179 | 0.185 | 0.191 | 0.198 | | |
| 90 | 0.173 | 0.180 | 0.185 | 0.191 | | |
| 105 | 0.168 | 0.174 | 0.180 | 0.187 | | |
| 120 | 0.163 | 0.169 | 0.175 | 0.181 | 0.185 | |
| 135 | 0.160 | 0.165 | 0.171 | 0.176 | 0.180 | |
| 150 | 0.156 | 0.162 | 0.167 | 0.172 | 0.175 | |
| 165 | 0.153 | 0.158 | 0.163 | 0.168 | 0.171 | |
| 180 | 0.151 | 0.155 | 0.159 | 0.164 | 0.167 | 0.169 |
| 195 | | | 0.156 | 0.162 | 0.164 | 0.168 |
| 210 | | | 0.154 | 0.158 | 0.161 | 0.163 |
| 225 | | | 0.151 | 0.156 | 0.158 | 0.161 |
| 240 | | | 0.149 | 0.153 | 0.156 | 0.158 |

**Table F.4.  Curve Fit Data for the Radial Heat Loss for an Applied Heat Load of 60 W.**

| Flow Rate | Heat Loss /Heat Applied | | | | | |
|---|---|---|---|---|---|---|
| | Coolant Temperature | | | | | |
| kg/hr | -10°C | 0°C | 10°C | 20°C | 30°C | 40°C |
| 60 | 0.177 | 0.181 | 0.187 | 0.191 | | |
| 75 | 0.171 | 0.176 | 0.181 | 0.184 | | |
| 90 | 0.165 | 0.170 | 0.174 | 0.178 | | |
| 105 | 0.160 | 0.165 | 0.169 | 0.172 | | |
| 120 | 0.155 | 0.160 | 0.164 | 0.168 | 0.171 | |
| 135 | 0.151 | 0.156 | 0.161 | 0.163 | 0.167 | |
| 150 | 0.148 | 0.152 | 0.157 | 0.159 | 0.163 | |
| 165 | 0.145 | 0.149 | 0.153 | 0.156 | 0.159 | |
| 180 | 0.142 | 0.146 | 0.150 | 0.152 | 0.155 | 0.159 |
| 195 | | | 0.148 | 0.150 | 0.152 | 0.156 |
| 210 | | | 0.145 | 0.146 | 0.149 | 0.153 |
| 225 | | | 0.143 | 0.145 | 0.147 | 0.150 |
| 240 | | | 0.140 | 0.143 | 0.146 | 0.148 |

**Table F.5.  Curve Fit Data for the Radial Heat Loss for an Applied Heat Load of 80 W.**

| Flow Rate | Heat Loss /Heat Applied | | | | | |
|-----------|-------|------|------|------|------|------|
| | Coolant     Temperature | | | | | |
| kg/hr | -10°C | 0°C | 10°C | 20°C | 30°C | 40°C |
| 60  | 0.169 | 0.173 | 0.178 | 0.182 | | |
| 75  | 0.165 | 0.169 | 0.172 | 0.177 | | |
| 90  | 0.159 | 0.164 | 0.167 | 0.171 | | |
| 105 | 0.154 | 0.159 | 0.163 | 0.166 | | |
| 120 | 0.150 | 0.155 | 0.158 | 0.162 | 0.164 | |
| 135 | 0.147 | 0.151 | 0.154 | 0.157 | 0.160 | |
| 150 | 0.144 | 0.148 | 0.150 | 0.154 | 0.156 | |
| 165 | 0.141 | 0.145 | 0.148 | 0.151 | 0.153 | |
| 180 | 0.139 | 0.142 | 0.145 | 0.148 | 0.151 | |
| 195 | | | 0.143 | 0.145 | 0.148 | |
| 210 | | | 0.141 | 0.143 | 0.146 | |
| 225 | | | 0.140 | 0.142 | 0.144 | |
| 240 | | | 0.139 | 0.141 | 0.143 | |

**Table F.6. Curve Fit Data for the Radial Heat Loss for an Applied Heat Load of 100 W.**

| Flow Rate | Heat Loss /Heat Applied | | | | | |
|---|---|---|---|---|---|---|
| | Coolant Temperature | | | | | |
| kg/hr | -10°C | 0°C | 10°C | 20°C | 30°C | 40°C |
| 60 | 0.166 | 0.170 | 0.176 | 0.178 | | |
| 75 | 0.160 | 0.164 | 0.170 | 0.172 | | |
| 90 | 0.155 | 0.158 | 0.163 | 0.166 | | |
| 105 | 0.150 | 0.154 | 0.158 | 0.161 | | |
| 120 | 0.146 | 0.150 | 0.155 | 0.157 | | |
| 135 | 0.143 | 0.146 | 0.151 | 0.153 | | |
| 150 | 0.140 | 0.143 | 0.147 | 0.150 | | |
| 165 | 0.137 | 0.140 | 0.144 | 0.146 | | |
| 180 | 0.134 | 0.138 | 0.142 | 0.143 | | |
| 195 | | | 0.139 | 0.141 | | |
| 210 | | | 0.137 | 0.138 | | |
| 225 | | | 0.135 | 0.137 | | |
| 240 | | | 0.133 | 0.135 | | |